NASA CR-72500
LMSC-A944673

SMALL AMPLITUDE LATERAL SLOSHING IN SPHEROIDAL CONTAINERS UNDER LOW GRAVITATIONAL CONDITIONS

by

P. Concus, G. E. Crane, H. M. Satterlee

Prepared for
NATIONAL AERONAUTICS AND SPACE ADMINISTRATION

NASA Lewis Research Center
CONTRACT NAS 3-9704
W. J. Masica, Project Manager

Lockheed

MISSILES & SPACE COMPANY
A GROUP DIVISION OF LOCKHEED AIRCRAFT CORPORATION
SUNNYVALE, CALIFORNIA

NOTICE

This report was prepared as an account of Government-sponsored work. Neither the United States, nor the National Aeronautics and Space Administration (NASA), nor any person acting on behalf of NASA:

A.) Makes any warranty or representation, expressed or implied, with respect to the accuracy, completeness, or usefulness of the information contained in this report, or that the use of any information, apparatus, method, or process disclosed in this report may not infringe privately-owned rights; or

B.) Assumes any liabilities with respect to the use of, or for damages resulting from the use of, any information, apparatus, method or process disclosed in this report.

As used above, "person acting on behalf of NASA" includes any employee or contractor of NASA, or employee of such contractor, to the extent that such employee or contractor of NASA or employee of such contractor prepares, disseminates, or provides access to any information pursuant to his employment or contract with NASA, or his employment with such contractor.

NASA CR-72500
LMSC/A944673

FINAL REPORT

SMALL AMPLITUDE LATERAL SLOSHING IN SPHEROIDAL CONTAINERS UNDER LOW GRAVITATIONAL CONDITIONS

by

P. Concus, G. E. Crane, and H. M. Satterlee

LOCKHEED MISSILES AND SPACE COMPANY
1111 Lockheed Way
Sunnyvale, California

Prepared for

NATIONAL AERONAUTICS AND SPACE ADMINISTRATION
February 4, 1969

NASA Lewis Research Center
Cleveland, Ohio

W. J. Masica, Project Manager
Space Technology Division

TABLE OF CONTENTS

LIST OF ILLUSTRATIONS

LIST OF TABLES

ABSTRACT

A finite difference technique utilizing an irregular-triangular mesh and the Wielandt inverse-iteration method is used to compute normal mode sloshing in spheroidal tanks of eccentricities ranging from zero to 0.8 under zero and low gravitational conditions for a contact angle of 5 degrees. The results are used to calculate, using a finite Fourier series expansion, liquid response to sinusoidal, square-wave, and periodic pulse lateral perturbing accelerations. Reduction of either liquid volume or gravity level decreases the fundamental sloshing frequency.

SUMMARY

The small-amplitude lateral sloshing of an incompressible inviscid liquid partially filling a spheroidal tank, as determined by surface and gravitational forces, is studied for zero- and low-g conditions. The problem is formulated in a curvilinear coordinate system parallel to the equilibrium free-surface. The first few normal modes of oscillation having one nodal diameter and the corresponding eigenfrequencies are calculated numerically for a liquid-tank contact angle of 5 degrees. These modes are computed by a finite difference method using an irregular triangular mesh and a Wielandt inverse iteration technique. The forced response to lateral perturbing accelerations is developed in terms of the calculated modes using a finite Fourier analysis. The calculations are carried out for tanks of eccentricity 0., 0.5, 0.68, and 0.8 and for liquid volumes ranging from 1/8 to 7/8 of a full tank. The (dimensionless) Bond number $B_\alpha = \rho g_\alpha a^2/\sigma$ (ρ, g_α, a, and σ are the liquid density, steady axial acceleration, tank semi-major axis, and surface tension) ranges from zero to 100. At the lower values of B_α, the equilibrium meniscus may leave dry spots at both the bottom and the top of the tank.

General conclusions include: (a) The fundamental sloshing frequency is generally an increasing function of Bond number B_α and liquid volume. The fundamental sloshing frequency is zero or near zero for $B_\alpha = 0$ when the equilibrium free-surface intersects the tank wall in a single circle and is generally positive for $B_\alpha = 0$ when the tank wall and free-surface intersect in two circles. (b) Computation of the response to lateral perturbing accelerations can be effected by use of the finite Fourier analysis, but, where appropriate, engineering computations may be more easily made using a spring-mass analog for normal mode liquid sloshing. Parameters for this analog are presented for first mode sloshing. These are adequate for engineering computations when the first term is dominant in the Fourier series for the forced motion. (c) The irregular-triangular, finite-difference, Wielandt inverse-iteration scheme appears adaptable for this type of problem in a wide variety of tank shapes when currently available digital computers are fully utilized.

INTRODUCTION

In the recent past, considerable attention has been given to the sloshing of liquids in containers of the shapes used in modern propulsion systems, such as cylindrical containers with spheroidal ends (sometimes inverted) or simple spheroidal ones. Interest has focused more recently on sloshing under low-g conditions, where surface tension effects can dominate the behavior of the liquid.

There now exists a large body of literature concerning sloshing under conditions where surface tension is not important.[1] However, comparatively little work has been done on investigating low-g sloshing,[2-8] and much of it has been limited to conditions in which the effects of surface tension are slight so that gravitational forces still essentially dominate.[3,7]

The object of this study is to investigate linearized low-gravity sloshing in spheroidal tanks of zero to moderate eccentricity. Specific objectives include: (a) Determination of the normal lateral sloshing modes and frequencies as a function of the axial acceleration level, the surface tension and density of the liquid, and the liquid volume in the tank. (b) Determination of the forced response of the liquid to lateral perturbing accelerations. (c) Computation of the lateral forces and moments acting on the tank.

The linear analysis employed here describes small amplitude oscillations of the liquid about its equilibrium shape and neglects the influence of viscosity. (Experiments have shown that viscosity can be safely neglected for determining the natural frequency of even quite small scale models.[2,3,7]) It is assumed that the fluid properties and the contact angle of the liquid are constant and do not vary dynamically.

The frame of reference used for this study is fixed to the container as shown in Figure 1. The liquid in tanks of a space vehicle will not be acted upon directly by a lateral force that acts on the vehicle, but rather acted upon indirectly by the moving walls of the tank. For convenience, however, the tank is considered fixed and the liquid as being influenced directly by a lateral perturbing acceleration in the tank-fixed coordinate system.

The mathematical problem describing the sloshing is a linear boundary value problem. In the tank-fixed coordinate system it can be assumed that the liquid motion is irrotational so that the governing equation is Laplace's equation, the equation of continuity for an ideal liquid. The solution of Laplace's equation in the domain occupied by the liquid must satisfy a zero normal velocity boundary condition at the tank walls and dynamical and kinematic conditions at the free-surface. The dynamical condition is obtained from the unsteady form of the Bernoulli equation and the kinematic condition relates the velocity potential to the motion of the free-surface. The motion of the free surface is constrained to preserve the contact angle constant at the tank wall.

Previous analysis related to sloshing in spheroidal tanks has been limited to the simpler high-g (zero surface tension) case. It was found, even for this case, that the use of approximate methods is required, in general, for solving the governing equations.[9,10,11] In the more complex low-g case studied here, approximate methods are also required. To solve the boundary value problem, an extension of the numerical technique successfully applied previously to low-g sloshing in hemispherically bottomed cylindrical tanks is used.[4,5]

The numerical solution of the sloshing problem is carried out in three stages: (a) The equilibrium meniscus shape is computed for each combination of Bond number (dimensionless ratio of gravitational to surface tension forces) and liquid volume. (b) A suitable finite difference mesh is constructed by mapping a cross section of the liquid conformally onto the unit circle, by constructing a mesh within the circular domain, and by mapping this mesh conformally back into the liquid cross section. (c) The eigenfrequencies and eigenfunctions of the discretized system of equations are determined. The forced response to lateral perturbing accelerations, as well as other engineering data, is then developed in terms of the solutions.

PROBLEM FORMULATION

In this section the mathematical formulation for lateral sloshing in a spheroidal container is presented. It closely follows that presented previously for a hemispherically bottomed cylindrical container and, wherever possible, similar notation is used to facilitate comparison.[4,5]* A new formulation is required primarily because the one used earlier is based upon representing the free surface as a single valued function of the radial coordinate in circular cylindrical coordinates, a representation that is not general enough for a spheroidal container. The possibility of representing a free surface double-valued in those coordinates is allowed for here by employing a surface polar normal coordinate system to express the free-surface boundary conditions.

Surface Polar Normal Coordinates

Let the unit vectors associated with the coordinate directions in circular cylindrical coordinates (r,θ,z) be denoted by the triple $[\underline{e}_r,\underline{e}_\theta,\underline{k}]$, and let the equations of a meridian of the equilibrium free-surface be

$$r = R(s) \qquad \text{and} \qquad z = Z(s) \ ,$$

where the parameter s is arc length along the curve measured from the lowest point on the surface (see Figure 1).** Then the position vector of a point on the equilibrium free-surface, a surface of revolution about the z-axis, can be represented by

---

*Reference numbers are superscripted in parentheses.

**Variables appearing in this report are dimensionless, unless otherwise stated. They are defined in the Nomenclature List, Appendix A, where the relationships to the physical dimensioned variables are given.

$$\underline{r} = R(s)\,\underline{e}_r + Z(s)\,\underline{k} \tag{1}$$

The surface polar normal coordinates are defined relative to the equilibrium free-surface by taking $\underline{e}_s$ and $\underline{e}_n$ to be unit vectors tangent and normal to a meridian. Let $\underline{e}_n$ point from the liquid into the gas and $\underline{e}_s$ point in the direction of increasing s so that the unit vectors $[\underline{e}_s, \underline{e}_\theta, \underline{e}_n]$ form a right-handed triple. This triple is associated with the coordinate directions in surface polar normal coordinates (s,θ,η), where η is the distance of a point from the equilibrium free-surface along $\underline{e}_n$. In terms of circular cylindrical coordinates the unit vectors are

$$\underline{e}_s = R_s\,\underline{e}_r + Z_s\,\underline{k} \quad \text{and} \quad \underline{e}_n = -Z_s\,\underline{e}_r + R_s\,\underline{k}\,,$$

and conversely (2)

$$\underline{e}_r = R_s\,\underline{e}_s - Z_s\,\underline{e}_n \quad \text{and} \quad \underline{k} = Z_s\,\underline{e}_s + R_s\,\underline{e}_n\,.^*$$

As a sphere of radius η rolls over the equilibrium free-surface, the center generates a "parallel" surface. These parallel surfaces have no self-intersections so long as

$$\eta < \min\,(R_1, R_2) \tag{3}$$

where

$$R_1 = [Z_{ss}R_s - Z_sR_{ss}]^{-1} \text{ and } R_2 = [R/Z_s]^{-1}$$

are the principal radii of curvature of the equilibrium free-surface. Consequently, a perturbed free-surface can be described in surface polar normal coordinates by the relation

$$\eta = H(s,\theta;t) \tag{4}$$

*The subscripts on R and Z denote differentiation. Throughout the paper such notation is used to denote differentiation of a dependent variable with respect to an independent variable, when the context makes it clear that such differentiation is intended.

provided that departure from the equilibrium surface $\eta = 0$ is small enough so that

$$\max H < \min (R_1, R_2) \ . \tag{5}$$

(The relation (5) is not a significant restriction for the small amplitude sloshing problems considered here.) Let ψ be the angle from $\underline{e}_r$ to $\underline{e}_s$ (alternately from $\underline{k}$ to $\underline{e}_n$) so that $Z_s = \sin\psi$ and $R_s = \cos\psi$, then one obtains directly that the position vector of a point can be described in surface polar normal coordinates by

$$\underline{r} = \underline{r}(s,\theta,\eta) = (R - \eta Z_s)\, \underline{e}_r + (Z + \eta R_s)\, \underline{k} \ ; \tag{6}$$

when $\eta = H(s,\theta;t)$ the point lies on the perturbed surface; when $\eta = 0$ the point lies on the equilibrium surface and (6) reduces to (1).

The Governing Equation

The liquid is assumed to be incompressible and inviscid and its motion irrotational so that the velocity potential satisfies Laplace's equation

$$\Phi_{rr} + \frac{1}{r}\Phi_r + \frac{1}{r^2}\Phi_{\theta\theta} + \Phi_{zz} = 0 \tag{7}$$

within the liquid, subject to the boundary condition on the container wall that the normal velocity be zero,

$$\frac{\partial \Phi}{\partial n} = 0 \tag{8}$$

on w. The boundary conditions on the free-surface present the major complexity and are derived in the next parts of this section.

Free-Surface Boundary Conditions

Bernoulli Equation. One of the free-surface boundary conditions is obtained from the nonsteady state Bernoulli equation, which in surface polar normal

coordinates takes the form

$$p + B_\alpha(Z+HR_s) - B_{tr}(R-HZ_s)\cos\theta + (1+B_\alpha)\,\Phi_t + \frac{1+B_\alpha}{2}\left[\|\underline{\nabla}\Phi-\underline{\Omega}x\underline{r}\|^2 + (\underline{\Omega}\cdot\underline{r})^2 - \|\underline{\Omega}\|^2\,\|\underline{r}\|^2\right] = f(t) \tag{9}$$

on $\eta = H(s,\theta;t)$, where the sign of the velocity potential Φ is chosen so that the velocity $\underline{v}$ is

$$\underline{v} = \underline{\nabla}\Phi = \Phi_r\underline{e}_r + \frac{1}{r}\Phi_\theta\underline{e}_\theta + \Phi_z\underline{k}\,. \tag{10}$$

Equations (9) and (10) are for fluid motion relative to the container in a coordinate system fixed to the container. The choice of the function on the right hand side of (9) is arbitrary and, for convenience, is set equal to p_o, the static liquid pressure at a fixed point on the equilibrium meniscus. The liquid pressure at the interface is related to the gas pressure through the surface-tension and the mean curvature of the free-surface by means of the relation

$$p_g - p = 2\mathcal{H}. \tag{11}$$

Substitution of this relation and p_o for $f(t)$ into (9) results in

$$2\mathcal{H} - B_\alpha(Z+HR_s) + B_{tr}(R-HZ_s)\cos\theta - (1+B_\alpha)\,\Phi_t - \frac{1+B_\alpha}{2}\left[\|\underline{\nabla}\Phi - \underline{\Omega}x\underline{r}\|^2 + (\underline{\Omega}\cdot\underline{r})^2 - \|\underline{\Omega}\|^2\,\|\underline{r}\|^2\right] = p_g - p_o \text{ on } \eta = H. \tag{12}$$

The form that the mean curvature $\mathcal{H}$ in (12) takes in surface polar normal coordinates can be calculated from the relation[13] that for a surface defined by $F = 0$

$$2\mathcal{H} = -\,\mathrm{div}(\underline{\mathrm{grad}}F/\|\underline{\mathrm{grad}}F\|)\Big]_{F=0} \tag{13}$$

The vector $\underline{\text{grad}}F/\|\underline{\text{grad}}F\|$ is the unit normal to the surfaces F = constant, and (13) states that the negative of its divergence when evaluated on the surface $F = 0$ is twice the mean curvature of that surface. The desired form for $\mathcal{H}$ is thus obtained by taking $F = \eta - H(s,\theta;t)$ in (13) and using the expressions for the divergence and gradient in surface polar normal coordinates.

The standard formulas expressing the gradient of a function F and the divergence of a vector $\underline{G}$ in orthogonal curvilinear coordinates specialize in the case of surface polar normal coordinates to

$$\underline{\text{grad}}\ F = \frac{F_s}{h_1}\,\underline{e}_s + \frac{F_\theta}{h_2}\,\underline{e}_\theta + \frac{F_\eta}{h_3}\,\underline{e}_n \tag{14}$$

and for

$$\underline{G} = g_1\,\underline{e}_s + g_2\,\underline{e}_\theta + g_3\,\underline{e}_n\ ,$$

to

$$\text{div}\ \underline{G} = \frac{1}{h_1h_2h_3}\left[(h_2h_3g_1)_s + (h_3h_1g_2)_\theta + (h_1h_2g_3)_\eta\right] \tag{15}$$

where h_1, h_2, and h_3 are the magnitudes of the derivatives of the position vector (6) with respect to the coordinates, that is,

$$h_1\,\underline{e}_s = \frac{\partial \underline{r}}{\partial s}\ ,\quad h_2\,\underline{e}_\theta = \frac{\partial \underline{r}}{\partial \theta}\ ,\ \text{and}\ h_3\,\underline{e}_n = \frac{\partial \underline{r}}{\partial \eta}\ .$$

or

$$\left.\begin{aligned} h_1 &= 1 - \eta(Z_{ss}R_s - Z_sR_{ss}) = 1 - \eta/R_1\ , \\ h_2 &= R - \eta\, Z_s = R(1-\eta/R_2),\ \text{and} \\ h_3 &= 1\ . \end{aligned}\right\} \tag{16}$$

Observe that $h_1 > 0$ and $h_2 > 0$ imply that $\eta < \min\,(R_1,R_2)$, which is equivalent to (3). (The identity

$$(Z_{ss}R_s - Z_sR_{ss})^2 = Z_{ss}^{\ 2} + R_{ss}^{\ 2}\ ,$$

which follows from the fact that the parameter s is arc length, is useful in evaluating h_1.)

If the perturbed surface is

$$F(s,\theta,\eta;t) = \eta - H(s,\theta;t) = 0 \ , \tag{17}$$

then (14) becomes

$$\underline{\text{grad}}\ F = -\frac{H_s}{h_1}\underline{e}_s - \frac{H_\theta}{h_2}\underline{e}_\theta + \underline{e}_n \ ;$$

so that

$$\underline{G} = \frac{\underline{\text{grad}}\ F}{\|\underline{\text{grad}}\ F\|} = -\frac{h_2 H_s}{Q}\underline{e}_s - \frac{h_1 H_\theta}{Q} + \frac{h_1 h_2}{Q}\underline{e}_n \tag{18}$$

where

$$Q = h_1 h_2 \|\underline{\text{grad}}\ F\| = \left[h_2^2 H_s^2 + h_1^2 H_\theta^2 + h_1^2 h_2^2\right]^{1/2} .$$

Using (15), (17), and (18) to evaluate (13) yields the desired expression for $\mathcal{H}$,

$$2\mathcal{H} = \frac{1}{h_1 h_2}\left[\left(\frac{h_2^2 H_s}{Q}\right)_s + \left(\frac{h_1^2 H_\theta}{Q}\right)_\theta - \left(\frac{h_1^2 h_2^2}{Q}\right)_\eta\right] \tag{19}$$

on $\eta = H(s,\theta;t)$ with h_1 and h_2 given by (16).

Contact Angle Condition. The end condition for the free-surface boundary condition (12) and (19) is given by specifying the contact angle between the free-surface and the container wall. The condition that the contact angle remain fixed at the value Θ during the motion is that

$$\cos\Theta = \underline{n}_H \cdot \underline{n}_w \tag{20}$$

along the curve of intersection, where $\underline{n}_H$ is the unit normal to the free-surface pointing from the liquid into the gas and $\underline{n}_w$ is the unit inward normal to the container wall. The expression for $\underline{n}_H$ is given by (18) when

it is evaluated on the free surface $\eta = H(s,\theta;t)$ at the intersection with the wall. If the equations of a meridian of the container wall are

$$r = X(\tau) \quad \text{and} \quad z = Y(\tau) \ ,$$

where τ is arclength measured along the curve from the lower pole of the container, then $\underline{n}_w$ is given by the expression

$$\underline{n}_w = - Y_\tau \underline{e}_r + X_\tau \underline{k}$$

evaluated at the intersection with the free-surface. With respect to the unit vectors of surface polar normal coordinates the expression becomes, by use of (2),

$$\underline{n}_w = (-Y_\tau R_s + X_\tau Z_s)\, \underline{e}_s + (Y_\tau Z_s + X_\tau R_s)\, \underline{e}_n \ .$$

Substituting into (20) then yields the desired contact angle condition,

$$\cos\Theta = - \frac{h_2 H_s}{Q} (-Y_\tau R_s + X_\tau Z_s) + \frac{h_1 h_2}{Q} (Y_\tau Z_s + X_\tau R_s) \qquad (21)$$

along the curve(s) of intersection

$$R - \eta\, Z_s = X \quad , \quad Z + \eta\, R_s = Y \ .$$

Kinematic Condition. The remaining free-surface boundary condition is the kinematic condition, which connects the motion of the free surface with the velocity potential. It is derived from the total derivative with respect to time of the equation defining the free-surface, which is

$$\frac{d}{dt} [\eta - H(s,\theta;t)] = H_t + \underline{\text{grad}}[\eta - H(s,\theta;t)] \cdot \underline{\text{grad}}\ \Phi = 0 \text{ on } \eta = H \ .$$

Expressing the gradient in surface polar normal coordinates then yields the kinematic condition as

$$H_t = \Phi_\eta - \frac{\Phi_s H_s}{h_1^2} - \frac{\Phi_\theta H_\theta}{h_2^2} \text{ on } \eta = H \, . \tag{22}$$

Linearization

The only nonlinearities of the problem appear in the free-surface boundary conditions, (12), (19), (21), and (22). These can be linearized by assuming that the perturbing Bond number B_{tr} is small enough so that H is small compared to the principal radii of curvature of the equilibrium free-surface, that is,

$$H \ll \min \left[\frac{1}{Z_{ss}R_s - Z_s R_{ss}} \, , \, \frac{R}{Z_s} \right] \tag{23}$$

where $(Z_{ss}R_s - Z_s R_{ss}) = \psi_s$ is the curvature of a meridian and $Z_s/R = \sin\psi/R$ is the other principal curvature. Neglecting the $O(H^2)$ terms in (12)(all angular velocity terms are of this order) then yields

$$\frac{1}{R}(R\,H_s)_s + \frac{1}{R^2} H_{\theta\theta} + \left[(Z_{ss}R_s - Z_s R_{ss})^2 + \left(\frac{Z_s}{R} \right)^2 \right] H$$

$$+ (Z_{ss}R_s - Z_s R_{ss}) + \frac{Z_s}{R} - B_\alpha Z - B_\alpha H R_s + B_{tr} R \cos\theta$$

$$- (1 + B_\alpha) \Phi_t - \lambda = 0 \text{ on } \eta = 0 \, ,$$

where the constant λ is equal to $p_g - p_o = 2\mathcal{H}_o$, twice the mean curvature at the point at which p_o is evaluated (11). The terms

$$(Z_{ss}R_s - Z_s R_{ss}) + \frac{Z_s}{R} - B_\alpha Z - \lambda = 0 \, , \tag{24}$$

form the equation of the equilibrium free-surface. With these deleted, the equation becomes

$$\frac{1}{R}(R\,H_s)_s + \frac{1}{R^2}H_{\theta\theta} + \left[(Z_{ss}R_s - Z_sR_{ss})^2 + \left(\frac{Z_s}{R}\right)^2\right]H$$

$$- B_\alpha HR_s + B_{tr}\,R\cos\theta - (1 + B_\alpha)\,\Phi_t = 0 \text{ on } \eta = 0\,. \tag{25}$$

The end conditions for (24) and (25) are found from (21). For the equilibrium free-surface (24), where $\eta = 0$, (21) yields the terminal end condition

$$\cos\Theta = Y_\tau Z_s + X_\tau R_s\Big]_{\substack{s=s_u \\ \tau=\tau_u}} \tag{26a}$$

where s_u and τ_u are the values of s and τ, respectively, at the uppermost intersection of the equilibrium free-surface and the container wall,

$$Z(s_u) = Y(\tau_u) \quad , \quad R(s_u) = X(\tau_u)\,.$$

If there is sufficient liquid to cover the container bottom, then the intersection at $s = s_u$ and $\tau = \tau_u$ is the only one, and the initial end condition is the symmetry condition about the axis of revolution, namely

$$Z_s = 0 \quad \text{at} \quad s = 0\,. \tag{26b}$$

If there is insufficient liquid to cover the bottom, then there is another (lower) circle of intersection at $s = 0$ and $\tau = \tau_\ell$, and the initial end condition is (26a) at $s = 0$ and $\tau = \tau_\ell$ as well. (Recall that s is zero at the lowest point on the equilibrium free-surface -- at the axis $r = 0$ if there is only one circle of intersection; at the lower circle of intersection if there are two.)

The terminal end condition for (25) is derived from the expressions for the unit normals at the intersection of the container wall and the equilibrium free surface, which are

$$\left[\underline{n}_w\right]_{\tau=\tau_u} = -\sin\Theta\,\underline{e}_s + \cos\Theta\,\underline{e}_n$$

and

$$\left[\underline{n}_H\right]_{\substack{s=s_u \\ \eta=0}} = \underline{e}_n \ ,$$

respectively. The unit tangent to the container wall at the intersection in the direction of increasing τ is also required; it is

$$\left[\underline{e}_\tau\right]_{\tau=\tau_u} = \cos\Theta\,\underline{e}_s + \sin\Theta\,\underline{e}_n \ .$$

At the intersection of a meridian of the perturbed free surface $\eta = H(s,\theta;t)$ with the container wall let the values of s, η, and τ be denoted by s_1, η_1, and τ_1. Then if χ denotes the angle from $\underline{e}_r$ to $\underline{e}_\tau$ (alternately from $\underline{k}$ to $\underline{n}_w$) so that

$$\frac{d\underline{n}_w}{d\tau} = -\frac{d\chi}{d\tau}\,\underline{e}_\tau \ ,$$

then the linearized expression for the wall normal is

$$\left[\underline{n}_w\right]_{\tau=\tau_1} = \left[\underline{n}_w - (\tau_1-\tau_u)\,\frac{d\chi}{d\tau}\,\underline{e}_\tau\right]_{\tau=\tau_u}$$

to first order. Similarly, since

$$\frac{d\underline{e}_n}{ds} = -\frac{d\psi}{ds}\,\underline{e}_s \ ,$$

one obtains for the surface normal

$$\left[\underline{n}_H\right]_{\substack{s=s_1 \\ \eta=\eta_1}} = \left[\underline{n}_H\right]_{\substack{s=s_u \\ \eta=\eta_1}} - \left[(s_1-s_u)\,\frac{d\psi}{ds}\,\underline{e}_s\right]_{\substack{s=s_u \\ \eta=0}}$$

to first order. This latter expression becomes

$$\left[\underline{n}_H\right]_{\substack{s=s_1 \\ \eta=\eta_1}} = \left[- H_s \underline{e}_s - \frac{H_\theta}{R}\,\underline{e}_\theta + \underline{e}_n - (s_1 - s_u)\,\frac{d\psi}{ds}\,\underline{e}_s\right]_{\substack{s=s_u \\ \eta=0}}$$

when (19), with $O(H^2)$ terms neglected, is used.

The relationship between (s_1-s_u), $(\tau_1-\tau_u)$, and H can be observed from a curvilinear triangle obtained when the perturbed surface lies "above" the equilibrium free surface, by extending the equilibrium free surface beyond the intersection with the container wall (see Figure 2). In the triangle with vertices at

$$[s_u,0] = (X(\tau_u),\ Y(\tau_u)) ,$$

$$[s_1,0] , \quad \text{and}$$

$$[s_1,\eta_1] = (X(\tau_1),\ Y(\tau_1)) ,$$

the angle at $[s_u,0]$ is Θ, the angle at $[s_1,0]$ is right, and the lengths of the sides are $s_1 - s_u$, $H(s_1,\theta)$, and $\tau_1 - \tau_u$. Hence, to first order

$$s_1 - s_u = H \cot\Theta$$

and

$$\tau_1 - \tau_u = H/\sin\Theta .$$

By substitution into the requirement that

$$\cos\Theta = \left[\underline{n}_H \cdot \underline{n}_w\right]_{\tau=\tau_1}$$

one then obtains the desired linearized terminal contact angle condition

$$H_s \sin\Theta + \left(\frac{d\psi}{ds}\cos\Theta - \frac{d\chi}{d\tau}\right) H = 0 \qquad (27a)$$

at $s = s_u$, $\eta = 0$.

When there is insufficient liquid to cover the tank bottom, then the initial contact angle condition required at the lower circle of intersection is similarly found to be

$$H_s \sin\Theta - \left(\frac{d\psi}{ds}\cos\Theta - \frac{d\chi}{d\tau}\right) H = 0 \qquad (27b)$$

at $s = 0$, $\eta = 0$.

Finally, the linearized kinematic condition (22) is

$$H_t = \Phi_\eta = \frac{\partial\Phi}{\partial n} \text{ on } \eta = 0 \ . \qquad (28)$$

The task, then, is to solve the linear boundary value problem (7), (8), (25), (27), and (28), where the equilibrium free-surface is defined by (24), (26), and the given volume of liquid. In the foregoing, it is assumed that $B_\alpha \geq 0$; negative values of B_α are not considered in this study.

The Eigenvalue (Normal Mode) Problem

The linear boundary value problem posed above is inhomogeneous because of the transverse perturbing acceleration proportional to B_{tr} in (25). The solution can be obtained in two parts. The problem is first made homogeneous by setting B_{tr} to zero and solving the normal mode problem. The result is a set of eigenfunctions that may then be used in a Fourier series expansion to obtain the response to the transverse perturbing acceleration.

Normal Modes. Let the periodic time dependence and the angular dependence of Φ and H for the kth normal mode be

$$\Phi = \Phi_k(r,z)\cos\theta\cos(\omega_k t)$$
$$H = H_k(s)\cos\theta\sin(\omega_k t)\ . \tag{29}$$

The θ dependence chosen in (29) corresponds to the modes having one diametral node excited by the lateral perturbing acceleration $B_{tr}\cos\theta$. Substituting (29) into (25) with $B_{tr} = 0$ and into (28) gives

$$\left.\begin{aligned}(1 + B_\alpha)\,\omega_k\Phi_k - B_\alpha R_s H_k + \frac{1}{R}\left(RH_{k_s}\right)_s - \frac{1}{R^2}H_k \\ + \left[(Z_{ss}R_s - Z_s R_{ss})^2 + \left(\frac{Z_s}{R}\right)^2\right]H_k = 0\end{aligned}\right\}\ \text{on}\ \eta = 0\ . \tag{30}$$

and

$$\left.\omega_k H_k(s) = \Phi_{k_n}(r,z) = \Phi_{k_n}(s,0) = \Phi_{k_\eta}(s,0)\right\}$$

The boundary conditions on H_k and Φ_k are the one on H in (27) and

$$\Phi_{k_n} = 0 \quad \text{on} \quad w\ ; \tag{31}$$

and also, $\Phi_k(0,z) = 0$ and $H_k(0) = 0$,

if the liquid covers the container bottom. Solution of this problem yields a set of eigenfunctions $\{\Phi_k\}$, eigenvalues $\{\omega_k{}^2\}$, and eigenmodes $\{H_k\}$.

Response to Perturbing Accelerations. For a sinusoidal perturbation of amplitude $\hat{B}_{tr}$,

$$B_{tr} = \hat{B}_{tr}\sin(\omega_o t)\ ,$$

the velocity potential of the perturbed motion can be represented as a Fourier series

$$\Phi = \cos\theta\cos(\omega_o t)\sum_k A_k\Phi_k(r,z)\ , \tag{32}$$

where the solution to the normal mode problem, $\Phi_k(r,z)$, satisfies (30) and (31), but not (25) and (28). Inserting the series into (25) and (28), the free-surface and kinematic boundary conditions for the perturbed motion, and combining the results lead to

$$(1 + B_\alpha) \sum_k (\omega_k^2 - \omega_o^2) A_k \Phi_k = \hat{B}_{tr} \omega_o R$$

on the equilibrium free-surface, $r = R(s)$ and $z = Z(s)$. Now, R can be expressed as an expression in the Φ_k evaluated on $r = R(s)$ and $z = Z(s)$,

$$R = \sum_k D_k \Phi_k [R(s), Z(s)] . \tag{33}$$

It can be shown that the Φ_k's and the corresponding H_k's form a biorthogonal set with the orthogonality condition,

$$\int_o^{s_u} \Phi_k H_m R \, ds \begin{cases} = 0 & \text{for } k \neq m , \\ \neq 0 & \text{for } k = m , \end{cases}$$

where s_u is the length of a meridian of the equilibrium free-surface, measured from the axis when there is a single circle of intersection and from the lower circle when there are two. Consequently, the expression for the Fourier coefficients in (33) take the form

$$D_k = \frac{\int_o^{s_u} H_k R^2 \, ds}{\int_o^{s_u} \Phi_k H_k R \, ds} . \tag{34}$$

Thus, for sinusoidal excitation, the coefficient A_k in (32) is

$$A_k = \frac{1}{(1 + B_\alpha)} \frac{\hat{B}_{tr} D_k \omega_o}{\omega_k^2 - \omega_o^2} \tag{35}$$

and the velocity potential for the sinusoidally perturbed motion becomes

$$\Phi = \frac{\hat{B}_{tr} \cos\theta \cos(\omega_o t)}{1 + B_\alpha} \sum_k \frac{D_k \omega_o}{\omega_k^2 - \omega_o^2} \Phi_k(r,z) \ . \qquad (36)$$

The procedure for obtaining the solution for any periodic perturbation that possesses a Fourier series expansion of the form

$$B_{tr} = \hat{B}_{tr} \sum_m C_m \sin(m\omega_o t)$$

is similar. The solution is

$$\Phi = \cos\theta \sum_k \Phi_k(r,z) \sum_m A_k^{(m)} \cos(m\omega_o t) \ , \qquad (37)$$

where

$$A_k^{(m)} = \frac{D_k \hat{B}_{tr}}{(1 + B_\alpha)} \frac{m C_m \omega_o}{\omega_k^2 - m^2\omega_o^2} \ .$$

Particular perturbations of interest are the square wave and the periodic pulsing accelerations, for which the Fourier coefficients are

$$C_m = \begin{cases} 0 \ , & m \ \text{even} \\ \dfrac{4}{m\pi} \ , & m \ \text{odd} \end{cases} \qquad \text{for the square wave}$$

and

$$C_m = \begin{cases} 0 \ , & m \ \text{even} \\ \dfrac{4}{m\pi} (-1)^{\frac{m-1}{2}} \sin\dfrac{m\delta\pi}{2} \ , & m \ \text{odd} \end{cases} \qquad \text{for the periodic pulse ,}$$

where δ is the ratio of Δt, the perturbing pulse width, to $\frac{1}{2} T = \pi/\omega_o$, half its period (see Figure 3).

The explicit expressions for the normal surface displacement at the wall, the item of principal interest, are then found from (28). They are

$$H]_{\substack{\theta=0 \\ s=s_u}} = \frac{\hat{B}_{tr}}{1 + B_\alpha} \sin\omega_o t \sum_{k=1}^{\infty} \frac{D_k}{\omega_k^2 - \omega_o^2} \Phi_{k_n}]_{\substack{z=Z(s_u) \\ r=R(s_u)}} \quad \text{for sinusoidal,} \tag{38}$$

$$H]_{\substack{\theta=0 \\ s=s_u}} = \frac{\hat{B}_{tr}}{1 + B_\alpha} \frac{4}{\pi} \sum_{k=1}^{\infty} D_k \Big[\sum_{\substack{m=1 \\ m \text{ odd}}}^{\infty} \frac{\sin(m\omega_o t)}{m(\omega_k^2 - m^2\omega_o^2)} \Big] \Phi_{k_n}]_{\substack{z=Z(s_u) \\ r=R(s_u)}} \quad \text{for square wave,} \tag{39}$$

and

$$H]_{\substack{\theta=0 \\ s=s_u}} = \frac{\hat{B}_{tr}}{1 + B_\alpha} \frac{4}{\pi} \sum_{k=1}^{\infty} D_k \Big[\sum_{\substack{m=1 \\ m \text{ odd}}}^{\infty} \frac{(-1)^{\frac{m-1}{2}} \sin\frac{m\delta\pi}{2} \sin(m\omega_o t)}{m(\omega_k^2 - m^2\omega_o^2)} \Big] \Phi_{k_n}]_{\substack{z=Z(s_u) \\ r=R(s_u)}} \tag{40}$$

for periodic pulse perturbations.

Mechanical Analogue. For practical design applications it is convenient to express each sloshing mode in terms of the fundamental mode of an equivalent spring-mass mechanical analogue. To calculate the parameters of this analogue it is necessary to obtain expressions for the lateral force and moment acting on the container wall, which, in turn, can be found from the pressure. The pressure at the wall is

$$p = \begin{cases} p_g - \lambda - B_\alpha Z - (1+B_\alpha)\Phi_t , & \text{in the liquid} \\ p_g , & \text{in the gas} , \end{cases} \tag{41}$$

where the first expression is the linearized form of the Bernoulli equation (9). When there is sufficient fluid to cover the container bottom, the lateral force on the wall is given by the integral

$$F_x = \int_0^{2\pi} \int_0^{\tau_L} p \sin\chi \cos\theta \, X d\tau \, d\theta .$$

This integral, which is taken over the entire container wall, becomes, upon substituting (41) and discarding terms of higher than first order,

$$F_x = \int_o^{2\pi} \int_o^{\tau_L} p_g \sin\chi \cos\theta \, X d\tau \, d\theta$$

$$- \int_o^{2\pi} \int_o^{\tau_u + H_u \csc\Theta} (\lambda + B_\alpha Z) \sin\chi \cos\theta \, X d\tau \, d\theta$$

$$- (1+B_\alpha) \int_o^{2\pi} \int_o^{\tau_u} \Phi_t \sin\chi \cos\theta \, X d\tau \, d\theta$$

The θ integration yields zero for the first integral and for the part of the second between the limits 0 and τ_u. Thus

$$F_x = - (\lambda + B_\alpha Z_u) \sin\chi_u X_u \csc\Theta \int_o^{2\pi} H_u \cos\theta \, d\theta$$

$$- (1 + B_\alpha) \int_o^{2\pi} \int_o^{\tau_u} \Phi_t \sin\chi \cos\theta \, X d\tau \, d\theta \, .$$

For the kth normal mode one obtains, after substituting (29) and the second of (30),

$$F_{x_k} = \pi \left[-(\lambda + B_\alpha Z_u) \sin\chi_u X_u \csc\Theta + \frac{\omega_k^2 (1+B_\alpha)}{\Phi_{k_{nu}}} \int_o^{\tau_u} \Phi_k \sin\chi X d\tau \right] H_{ku} \sin(\omega_k t) \, . \qquad (42)$$

The moment of the lateral force is given by the integral

$$M_y = - \int_o^{2\pi} \int_o^{\tau_L} pX \cos\theta \, (Y \sin\chi + X \cos\chi) \, d\tau \, d\theta$$

which becomes simply

$$M_y = - \left(1 - \frac{1}{b^2}\right) \int_o^{2\pi} \int_o^{\tau_L} pXY \cos\theta \sin\chi \, d\tau \, d\theta$$

for the spheroidal tank with origin at the tank center (Figure 1a),

$$X \cos\chi = - \frac{1}{b^2} Y \sin\chi \ .$$

Using the same technique as above, one obtains in general

$$M_y = (1 - \frac{1}{b^2}) \left[(\lambda + B_\alpha Z_u) \sin\chi_u X_u Y_u \csc\Theta \int_o^{2\pi} H_u \cos\theta \, d\theta \right.$$

$$\left. + (1+B_\alpha) \int_o^{2\pi} \int_o^{\tau_u} Y \Phi_t \sin\chi \cos\theta \, X d\tau \, d\theta \right] ,$$

and for the kth normal mode

$$M_{y_k} = \pi(1-\frac{1}{b^2}) \left[(\lambda + B_\alpha Z_u) \sin\chi_u X_u Y_u \csc\Theta - \frac{\omega_k^2 (1+B_\alpha)}{\Phi_{k_{nu}}} \int_o^{\tau_u} \Phi_k \sin\chi \, XY d\tau \right] H_{ku} \sin(\omega_k t). \tag{43}$$

For the case when there is not sufficient liquid to cover the container bottom, the same procedure yields the expressions

$$F_{x_k} = \pi \left[-(\lambda + B_\alpha Z_\ell) \sin\chi_\ell X_\ell \csc\Theta \frac{H_{k\ell}}{H_{ku}} - (\lambda + B_\alpha Z_u) \sin\chi_u X_u \csc\Theta \right.$$

$$\left. + \frac{\omega_k^2 (1+B_\alpha)}{\Phi_{k_{nu}}} \int_{\tau_\ell}^{\tau_u} \Phi_k \sin\chi X d\tau \right] H_{ku} \sin(\omega_k t) , \tag{44}$$

and

$$M_{y_k} = \pi(1 - \frac{1}{b^2}) \left[(\lambda + B_\alpha Z_\ell) \sin\chi_\ell X_\ell Y_\ell \csc\Theta \frac{H_{k\ell}}{H_{ku}} + (\lambda + B_\alpha Z_u) \sin\chi_u X_u Y_u \csc\Theta \right.$$

$$\left. - \frac{\omega_k^2 (1+B_\alpha)}{\Phi_{k_{nu}}} \int_{\tau_\ell}^{\tau_u} \Phi_k \sin\chi XY d\tau \right] H_{ku} \sin(\omega_k t) \ . \tag{45}$$

The point of action z_k on the container axis of the single force to which the mechanical analogue is made equivalent is then the ratio

$$z_k = M_{y_k}/F_{x_k} , \tag{46}$$

where z_k is measured from the center of the tank. Because the amplitude of the force imposed by a spring-mass oscillator, which is made equal to the amplitude of F_{x_k}, is $\varkappa_k \hat{x}$, and the amplitude of the energy is $\varkappa_k \hat{x}^2/2$, the spring constant of the analogue must be

$$\varkappa_k = F_{x_k}^2/2V_k , \tag{47}$$

where V_k is the amplitude of the energy of the kth mode of the liquid,

$$V_k = \frac{\pi}{2}(1+B_\alpha)\int_o^{s_u} \Phi_k \frac{\partial \Phi_k}{\partial n} R\, ds . \tag{48}$$

For the mechanical analogue to have the fundamental frequency ω_k, its mass must therefore be

$$\mathcal{M}_k = \varkappa_k/\omega_k^2 . \tag{49}$$

NUMERICAL ANALYSIS

The common angular variation of the velocity potential and normal displacement for the kth normal mode is explicitly exhibited by the factor $\cos\theta$ in (29) and (30). Consequently, the domain in which the eigenvalue problem developed in the preceding section must be solved can be taken as a radial section of the liquid within the tank in the plane perpendicular to the single diametral node. When the volume of liquid is large enough to insure that the bottom is completely covered, the radial section is bounded by the axis of revolution, the meridian of the tank, and the meridian of the free-surface (Figure 1a). When the bottom is uncovered, the radial section is a lunar region between the meridians of the free-surface and the tank (Figure 1b).

Throughout this section of the report, when no confusion will result, the subscript k attached to H and Φ will be suppressed to simplify the notation. By using the relation (30), written as

$$\omega H(s) = \Phi_n(r,z) = \Phi_n(s,0) \ ,$$

the eigenvalue problem can be reformulated in terms of the kth velocity potential and its normal derivative on the equilibrium free-surface. For the bottom covered case the complete restatement follows. The velocity potential satisfies

$$-\left(\Phi_{rr} + \frac{1}{r}\Phi_r + \Phi_{zz}\right) + \frac{1}{r^2}\Phi = 0 \qquad (50)$$

within the liquid subject to the boundary conditions

$$\Phi(0,z) = 0 \qquad (51)$$

along the axis within the liquid,

$$\Phi_n = 0 \tag{52}$$

on the wetted tank meridian, and

$$-\frac{1}{R}\left(R\left[\Phi_n\right]_s\right)_s + \left\{B_\alpha R_s + \frac{1}{R^2} - \left[(Z_{ss}R_s - Z_s R_{ss})^2 + \left(\frac{Z_s}{R}\right)^2\right]\right\}\Phi_n = (1+B_\alpha)\,\omega^2\,\Phi \tag{53}$$

on the equilibrium free-surface. The free-surface boundary condition (53) is subject to the end conditions

$$\left[\Phi_n\right]_s \sin\Theta + \left(\frac{d\psi}{ds}\cos\Theta - \frac{d\chi}{d\tau}\right)\Phi_n = 0 \tag{54}$$

at the intersection between the free-surface and tank meridians ($s = s_u$, $\eta = 0$) and

$$\Phi_n = 0 \tag{55}$$

at the intersection of the free-surface with the axis ($s = 0$). The meridian of the equilibrium free-surface is the solution to the differential equation,

$$\left[(Z_{ss}R_s - Z_s R_{ss}) + \frac{Z_s}{R}\right] - B_\alpha Z - \lambda = 0 \tag{56}$$

subject to the boundary conditions

$$\cos\Theta = Y_\tau Z_s + X_\tau R_s\Big]_{\substack{s=s_u \\ \tau=\tau_u}} \tag{57}$$

and

$$Z_s = 0 \tag{58}$$

at $s = 0$, that when rotated about the axis encloses a given volume of liquid within the spheroid.

When the fluid volume is so small that the bottom is uncovered, the axial boundary condition (51) disappears. The end condition (55) for the free-surface boundary condition is replaced by the constant contact angle condition

$$\left[\Phi_n\right]_s \sin\Theta - \left(\frac{d\Psi}{ds}\cos\Theta - \frac{\partial X}{d\tau}\right)\Phi_n = 0 \qquad (59)$$

at $s = 0$, $\eta = 0$, the lower intersection between the free-surface and tank meridians. Finally the constant contact angle condition

$$\cos\Theta = Y_\tau Z_s + X_\tau R_s\Big]_{\substack{s=0 \\ \tau=\tau_\ell}} \qquad (60)$$

replaces the symmetry boundary condition (58) for the equilibrium free-surface.

The computation of the eigenvalues, ω^2, the eigenfunctions, Φ, and the eigenmodes, H, falls into three major tasks:

- Determination of the meniscus shapes defining the domains filled by given volumes of liquid.
- Development of irregular triangular meshes within the radial sections of the liquid such that the finite difference approximations to the eigenvalue problems are symmetric.
- Solution of the approximate eigenvalue problems.

Finally, finite Fourier analyses in terms of the approximate eigensystems yield, almost immediately, predictions of the shape of the forced response of the liquid to lateral perturbing accelerations. Moreover, the values needed to set up an equivalent spring-mass mechanical analog ((44) through (49)) are an easy by-product of the computation. Each of the major tasks as well as the subsidiary calculations will be discussed in turn.

Computation of Meniscus Shapes

The Initial Value Problems. Combining the differential equation for the meridian of the equilibrium free-surface (56) with the relation

$$R_s R_{ss} + Z_s Z_{ss} = 0$$

derived from

$$R_s^2 + Z_s^2 = 1$$

(s is arc length) yields a 2 x 2 system with the solution

$$R_{ss} = - CZ_s \quad \text{and} \quad Z_{ss} = CR_s$$

where

$$C = B_\alpha Z + \lambda - Z_s/R = d\psi/ds \tag{61}$$

is the curvature of the meridian. Consequently, (56) is equivalent to the redundant first order system

$$\begin{aligned} Z_s &= W \\ W_s &= CU \\ U_s &= - CW \\ R_s &= U \\ U^2+W^2 &= 1 \end{aligned} \tag{62}$$

in which U and W are the r and z velocity components of a point moving with unit velocity along a curve with the function C (61) as curvature. When C is positive, the curve curls to the left as s increases.

Because only the tangent vectors are involved in the boundary condition (57), the difference between the z-data of the free-surface and the tank may be absorbed in the function $z = Y(\tau)$. Thus the tank may be permitted to slide

up and down the axis of symmetry relative to the surface. A convenient z-datum for the equilibrium free-surface when the bottom is covered is

$$Z(0) = 0 \ . \tag{63}$$

The conditions

$$R(0) = 0, \quad U(0) = 1, \quad \text{and} \quad W(0) = 0 \tag{64}$$

then follow from the boundary condition (58).

On the solution to the initial value problem (62), (63) and (64), there is at least one point (there may be three) at which the boundary condition (57) holds. Let the tank be translated so that the meridian passes through such a point. If the segment of the solution up to a point where (57) holds lies entirely within the tank, then the two-point boundary value problem (62), subject to (57) and (58) with λ to be determined so that the volume has a given value V, may be replaced by the problem of choosing λ so that the rotation of the segment of the solution of (62), (63), and (64) between the origin and a point where (57) holds encloses a given volume V.

To obtain an analogous reformulation in terms of an initial value problem when the bottom of the tank is dry, it is convenient to choose the z-datum for the tank so that the equation of the tank meridian is

$$X^2 + Y^2/b^2 = 1 \ . \tag{65}$$

Choose an initial point

$$R(0) = R_\ell = X(\tau_\ell) \quad \text{and} \quad Z(0) = Z_\ell = Y(\tau_\ell) \tag{66}$$

on the lower branch of (65). Re-expressing the contact angle condition (60) in the form $\psi = \chi - \Theta$ yields

$$U(0) = R_s(0) = \left[X_\tau \cos\Theta + Y_\tau \sin\Theta\right]_{\tau=\tau_\ell}$$

and (67)

$$W(0) = Z_s(0) = \left[Y_\tau \cos\Theta - X_\tau \sin\Theta\right]_{\tau=\tau_\ell}$$

as the other initial conditions needed to define a solution of (62) as an initial value problem.

In the family of solutions to the initial value problem (62) starting from (66) and (67) and characterized by positive values of λ, there is one for which the boundary condition (57) holds at the first intersection with the ellipse (65). Thus the two-point boundary value problem (62) subject to the conditions (57) and (60) with λ chosen so that the volume has a given value V may be replaced by the problem of choosing λ and either R_ℓ or Z_ℓ so that the volume enclosed by the rotation of the segment of the solution of (62), (66), and (67) between (R_ℓ, Z_ℓ) and the point where (57) holds encloses a given volume V.

Qualitative Behavior of the Solutions. In two special cases the solution to (62) subject to the initial conditions (63) and (64) can be written down.

For $\lambda = 0$, the solution is the straight line $Z \equiv 0$, for all B_α, because $C(0) = 0$ implies $C \equiv 0$. Clearly the tank can be positioned so that a horizontal plane makes the required contact angle.

From (61), it follows that

$$R_\psi = \cos\psi/C \quad \text{and} \quad Z_\psi = \sin\psi/C \tag{68}$$

are an alternate form for (56) or (62). For $B_\alpha = 0$, the circle

$$R(\psi) = (2\sin\psi)/\lambda \quad \text{and} \quad Z(\psi) = 2(1-\cos\psi)/\lambda \tag{69}$$

with radius $2/|\lambda|$ and centered at $(R = 0, Z = 2/\lambda)$ satisfies (68). The curvature of the meridian is the constant $C = \lambda/2$. An easy geometric construction shows that the contact angle condition determines the radius and hence λ. Thus for $B_\alpha = 0$, the equilibrium free-surface is a part of a sphere so long as the circle (69) intersects the elliptical cross section of the spheroid in two and only two points. For the spherical tank this is the case for any volume; and the planar solution is the limit of the spherical solutions as λ approaches zero.

For $B_\alpha > 0$, it can be shown that $C = d\psi/ds$ is a positive and monotone increasing function of s for $0 \leq \psi \leq \pi$. Thus from (68) it is apparent that for $\lambda > 0$ the solution starting from $\psi = 0$ (see (64)) lies in the first quadrant. Moreover, the R coordinate increases with s to a local maximum at $\psi = \pi/2$ and then decreases. The Z coordinate increases with s to a local maximum at $\psi = \pi$. Because the curvature C is monotonically increasing, (62) implies that the solution curls more and more tightly to the left. In fact beyond $\psi = \pi$, it curls so rapidly that it never crosses the axis again but becomes globally a spiral in the first quadrant. See Bakker[14] for such curves.

Only in the limiting case, $B_\alpha = 0$, when the solution is a sphere with constant curvature, does the solution ever return to the axis again as s increases. For $B_\alpha > 0$, the denominator of the term Z_s/R prevents the curve from crossing the axis.

For all sufficiently large λ, the solution to (62) or (68) starting from (63) and (64) is so tightly curled in the interval $0 \leq \psi \leq \pi$ that

$$R(\pi) < 2b$$

holds. For such cases the tank may slide along the common axis of symmetry so that the upper branch of its cross section is tangent to the solution near $\psi = \pi$. Lowering the cross section slightly will produce a position in

which the contact angle condition holds when Θ is small. Decreasing λ will uncurl the solution, raise the point at which the contact angle condition holds, and decrease the volume enclosed between the meniscus and the tank. Thus for large λ, volume is a decreasing function of λ. Unfortunately there may be, for a fixed λ, several points on the solution to (62), (63), and (64) that both satisfy the contact angle condition and the condition that the solution lie entirely within the tank. Consequently, volume V is a multivalued function of λ. However, λ is single valued as a function of V.

Applying the uncurling argument to the two-circle case shows that through each initial point (R_ℓ, Z_ℓ) there is at least one solution to (62), (66), and (67) that satisfies the contact angle condition. What is not clear is whether there may be more than one.

The One Circle Algorithm

The Basic Procedure. For a fixed Bond number, the meridian of a meniscus that has a single circle of intersection with the tank is determined by specifying $\lambda/2$, the curvature at the axis of symmetry when the initial point of the meridian is the origin. The shape of a spheroidal tank with equatorial semi-axis unity is specified by the eccentricity e of its polar cross section or by its polar semi-axis $b = (1 - e^2)^{1/2}$. Testing is facilitated by fixing the center of the tank at $(0,0,b)$ so that its cross section in the plane of the meniscus meridian is the ellipse

$$r^2 + ((z-b)/b)^2 = 1 \tag{70}$$

that passes through the origin and is tangent to the meniscus meridian there.

At each step in the numerical integration of (62), the basic procedure is to slide the tank cross section down along the axis of symmetry, common to the ellipse and the meniscus meridian, until the former passes through the point just generated on the latter. With the ellipse so positioned there are two questions to be resolved.

(1) Does the meridian so far developed lie entirely within the ellipse?

(2) Could the contact angle condition be satisfied within the integration step just completed?

If both answers are affirmative, the basic procedure concludes by cubic inverse interpolation for the value of s at which the contact angle condition holds and by calculating the cosine of the contact angle achieved, the volume V included between the adjusted meniscus and the tank, and the derivative $dV/d\lambda$.

Testing for Inclusion. Were the meridian of a meniscus to intersect the tank at its equator and to satisfy the contact angle condition there, $R_s = \cos\psi = \sin\Theta$ would hold. So long as

$$R_s > \sin\Theta \tag{71}$$

holds, an intersection between the two meridians (tank and meniscus) at which the contact angle condition holds must lie on the lower branch of the ellipse. When (71) fails, a satisfactory intersection must lie on the upper branch.

In the latter case, the algorithm computes the distance

$$Q = z - Z = b(1 + [1-R^2]^{1/2}) - Z \tag{72}$$

along the line $r = R$ between the terminal point of the meniscus (R,Z) and the upper branch of the fixed ellipse (70). A negative Q shows that the meniscus meridian has escaped from the fixed ellipse and is an indication that the integration should be terminated. If the curvature $\lambda/2$ of the meniscus exceeds the curvature of the ellipse at the origin, a nonnegative Q suffices to guarantee that the entire meniscus lies within the ellipse. This has been the case for all menisci with satisfactory intersections on the upper branch within the range of eccentricities, Bond numbers, and volumes considered in this report. Consequently, detailed checking for inclusion

along the upper branch has not been included in the present version of the algorithm.

For intersections along the lower branch of the ellipse, where (71) holds, the situation is more complicated. The algorithm computes the distance

$$P = z - Z = b(1 - [1-R^2]^{1/2}) - Z$$

along the line $r = R$ between the terminal point of the meniscus and the lower branch of the fixed ellipse (70) and maintains a maximum of the values of P previously computed, namely

$$P_m = \max_{[0,s-\Delta s]} [P]$$

for a positive Δs less than the length of the last integration step. Because $P = 0$ at $s = 0$, $P_m \geq 0$.

If

$$P \leq P_m \tag{73}$$

holds, then translating the fixed ellipse downward through a distance P will still leave the meniscus point at which P_m was attained on or below the tank meridian. Thus when (73) occurs, the algorithm ceases testing and returns to the meniscus integration.

If

$$P > P_m \tag{74}$$

holds, then translating the fixed ellipse downward through a distance P will put all previously computed meniscus points above the translated tank meridian. Provided the mesh spacing is small enough,

$$dP/ds = \cos\psi(\tan\chi - \tan\psi)$$

will be positive throughout an integration interval that contains a point s at which the contact angle condition is satisfied because the inequality $\chi > \psi$ must hold not only at s but also in a neighborhood thereof. Consequently, P evaluated at s will also exceed P_m. Thus with small mesh intervals it suffices to check (74) at the end of an integration step.

Testing the Contact Angle Condition. Four functions derived from the relations

$$\chi = \psi + \Theta \quad \text{and} \quad \psi = \chi - \Theta \tag{75}$$

by taking sines and cosines are used to test for the satisfaction of the contact angle condition. For example, a point s at which

$$F_1(s) = \sin\chi - (\sin\psi \cos\Theta + \cos\psi \sin\Theta)$$

or

$$F_1(s) = Y_\tau - (R_s \sin\Theta + Z_s \cos\Theta)$$

has a zero is a point at which the contact angle condition (75) is satisfied. It is an appropriate test function to use when

$$dF_1/ds = X_\tau \, d\tau/ds$$

is large so that the change of sign of F_1 between the ends of an integration interval is easily detected numerically. So long as small puddles are not in consideration, F_1 may be used when $1 > R_s > 2^{-1/2}$ holds. There are two principles for choice among F_1 and its three analogues. First, the derivative must be large; second, difficulty in evaluating the function up to the final subtraction must be avoided. Each test function derived from the relation $\Theta = \chi - \psi$ violates one of these two principles.

Because the sine is monotone increasing in $[0,\pi/2]$, the inequality

$$Y_\tau = \sin\chi > \sin\psi = Z_s \tag{76}$$

is equivalent to the inequality

$$\chi > \psi$$

derived from (75). These inequalities hold not only at the point where the contact angle condition is satisfied but also in a full neighborhood of such a point. Provided that the integration intervals are so small that a computed meniscus point terminating an interval within which the contact angle condition is satisfied is within the neighborhood in which (76) holds, it is safe to use the failure of (76) as a criterion for discontinuing the testing procedure. (Practical experience shows that this is safe except near the equator, for example, when R, Y_τ, and Z_s all exceed .99.) The basic procedure can be visualized by sliding the tank up and down along the axis of symmetry, common to the tank and the meniscus, until the tank meridian passes through the current terminal point of the meridian.

The Strategy. When, for a fixed tank and Bond number, the detail of the relation between λ and V, the volume enclosed by the meniscus, is still not determined, the basic procedure may be used to survey all possible points on the meridian at which the contact angle condition holds. For such a survey the numerical integration continues until the meridian satisfies one of three conditions that guarantee no further points at which the contact angle holds:

(1) The current terminal point lies beyond the line $R = 1$.

(2) The distance Q (72) has become negative.

(3) The meridian has passed beyond the point where it has a second horizontal tangent, $\psi \geq \pi$.

By carrying out such a survey for a suitable set of λ, enough points on the curve representing λ as a function of V can be determined to permit iterating toward the λ which correspond to a given set of V via secant interpolation. When λ is so close to the value corresponding to a given

V that, in a neighborhood of the goal, V is a single valued function of λ and $|dV/d\lambda|$ is neither too large nor too small, convergence is speeded by choosing the next value of λ via Newtonian extrapolation.

Very near the equator, λ as a function of V resembles an extremely flat parabola and large changes in volume correspond to very small changes in λ. Consequently, determining menisci which end near the equator is numerically difficult. Nevertheless, the strategy described above, occasionally refined by using double precision arithmetic and extremely fine mesh spacing, with some human intervention, successfully determined 195 of the 196 menisci attempted in the survey reported here.

The Two Circle Algorithm

Here it is convenient to fix the elliptical tank cross section in the position of (70). The starting point (66) for the meniscus meridian on the lower branch of the ellipse may be specified by giving either $R_\ell = X(\tau_\ell)$ or $Z_\ell = Y(\tau_\ell)$. Choosing the latter as parameter leads to simpler derivatives to evaluate; however, this may not be the best choice. The contact angle prescribes the initial direction of the curve via (67). To complete the specification of the putative meridian, a guess for the value of λ is needed.

The initial points on the meridian are computed from the power series expansion of R and Z as functions of s, λ, and Z_ℓ about the initial point. The numerical integration is then straightforward and is continued until the vertical distance Q (72) between the solution and the fixed ellipse turns negative. The point at which the putative meridian crosses the ellipse is determined by inverse cubic interpolation. The cosine of the contact angle achieved, the volume enclosed between the meridian and the tank, and the derivatives needed for the various alternative improvement schemes are also computed.

The most desirable of the alternates is to improve the guess for Z_ℓ and λ by a two-dimensional Newtonian iteration scheme with the goal of simultaneously

satisfying the contact angle condition and the requirement that the volume have a prescribed value. Sometimes it worked. More often it diverged, but in so doing frequently gave information about the volume and contact angle at nearby starting points. Another alternate, which proved useful when the contact angle was far from being satisfied, is to fix Z_ℓ and to improve λ until the approximation to the contact angle condition is satisfactory and then to try the Newtonian iteration again.

From the experiments in attempting to develop a systematic way for choosing starting values, enough information was gained about the relation between λ and Z_ℓ for each of the thirteen two-circle cases in the survey to permit the computation of meniscus shapes of comparable accuracy to those produced automatically for the one-circle cases.

Were there a reason to construct a good two-circle algorithm, it would seem that a combination of the second alternate with the secant interpolation used for the one-circle case followed by a two-dimensional Newtonian iteration when the volume was well bracketed might succeed.

Variable Mesh Spacing

In the one-circle case the mesh spacing along the free-surface near the axis need not be fine. However, when the surface is highly curved, fine mesh spacing is needed near the tank wall to represent the surface accurately. Moreover, by making it possible to pack mesh triangles into long thin regions, finer mesh near the tank wall has helped produce satisfactory irregular triangular meshes.

The penalty term in the discretization error for using unequal mesh spacing is proportional to the difference in lengths between adjacent intervals. Thus meshes with intervals in a geometric progression minimize the penalty and allow a wider mesh spacing at one end of a mesh than at the other without materially increasing the number of points or incurring an unusually large discretization error at any point.

It is a simple exercise to verify that the Lagrangian interpolation coefficients on such a mesh can be expressed in terms of the constant ratio between adjacent intervals and the length of one of the intervals, say the first. The Adams integration methods can be obtained by integrating a Lagrangian interpolation polynomial (with equal mesh spacing) over the first interval in the interpolation for the corrector and over the next interval for the predictor. Consequently, when Adams type integration formulas are derived from a Lagrangian interpolation polynomial on a mesh with intervals in a geometric progression, it turns out that the coefficients are constants times the length of the leading interval. Thus replacing an equal mesh by one in a geometric progression as the basis for an Adams type integration requires the following additional work: a multiplication to form the current mesh length and two extra multiplications per integration step per equation (assuming a single correction), one each for the predictor and corrector sums.

The computation of the constant coefficients for a geometric Adams method is easy, provided that the mesh ratio is near 1, as it should be. Here where order four is used, the computation involves solving two three-by-three systems accurately. Because this computation is so simple, it is relatively easy to change the mesh ratio. To switch from one mesh ratio to another, four recomputations of the geometric Adams coefficients are needed. Such a procedure facilitates the development of the triangular meshes for two-circle cases where it is desirable to pack triangles into the two corners. As to accuracy for the cases at hand the geometric Adams methods are only a little less satisfactory than the ordinary Adams methods.

Mesh Generation

The second major task is the development of a suitable irregular triangular mesh within half an axial cross section of the liquid-filled region. The goal is to obtain a mesh nearly free of obtuse triangles -- none near the free-surface or upper tank wall. In a regular triangular mesh, lay off along a horizontal line the number of mesh points to be used on the equilibrium free-surface; at the left end point draw a line downward to the left; at the

right end point leave just one triangle in the corner and again draw a line downward to the left; finally close the figure by another horizontal line. This parallelogram is the logical diagram; the mesh lines in the interior and on the boundary are mapped into curved lines in the interior and on the boundary of the half cross section of the liquid-filled region (logical into real free-surface) by a numerical algorithm. In addition to the number of mesh points on the free-surface and the number of mesh lines parallel to the free-surface, the mesh spacing along the free-surface may be varied to force more triangles into the corner near the contact angle. The details of the mesh are controlled by prescribing the location of some of the physical images of the logical boundary points. The computing mesh points are the intersections of the curved mesh lines within and on the boundaries of the half cross section.

Figure 4 shows an irregular triangular mesh used in this study. The free-surface and the tank wall, from the axis to the point where only two triangles meet at the wall, correspond to the longer, horizontal sides of the parallelogram; the axis and the remainder of the wall correspond to the slanting sides. The darker lines in the interior are the images of an integral, rectangular coordinate system used to locate vertices in the regular triangular mesh. By mentally distorting the mesh so that all triangles are equilateral, the user can recover a picture of the underlying logical diagram.

The ellipse with eccentricity e and unit major semi-axis

$$r^2 + (z/b)^2 = 1 \tag{77}$$

in the $\zeta = r + iz$ plane is mapped onto the unit circle in the $w = x + iy$ plane with the origin going into the origin and the real axis onto the real axis by the complex function

$$w = k^{1/2} \, sn\left[(2K/\pi) \arcsin(\zeta/e)\right] \tag{78}$$

where k is the modulus and K the real quarter period of the Jacobian elliptic function sn.[15,16,17] The terminology here follows the NBS Handbook of Mathematical Functions....[18] The inverse map

$$\zeta = e \sin\left[(\pi/2K)\int_0^{w/k^{1/2}} ([1-t^2][1-k^2t^2])^{-1/2}\, dt\right] \qquad (79)$$

which carries the unit circle back into the ellipse involves an elliptic integral of the first kind. The evaluations of the elliptic functions and integrals needed to effect (78) and (79) are made by algorithms derived from those of Bulirsch[19] and the computation of the complex inverse sine follows Wynn.[20]

Using (78) to map the meridian of the free-surface

$$\zeta(s) = R(s) + i\, Z(s)$$

into the unit circle produces, from the half cross section of the liquid filled region bounded by a part of an ellipse, a standardized domain bounded by a piece of the unit circle. Figure 5 shows the standardized domain for Figure 4. A triangular mesh is produced within the standardized domain by using an algorithm described by Winslow.[21] The computing mesh (Figure 4) is generated by applying the inverse map (79) to the standardized map (Figure 5).

An obvious advantage of the standardized domains is the ease with which points and distances on the unit circle may be described in terms of a central angle. The decisive advantage is that experience gained in producing a suitable mesh in one standard domain may be immediately applied to the development of meshes within similar standardized domains. Thus meshes developed for spherical tanks, where no mapping is necessary, have frequently served as time-saving models of meshes for spheroidal tanks with moderate eccentricity. Because (79) preserves angles locally but not in the larger scale of the mesh triangles, a mesh that is satisfactory in the standardized domain may not be so

when mapped into the original elliptical domain. The converse may occur. Consequently, the practical procedure is to control the mesh by prescribing the location of some boundary points on the standardized domain and to decide the acceptability of the mesh in terms of the number and location of the obtuse triangles that appear in the final computing mesh.

As an example consider Figure 6, the computing mesh, and Figure 7, the standardized domain, for a typical two-circle case. In the lower tip of Figure 7 there is a cluster of obtuse triangles near the free-surface, marked by "0" at their centroids. These disappear in the computing mesh, Figure 6.

The logical domain for a two-circle case is an isosceles trapezoid built from equilateral triangles with its longer side corresponding to the free-surface. The obtuse triangles that are marked on Figure 6 are associated with the two corners of the trapezoid where only two triangles meet at a boundary point. In Figure 4 there is exactly one such obtuse triangle in a similar location. Further adjusting of the input parameters may remove such triangles. However, experience shows that the expenditure of effort is unwarranted. Improvement comes slowly with change and more objectionable obtuse triangles at the free-surface frequently appear as a consequence of the readjustment.

Figure 6 shows a discernable discontinuity of the mesh spacing along the tank boundary at the equator. Following the broken line parallel to the darker broken lines from the equatorial point on the tank boundary to the free-surface locates the equatorial point there. Close examination of the mesh spacing along the free-surface will indicate that it decreases in both directions from the equator and in part accounts for the desirable crowding of mesh triangles into the tips of the half cross section. The broken line connecting the images of the equatorial points in the logical domain decomposes the isosceles trapezoid into two unequal "right" trapezoids which resemble the logical diagrams used in the previous report.[4] The user

prepares input for each half of the logical diagram separately. This input is rotated by $\pi/2$ to the left in a special input program to allow main mesh generation routines to operate unchanged, and a special output program rerotates the mesh by $\pi/2$ to the right to the position illustrated.

The procedures used to control the mesh within the standardized domains are described in the previous report.[4] They include prescribing the location of certain control (mesh) points on the unit circle, the number of mesh intervals in the group to be constructed between control points, and the length of the first interval of such a group. Whenever the data permits, the length of the mesh intervals in a group form a geometric progression; otherwise, they are equally spaced. In addition to the parallelogram used for Figure 4 and the isosceles trapezoid used for Figure 6, the program permits using the right trapezoid as in the previous report.[4] Moreover, such domains may be stacked on top of one another, provided that the right edge of the stack is along a mesh line slanting downward to the left and provided the left edge has no segments along horizontal mesh lines.

All meshes required in this survey can, in principle, be generated by the procedure described above. Additional programming is still needed to give more control over the location of mesh points along the unit circle to produce satisfactory meshes for some domains that are characterized by having free-surface and tank meridians of nearly equal length and relatively small centerline depth. One difficulty to be overcome is already exhibited in Figures 4 and 5. The fine mesh along the upper part of the circular boundary in Figure 5 maps a more widely spaced mesh along the periphery of the ellipse.

Solution of the Approximate Eigenvalue Problem

The Matrix Approximations. The introduction of surface polar normal coordinates results in a new form of the free-surface boundary condition (53) and new and easily interpretable constant contact angle conditions (54) and (59). With

$$Q(s) = B_\alpha R_s + (1/R^2) - \left[(Z_{ss}R_s - Z_s R_{ss})^2 + (Z_s/R)^2\right]$$

(53) may be written as

$$-\frac{1}{R}\left(R\left[\Phi_n\right]_s\right)_s + Q(s)\,\Phi_n = (1+B_\alpha)\,\omega^2\Phi \tag{80}$$

Let t_1 and t_2 be mid-points of two adjacent mesh intervals $[s_{j-1},s_j]$ and $[s_j,s_{j+1}]$. Integrating (80) with respect to R ds over the interval $[t_1,t_2]$ yields the "balance" equation

$$-R\left[\Phi_n\right]_s\Big]_{s=t_2} + R\left[\Phi_n\right]_s\Big]_{s=t_1} + \int_{t_1}^{t_2} Q(s)\,\Phi_n R\,ds = (1+B_\alpha)\,\omega^2\int_{t_1}^{t_2}\Phi\,R\,ds$$

and applying the usual two-point approximations for the derivatives and making one-point approximations for the unknown functions in the integrals yield the finite difference equation

$$-\Phi_{n_{j+1}}\frac{R(t_2)}{s_{j+1}-s_j} + \Phi_{n_j}\left(\frac{R(t_2)}{s_{j+1}-s_j} + \frac{R(t_1)}{s_j-s_{j-1}} + \int_{t_1}^{t_2} Q(s)\,R\,ds\right)$$

$$-\Phi_{n_{j-1}}\frac{R(t_1)}{s_j-s_{j-1}} = \Phi_j(1+B_\alpha)\,\omega^2\int_{t_1}^{t_2} R\,ds \tag{81}$$

with the two integrals to be approximated during the integration of the free-surface. Applying the same argument over an interval $[t_1,s_j]$, with $s_j = s_u$, adjacent to the tank wall yields in view of (56) the finite difference equation

$$\Phi_{n_j}\left(\frac{R(t_1)}{s_j-s_{j-1}}+\int_{t_1}^{s_j} Q(s)\,R\,ds+\left[\frac{R}{\sin\theta}\left(\frac{d\psi}{ds}\cos\theta-\frac{d\chi}{dt}\right)\right]_{s=s_u}\right)$$

$$-\Phi_{n_j}\frac{R(t_1)}{s_j-s_{j-1}}=\Phi_j\,(1+B_\alpha)\,\omega^2\int_{t_1}^{s_j} R\,ds \qquad (82)$$

as the analogue to (81) incorporating the constant contact angle boundary condition. For the two-circle case, applying the same argument over an interval $[0,t_2]$, with $s_j = 0$, adjacent to the tank wall yields a finite difference equation similar to (82) but incorporating the constant contact angle condition (59). Observe that all of the quantities needed to evaluate the difference equations (81) and (92) can be obtained in the course of the integration of the free-surface.

Assembling the difference equations and dividing by $(1+B_\alpha)$ yields a matrix-vector equation

$$T\,\underline{\varphi}_n-\lambda\,A\,\underline{\varphi}=0 \qquad (83)$$

where

$\underline{\varphi}$ and $\underline{\varphi}_n$ are vectors of values approximating the potential and its normal derivative at mesh points in the free-surface;

λ is an approximation to ω^2;

A is a diagonal matrix whose entries are $1/2\pi$ times the areas of the zones used to approximate the free surface; and

T is a tridiagonal, symmetric, irreducible matrix that approximates the differential operator on Φ_n in the free-surface boundary condition.

The matrix T is positive definite for all cases in this study with $B_\alpha \geq 1$; it is positive definite for all but one of the two-circle cases studied with $B_\alpha = 0$; and it fails to be positive definite for all but one of the one-circle cases studied with $B_\alpha = 0$.

The remainder of the matrix approximations are described in detail in the previous report.[4] The only difference occurs in the two-circle case; the condition $\Phi = 0$ on the axis is replaced by the condition $\Phi_n = 0$ on the tank wall at one end of each mesh line. However, a brief sketch of the arguments is included here.

At each interior mesh point the operator (50) has a seven-point finite difference approximation connecting the potential values at six neighboring points to the value at the central mesh point; at nonaxial boundary points a similar approximation using only points within the closed domain can be derived, provided the normal derivative is known.[21,22,23] On the free surface, (83) provides the missing normal derivatives. Let D be the matrix approximating (50) with $\Phi = 0$ on the axis and $\Phi_n = 0$ on the wall and the free-surface. Set $S^{-1} = 2AT^{-1}A$. Partition the vector of potential values as $\underline{\varphi} = [\underline{\varphi}_2, \underline{\varphi}_1]^T$ --the components of $\underline{\varphi}_2$ are values of $\underline{\varphi}$ not on the free-surface. When D is partitioned conformally with $\underline{\varphi}$, the finite difference approximation to the normal mode problem takes the form

$$\begin{bmatrix} D_{22} & D_{21} \\ D_{12} & D_{22}-\lambda S^{-1} \end{bmatrix} \begin{bmatrix} \underline{\varphi}_2 \\ \underline{\varphi}_1 \end{bmatrix} = 0 \qquad (84)$$

which emphasizes the role of the free-surface.

For meshes consisting entirely of acute triangles, the matrix D is symmetric, irreducible, positive on the diagonal, nonpositive off the diagonal, diagonally dominant and has at most seven nonzero entries in each row. Violent deviations from acuteness change the properties of D and affect the final results markedly; small departures from strict acuteness away from the free-surface have little effect. The matrix S inherits its properties from T; it is tridiagonal, symmetric, irreducible and for most cases in this study positive definite.

Because (84) can be reduced to a generalized eigenvalue problem of the form $[A - \lambda B]\,\underline{\varphi} = 0$, standard theory guarantees, when B is positive definite,

that (84) has solutions $[\lambda_k, \underline{\varphi}_k]$, $k = 1,2,\ldots,n$, where n is the number of points on the free-surface.[24]

When S fails to be positive definite, the numerical evidence so far obtained and the form of S support the conjecture that it has precisely one nonpositive eigenvalue and that the others are positive. If this is the case, working in the space orthogonal to the eigenvector corresponding to the nonpositive eigenvalue should restore the property of the preceding paragraph with n reduced by one.

The Modified Wielandt Inverse Iteration. Factor the matrix S into left and right triangular factors, $S = LR$, by a Cholesky decomposition modified when the product of diagonal entries is negative to set the left diagonal to the negative and the right diagonal to the positive value of the square root of the absolute value of the offending product. When S is positive definite, no modification is necessary and $R = L^T$. When S fails to be positive definite here, the modification takes place only for the final diagonal entries.

Multiply (84) on the left by

$$\begin{bmatrix} I & 0 \\ 0 & R \end{bmatrix}, \quad \text{insert} \quad I = \begin{bmatrix} I & 0 \\ 0 & L \end{bmatrix} \quad \begin{bmatrix} I & 0 \\ 0 & L^{-1} \end{bmatrix}$$

between the matrix and the vector in (84), and carry out the matrix multiplications to get an equivalent linear system

$$\begin{bmatrix} D_{22} & D_{21}L \\ RD_{12} & RD_{11}L - \lambda I \end{bmatrix} \begin{bmatrix} \underline{y} \\ \underline{z} \end{bmatrix} = 0 \qquad (85$$

where $\underline{y} = \underline{\varphi}_2$ and $\underline{z} = L^{-1}\underline{\varphi}_1$. As in the usual Wielandt inverse iteration[25], the one modified to take advantage of the form of (85) starts from a guessed eigenvalue $\lambda^{(o)}$ and a guessed eigenvector $\underline{z}^{(o)}$. The latter is improved by solving the linear system

$$\begin{bmatrix} D_{22} & D_{21}L \\ RD_{12} & RD_{11}L-\lambda I \end{bmatrix} \begin{bmatrix} \underline{y}^{(1)} \\ \underline{z}^{(1)} \end{bmatrix} = \begin{bmatrix} 0 \\ \underline{z}^{(o)} \end{bmatrix} . \tag{86}$$

The guess for the eigenvalue is improved by computing the Rayleigh quotient

$$\lambda^{(1)} = \frac{\underline{z}^{(1)T}\left[RD_{11}L\,\underline{z}^{(1)} + RD_{12}\underline{y}^{(1)}\right]}{\underline{z}^{(1)T}\,\underline{z}} \tag{87}$$

and $\lambda^{(1)}$ and $\underline{z}^{(1)}$ replace $\lambda^{(o)}$ and $z^{(o)}$ as the starting values for the next step in the iteration. The form of the linear system (86) accounts for the speed of the iteration. Because the leading entries in the right side are zero, when the system is solved by a factorization method, only a portion of the downsweep need be carried out. Moreover, because all the non-zero entries in RD_{12} are in the right portion of the matrix product, the up-sweep may be discontinued as soon as the corresponding values of $\underline{y}^{(1)}$ have been computed.

The iteration continues until the ratio $z_i^{(1)}/z_i^{(o)}$, for some fixed i, has grown so large that no further improvement can be obtained (10^{+5} is the value used here) or until the relative error $(\lambda^{(o)}-\lambda^{(1)})/\lambda^{(1)}$ is so small that further improvement is unlikely (10^{-4} seems suitable for the present problems).

When the iteration converges, the approximate potential throughout the tank $\underline{\varphi}_2 = \underline{y}$ is computed to obtain the values along the tank wall needed to evaluate the lateral force and moment integrals. The approximate eigenmode $\underline{H}$ is produced by solving the linear equation

$$R\,A\,\underline{H} = (\lambda^{1/2}/2)\,\underline{z} \tag{88}$$

and the approximate potential on the free-surface is determined by the matrix multiplication

$$\underline{\varphi}_1 = L\,\underline{z} .$$

When S is not positive definite and λ is negative, the square root in (88) is set to one because the eigenmode makes no sense.

Problems with $B_\alpha = 0$. On physical grounds the fundamental eigenvalue should be zero for $B_\alpha = 0$ when the tank is spherical. A finite-difference approximation to a continuous problem can at best yield an approximation to a zero eigenvalue. It can be shown for the one-circle problems that zero is not an eigenvalue of the approximate problem. Here the first approximate eigenvalue is small and positive for $V = 1/8$ and small and negative for $V = 7/8$. For $V = 1/2$ the approximation seems to be "too good"; the program quits under circumstances that suggest that the lowest eigenvalue of the finite difference approximation is zero to within machine accuracy. Unfortunately time has not permitted modifications to the program that would verify this hypothesis.

By continuity, the fundamental eigenvalue is expected to be small for the other spheroidal tanks. For all but one of the single circle cases with $B_\alpha = 0$ tried in the nonspherical tanks, the program produced an approximation for the fundamental eigenvalue. These values are small and uniformly negative. The exceptional case seems to be another example of "too good" an approximation, like $V = 1/2$ in the spherical tank. In two-circle cases with $B_\alpha = 0$ the program produced complete eigensystems; in one case, $V = 1/4$, $e = 0.5$, the fundamental eigenvalue turned out to be small and negative and in another, $V = 5/8$, $e = 0.8$, very small and positive. At a fixed volume, as the eccentricity of the tank increases, the fundamental eigenvalue also increases.

The pressing and unsolved problem here is to tell which of the small fundamental eigenvalues are truly nonzero. As eigenvalues of the finite difference problem approximating the continuous problem, they are only slightly less accurate than those in the remainder of the study, which are uniformly numerically acceptable. The question, therefore, would seem to center on the discretization error committed in passing from the continuous to the finite difference problem.

In principle, the program can and sometimes does produce some of the higher eigenvalues in the one-circle cases with $B_\alpha = 0$. When it fails to do so, it consistently slips back into the fundamental--even when provided with extremely large guesses for the eigenvalues. This circumstance suggests that modifying the construction of the starting eigenvector used in the Wielandt inverse iteration would improve the performance of the program for $B_\alpha = 0$. The fact that the chief difference between the one- and two-circle programs lies in this area reinforces this view.

Evaluation of the Forced Response

In principle, if enough frequencies ω_k and corresponding eigenmodes $H_k(s)$ are known, the shape assumed by the perturbed free-surface $H(s,\theta;t)$ in response to a periodic lateral perturbing acceleration which has a Fourier series expansion of the form

$$B_{tr} = \hat{B}_{tr} \Sigma_m C_m \sin(m\omega_o t)$$

can be calculated by evaluating the series

$$H(s,\theta;t) = \frac{\cos\theta \hat{B}_{tr}}{(1+B_\alpha)} \sum_k \omega_k D_k H_k(s) \sum_m \frac{C_m}{\omega_k^2 - m^2\omega_o^2} \sin(m\omega_o t) \qquad (89)$$

that follows from (37) with D_k given by (34).

For sinusoidal perturbations, where $C_1 = 1$ and $C_m = 0$ for $m > 1$, the inner sum in (89) disappears and the evaluation of the sum over k is straightforward provided that $\omega_k \neq \omega_o$. The numerical problem is to be sure that truncating the sum to the small set of natural frequencies and eigenmodes available does not omit a physically significant part of the response. For other perturbations, the evaluation of the inner sum presents an additional practical problem. The terms of largest magnitude in the sum over m usually occur for values of m near ω_k/ω_o, and this ratio grows rapidly with k. A feasible procedure for this initial survey is to carry each sum so far

beyond the neighborhood of ω_k/ω_o that there is no question of the convergence of the inner sum.

Thus the main question about the results here is whether enough terms have been included in the outer sum (89). With only 25 mesh intervals on the free surface, the accuracy of the representation of higher eigenmodes may be questioned. Consequently, five eigenmodes were used for the majority of the cases. The choice of five was also based on the fact that, with 44 mesh intervals on the free surface, doubling the number of eigenmodes from four to eight (and halving the time step) revealed no significant change in the computed response.

Granted that $H(s,0;t)$ can be evaluated satisfactorily, the question arises of when and where the maximum excursion produced by a given forcing function appears. An approximation to the desired answer can be given by computing $H(s,0;t)$ for a large number of values of t and noting the time at which $|H(s,0;t)|$ achieves its maximum among the values computed. In the present survey 30 time steps within 3/8 of the period of the fundamental or 60 time steps within 1/2 of the period of the fundamental are used. The shape of the perturbed surface is plotted at the time of the observed maximum and at intervals of 5 time steps going away from the maximum in both directions. The period of the fundamental was chosen as the unit of time to give a uniform time scale for varying forcing frequencies ω_o.

Because $H(s,0;t)$ represents the deviation of the perturbed surface from the equilibrium free-surface in the normal direction, this deviation is added vectorially to the free-surface to produce a graph of the perturbed surface shape in the plane $\theta = 0$ at each time plotted (cf. Figure 19). To save the user the trouble of reflecting the shape in the equilibrium free-surface, the reflected shape in the plane $\theta = \pi$ is also plotted on the same graph. The plotted values are normalized so that the maximum amplitude of the observed response ((89 computed with $\hat{B}_{tr} \cos\theta/(1+B_\alpha)$ set equal to 1) is equal to 1/10 of the length of the free-surface ($s_u = s_{max}$). Thus the amplitude of the

transverse Bond number reported in the plots is the value computed from the relation

$$(1+B_\alpha)\ s_{max}/10 = \hat{B}_{tr} \cdot \max_{s,t} |H(s,0;t)| \ .$$

This normalization is adopted to give the plots a large enough scale to make meaningful detail visible and at the same time prevent normals from crossing within the distance $s_{max}/10$ of the free-surface (see (3) and (23)). Thus the free-surface can be surrounded by a grid consisting of four parallels at distances of $\pm$ 1/10 and $\pm$ 1/20 of s_{max}. In addition the normals through every fifth point on the free-surface starting from s_{max} are drawn and labeled.

The question of whether or not the tank meridian should also be included in the plot can be argued either way. When it is present, it clutters the graph but does serve to emphasize that the present study is limited to small amplitude analysis and that the scale of the plots in the normal direction is, arbitrarily, set large to reveal detail of the computed perturbed shape. Clearly the perturbed surface cannot cross the tank wall and must extend to the wall when the displacement is positive at s_{max}.

The present program can certainly be used (with caution) to determine whether the computation of the perturbed shape is of enough practical use to warrant further refinement.

Evaluation of the Mechanical Analog Parameters

Because

$$\lambda + B_\alpha Z = 2H$$

and

$$\sin\chi = Y_\tau = bX/(1-e^2X^2)^{1/2} \ ,$$

the lateral force for the two-circle case (44) may be rewritten as

$$F_x = b\pi \left[-C_\ell \, H(0) - C_u H(s_u) + \omega(1+B_\alpha) \left(\int_{\tau_\ell}^{\tau_u} \left[(\Phi X^2)/(1-e^2X^2)^{1/2} \right] d\tau \right) H(s_u) \right] \tag{90}$$

with

$$C_\ell = 2\mathcal{H}\Big]_{s=0} \cdot \left[X \csc\Theta/(1-e^2X^2) \right]_{\tau=\tau_\ell}$$

and

$$C_u = 2\mathcal{H}\Big]_{s=s_u} \cdot \left[X \csc\Theta/(1-e^2X^2) \right]_{\tau=\tau_u} .$$

If C_ℓ is set to zero, (90) represents F_x for the one-circle case (42) as well.

The coefficients C_ℓ and C_u must be computed at the beginning and end of the final integration of the equilibrium free-surface. A natural form for the approximation to the integral in (90) is

$$\int_{\tau_\ell}^{\tau_u} \left[(\Phi X^2)/(1-e^2X^2)^{1/2} \right] d\tau = \sum_J \Phi_j \, w_j \tag{91}$$

where J is the set of indices that pick out values of the potential on the tank wall from the vector of potential values at all the mesh points. The set J and the corresponding weights w_j must be determined while the entries in the matrix D are being assembled. However, the final evaluation of the integral must wait until the potential is generated.

Because the tank wall is approximated by straight lines between mesh points, a mid-point approximation seems appropriate. Let (X_1,Y_1) and (X_2,Y_2) be two adjacent mesh points on the tank wall with Φ_μ and Φ_ν as corresponding potential values. Set

$$X_m = (X_1 + X_2)/2$$

and

$$\Delta\tau = \left[(X_2 - X_1)^2 + (Y_2 - Y_1)^2\right]^{1/2} .$$

Then the approximation

$$\int_{\tau_1}^{\tau_2} \left[(\Phi X^2)/(1-e^2X^2)^{1/2}\right] d\tau$$

$$\doteq (\Phi_\mu + \Phi_\nu)\, X_m^{\,2}\, \Delta\tau/2(1-e^2X_m^{\,2})^{1/2}$$

contributes the weight

$$X_m^{\,2}\, \Delta\tau/2(1-e^2X_m^{\,2})^{1/2} \tag{92}$$

to each of the weights w_μ and w_ν in (91). Each w_j, except at the ends of the tank meridian, is the sum of two terms of the form (92). An analogous procedure is used to compute the moment (43) or (45).

Because the potential is normalized so that $\Phi^T S^{-1} \Phi = 1$, it turns out that

$$V = \pi/2\ (1+B_\alpha) \int_o \Phi\Phi_n\, R\, ds = \pi(1+B_\alpha)\ \omega^2/4 .$$

Thus the evaluation of the remaining mechanical analog parameters (46), (47), (48), and (49) is straightforward.

RESULTS AND CONCLUSIONS

The Method

The problem of low gravity sloshing in spheroidal tanks has previously been investigated by approximate mathematical methods and by experimental methods. Even when surface tension forces are negligible, approximate solutions of the governing equations are the only ones possible.[9,10,11] No attempts have been made thus far to apply these methods to the case in which surface tension forces dominate the liquid motion. Experimental work has, with one exception, been limited to the case of zero surface tension, and even there physical limitations prevented experiments under conditions where surface tension actually dominated the liquid behavior. This report is the first attempt to study lateral sloshing in spheroidal tanks under such conditions.

The highly curved free-surface shapes characterized by large departures from the horizontal plane are accurately computed here by numerical means properly accounting for the equilibrium contact angle and, by iteration, the liquid volume in the spheroidal tank. Solution of Laplace's equation in the domain occupied by the liquid subject to appropriate boundary conditions at the tank wall and the free surface is accomplished using a finite difference technique on an irregular triangular mesh. Such a mesh is space filling allowing accurate approximation of curved tank and free-surface boundaries. The basic restriction inherent in the finite-difference approximation is that the contact angle be nonzero.

Demonstration that the computer program can feasibly produce the desired numerical calculations is a major result of this work. The basic program used in this project is an adaptation of one previously developed[4] for calculating low-g lateral sloshing in hemispherically bottomed cylindrical tanks. The principal output from the program includes:

1. Normal mode eigenvalues ω_k^2 ;
2. Normal mode eigenfunctions Φ_k ;
3. Normal eigenmodes H_k ; and
4. Fourier coefficients, D_k .

These have been used to compute, as a Fourier series expansion, the response to sinusoidal, square wave, and periodic pulse lateral perturbing accelerations and to compute the lateral force and moment imposed on the tank by the liquid in kth mode lateral sloshing. Where appropriate, the force and moment can be used to compute parameters of an equivalent spring-mass system to facilitate engineering computations.

The Present Study

The data reported here is a survey of small amplitude linearized sloshing in spheroidal tanks of eccentricity 0, 0.5, 0.68, and 0.8 with axial Bond number B_α ranging from zero to 100 and relative liquid volume ranging from 1/8 to 7/8 of the tank volume. All calculations have been carried out for a fixed contact angle of 5 degrees consistent with previous work,[4] which allows adequate representation of small-contact-angle low-g liquid sloshing behavior while keeping numerical difficulties inherent in the method for very small contact angles minimal.

Figures 8-14 show the meniscus shapes considered in the study. At the higher Bond numbers, the liquid cross section ranges from a flat puddle in the tank bottom to a deep body enclosing a flattened bubble at the top of the tank. At the lower Bond number, the liquid free-surface extends from the lower into the upper hemispheroid; and, at sufficiently small liquid volume and Bond number, the bottom of the tank is uncovered, the liquid being found in an annular region around the equator.

Eigenvalues ω_k^2

The variation of first mode (fundamental) eigenvalues as a function of Bond number B_α and liquid volume is shown in Figure 15 and Table I. The first mode eigenvalue ω_1^2 generally increases with Bond number and liquid volume for a given tank shape. The behavior of ω_1^2 , observed here, as a function

of liquid volume for $B_\alpha = 100$ and $e = 0$ is consistant with the known behavior [1] of ω_1^2 in a spherical tank for $B_\alpha = \infty$ (the case of zero surface tension). For $B_\alpha \geq 5$ and $e = 0$, the values of ω_k^2 in Table I replace the values reported earlier [4,5] for cases in which the liquid lies entirely within the lower hemisphere. The new values are consistently higher and are more reliable because they are based upon the exact constant contact angle condition ((27a) or (54)) rather than upon the approximation used in the earlier computations for the hemisphere. For $B_\alpha \leq 2$ and $e = 0$, the effect of the approximation in the hemisphere appears to be negligible. (Because the constant contact angle condition used on the vertical wall was exact, the data reported earlier [4,5] need be replaced by the present values only for $B_\alpha \geq 5$ and $e = 0$, cases with large Bond number and with small fill levels in which the liquid lies entirely within the hemispherical bottom.) The fundamental eigenvalue ω_1^2 for $B_\alpha = 0$, $e = 0$ is zero. (That it is exactly zero can be deduced from physical considerations. The computational results presented in Table I are, subject to the discretization error, considered to be consistent with this value.)

Table I also indicates that ω_1^2 is very nearly zero in spheroids with $e \neq 0$ when the meniscus intersects the tank wall in only one circle and in some cases, when it intersects it in two. In other two-circle cases, characterized by small fill level and large eccentricity, ω_1^2 is well away from zero. Note also that first mode eigenvalues for the two-circle cases do not fall on the curves in Figure 15. This may be explained as follows. Physically, lateral slosing in the one-circle and two-circle cases is much different. In one-circle cases, the motion is essentially lateral from one side to the tank to the other; the eigenmodes are all odd. First mode sloshing in two-circle cases is circumferential with liquid moving from one side of the tank to the other circumferentially; higher modes are characterized by an almost vertical motion in each side of the tank, and both odd and even modes (i.e. an odd or even number of equilibrium free-surface crossings) must be considered.

The first five eignevalues ω_k^2 for all cases considered are listed in Table I. Note that all eigenvalues for a given tank shape - Bond number combination increase with liquid volume V except for the two-circle of intersection

cases where the higher eigenvalues decrease as liquid volume increases.

Dimensional sloshing frequencies $\bar{\omega}_k$ can be obtained from values in Figure 15 or Table I from the relation

$$\bar{\omega}_k = \omega_k \left((1+B_\alpha)\sigma/\rho a^3\right)^{1/2} .$$

The centerline depth of liquid under the meniscus and other meniscus geometry may be obtained from Figures 8-14.

Eigenmodes H_k

The normal departure of the free surface from its equilibrium shape is shown in Figures 16-19 for six representative cases. Low Bond number and high Bond number shapes are shown in Figures 12 and 13 to illustrate the influence of tank shape on the eigenmodes. It is observed that the first eigenmode for the smaller Bond numbers is generally convex up in the region $0 \le s < s\,(H_{1_{max}})$, where $H_{1_{max}}$ is the maximum value of H_1 ; whereas, by contrast, H_1 is generally convex down in down in this same region for Bond numbers greater than 10. The dependence on the first eigenmode shape is not otherwise (except for two-circle cases) greatly affected by changes in tank shape, liquid volume, or Bond number.

Response to Lateral Perturbations

Practical application of the results of the present analysis centers on the response of the liquid to lateral perturbing accelerations. The response to sinusoidal perturbing accelerations is given by

$$H\Big|_{\theta=0} = \frac{\hat{B}_{tr}}{1+B_\alpha} \sin\omega_o t \sum_{k=1}^{\infty} \frac{D_k \omega_k^2}{\omega_k^2 - \omega_o^2} H_k(s) \qquad (93)$$

where D_k, defined by (34), is the Fourier coefficient in the expansion $R = \Sigma\, D_k \Phi_k$.

For all cases in the survey, the quantities needed to evaluate (93) at

$s = s_u$ (at the intersection of the tank wall with the equilibrium free surface) are tabulated for the first five modes: ω_k^2 in Table I, D_k in II, and $H_k(s_u)$ in III. (For cases in which the liquid lies entirely within the hemispherical bottom, the present tables should be used, as pointed out above, rather than those reported earlier (4,5).)

The forced response to sinusoidal, square wave, and periodic pulse lateral perturbing accelerations has been calculated for representative cases. In each case the transverse Bond number has been chosen to yield a maximum value of H equal to 1/10 of $s_u = s_{max}$. Surface-normal coordinates (s,H) where s is arclength along the free-surface and H is the displacement normal to the free-surface are used in plotting (see Figure 19). On each plot a surface-normal coordinate grid surrounds the free-surface. The lines of constant H in the grid are the parallels to the free-surface at $H = \pm s_{max}/10$ and $H = \pm s_{max}/20$ to show where the response reaches the maximum and half the maximum excursion. The lines of constant s are the normals to the free-surface drawn through $s = 0$, $s = s_{max}$, and every fifth mesh point starting from s_{max}. The normals are labeled with their s-coordinates.

The computed response of the liquid to a sinusoidal perturbing acceleration for the two-circle case $B_\alpha = 1$, $V = 3/8$, and $e = 0.8$ is shown in Figure 19. The response shown has a maximum excursion from equilibrium of 1/10 of s_u. The magnitude of the transverse Bond number required to force the response to have this amplitude is given. The simple form of (93) allows easy computation of the response to sinusoidal lateral perturbing accelerations of different magnitudes and at different ratios of perturbing to fundamental frequency. The plot of eigenmodes for this case is also included.

The response of the liquid to any periodic lateral perturbing acceleration is given by

$$H\Big|_{\theta=0} = \frac{\hat{B}_{tr}}{1+B_\alpha} \sum_{k=1}^{\infty} D_k \omega_k H_k(s) \sum_{m=1}^{\infty} \frac{C_m \sin m\omega_o t}{\omega_k^2 - m^2\omega_o^2} \qquad (94)$$

where the C_m's are the coefficients of the Fourier series expansion of the lateral acceleration. The response of liquid to square wave and periodic pulse perturbing accelerations for the same case is shown in Figures 20 and 21 for a forcing frequency 7/10 the fundamental eigenfrequency. Four plots are presented in each case showing the motion in the first half cycle leading to an amplitude approximating the maximum. In the last plot for each case, the maximum departure of the free-surface from its equilibrium shape is 1/10 the length of a meridian of the free-surface. The magnitude of the transverse Bond number $\hat{B}_{tr}$ resulting in this displacement is noted on each plot. The response near the maximum to sinusoidal, square wave and periodic pulse perturbations is given for the case $B_\alpha = 5$, $V = 3/4$, and $e = 0$ in Figure 22, and similarly for the case $B_\alpha = 5$, $V = 3/4$, and $e = 0.8$ in Figure 23 and for $B_\alpha = 2$, $V = 3/8$, and $e = 0.68$ in Figure 24.

The convergence of the series expansion for the forced response to sinusoidal lateral perturbations depends mainly on the requirement that the forcing frequency ω_o be markedly different from the natural frequencies ω_k. For $\omega_o < \omega_1$, the growth of ω_k^2 with k enforces the convergence and the five terms from Tables II and III are generally sufficient to give three significant figure accuracy.

More limitations must be imposed on the evaluation of (94). The inner series involving the C_m's is clearly convergent, depending only on the ratio ω_o/ω_k. However, the dominant term may occur far out in the series if ω_k/ω_o closely approximates an integer found in the definition of the C_m's. (In the case of square wave and periodic pulse perturbations, only odd integers are important in this connection.) Moreover, resonance can occur if ω_o is a submultiple of ω_1. It may be concluded that this method of finding the response to lateral perturbing accelerations must be used with caution in each specific case so that difficulties arising from submultiple resonances may be identified and avoided.

The Mechanical Analog

Much emphasis has in the past been placed on finding simple approximations to the lateral sloshing of liquids in tanks such as equivalent pendulums or spring-mass oscillators which, in principle, impose the same force on the tank as does the sloshing liquid. Such models are also useful in physically interpreting the results of studies like the present work. Mechanical analog parameters for first mode sloshing are shown in Figures 25-28. The lateral force obtained by integrating the component of the pressure force acting horizontally in the $\theta = 0$ direction is presented in Figure 25. The spring constant of the spring-mass oscillator producing lateral forces equivalent to first mode sloshing is shown in Figure 26. The lateral force action point is shown in Figure 27. This quantity gives the required attachment point of the spring-mass oscillator to produce the proper moment about the center of the tank.

Note in Figure 25 that the lateral force imposed by the liquid as it moves to the right (i.e. in the $\theta = 0$ direction) is negative for smaller values of B_α. This result arises from the fact that the liquid pressure near the free-surface is less than that over the liquid. The integral of this pressure depression is embodied in the first term on the right hand side of (42). It is observed that it is negative (i.e. it acts in the $\theta = \pi$ direction) and offsets the inertial behavior of the liquid embodied in the second term in (42). As the Bond number increases, the first term diminishes, compared to the second. When $B_\alpha = \infty$, only the second term found in similar analyses restricted to the case of zero surface tension remains. For the higher values of Bond number considered in this study the lateral force is always positive.

The spring constant and the mass are always positive as a consequence of (47) and (49). Because of this, the spring constant is plotted only in the region where the lateral force is positive. The mechanical analog is not considered valid when a positive displacement of the right hand limb of the free-surface results in a negative force (i.e. one directed to the left in Figure 1).

The magnitude of the mass in the mechanical analog may be obtained from (49)

$$\mathcal{M}_1 = \frac{\kappa_1}{\omega_1^2} .$$

The attachment point of the equivalent mechanical oscillator giving the proper moment is presented in Figure 27. It is observed from (43) that the net moment imposed by liquid sloshing in a spherical tank is zero. Heuristically, this is easily confirmed by noting that the moment of pressure forces acting anywhere in the tank is always zero because an elemental area at any point in the tank is normal to a radius vector from the center of the tank.

This is not true, however, in spheroidal tanks of nonzero eccentricity. It may be observed that a positive pressure acting on an element of the tank wall to the right and below the tank's center produces a generally negative moment (i.e. one tending to turn the tank in the clockwise direction). Negative pressures characteristic of the lower Bond numbers will produce generally positive moments, hence the positive value of z_1 noted at the smaller liquid volumes. Increasing liquid volume allows a greater hydrostatic pressure which has a greater negative moment. Thus for larger liquid volumes, the net moment will be negative and the value of z_1 also negative. The discontinuity between negative and positive values of z_1 corresponds to the point where the lateral force in Figure 25 is zero.

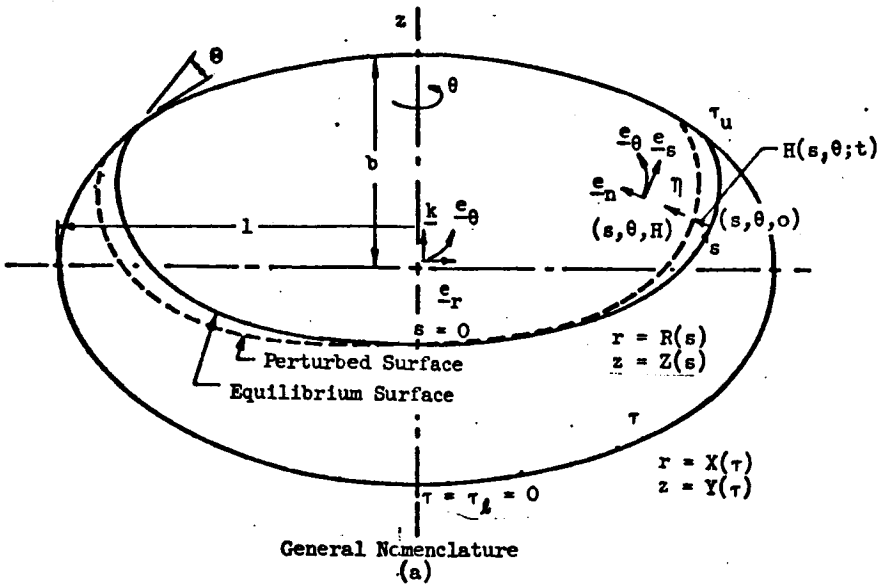

General Nomenclature
(a)

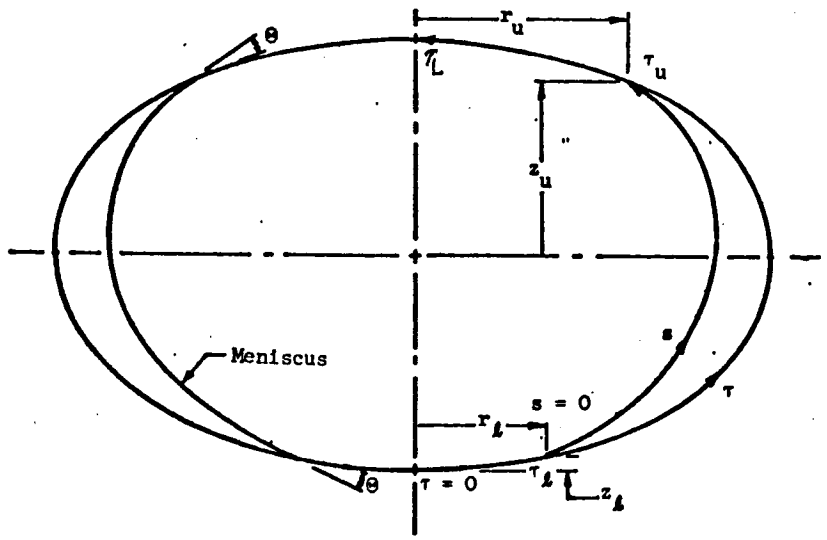

Two-Circle Meniscus Nomenclature
(b)

Dimensionless Tank and Liquid Geometry

Figure 1

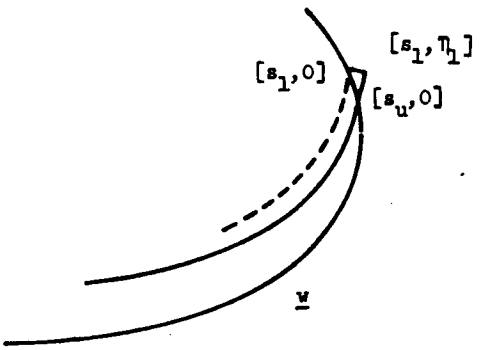

Detail at Contact Angle

Figure 2

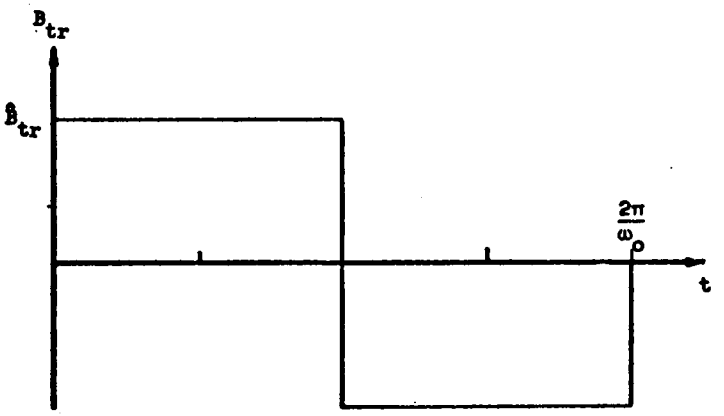

Square Wave Function

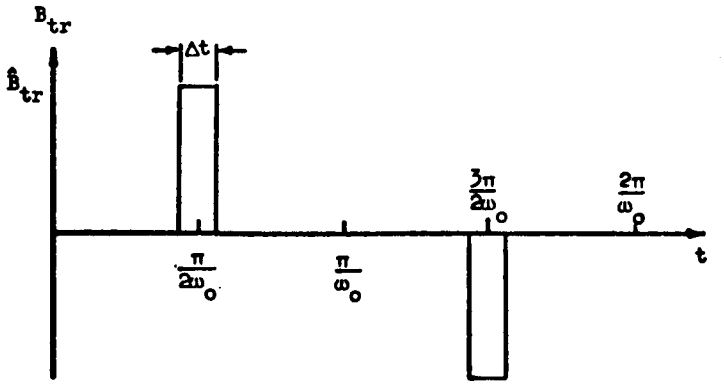

Periodic Pulse Function

Square Wave and Periodic Pulse Perturbing Accelerations

Figure 3

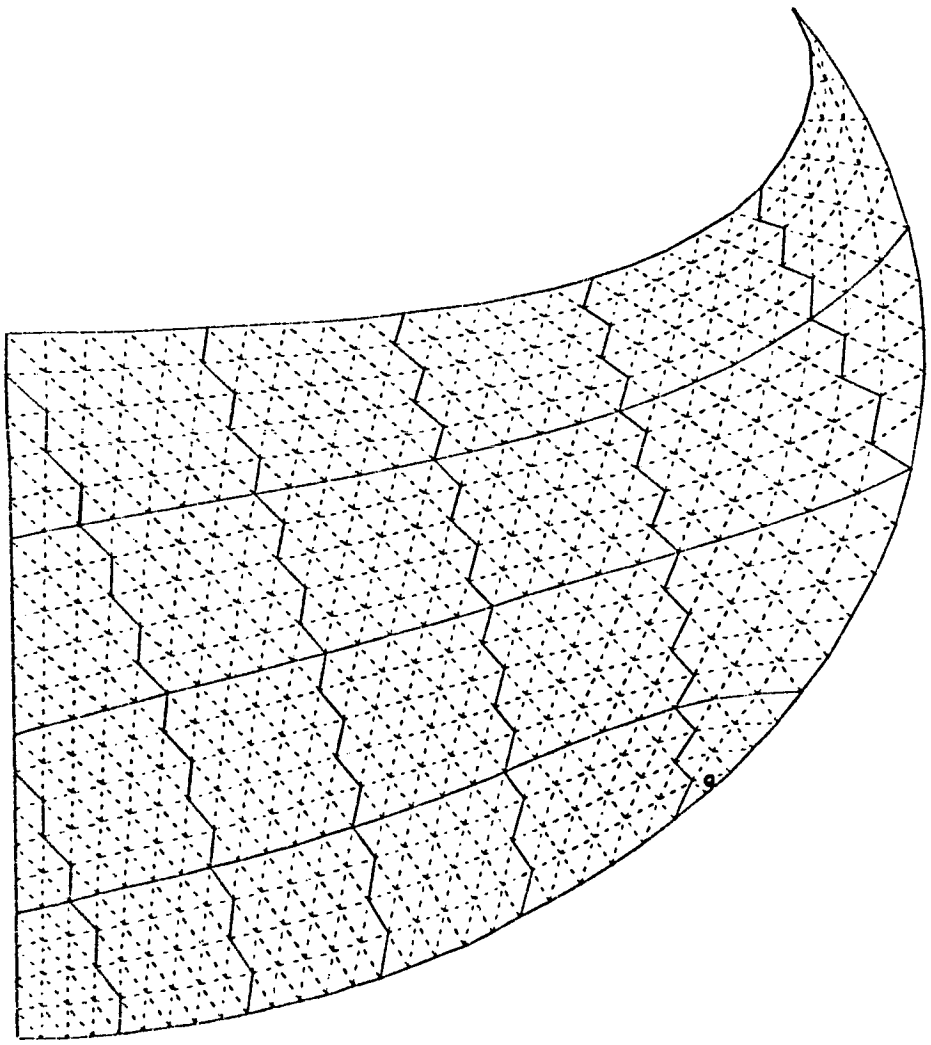

Triangular Mesh Used for $B_\alpha = 30$, $V = 5/8$, and $e = 0.68$

Figure 4

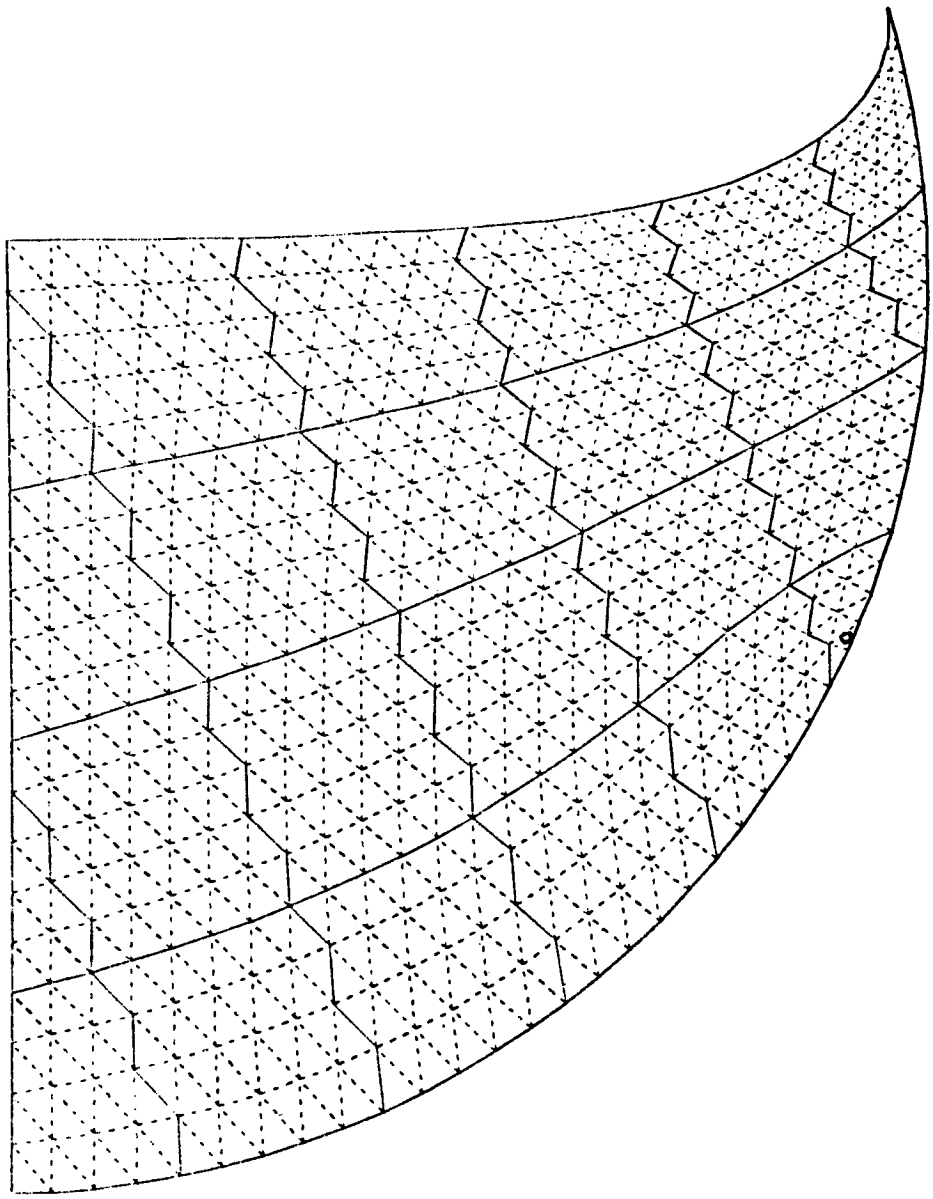

Conformal Map of Figure 4 into the Unit Circle

Figure 5

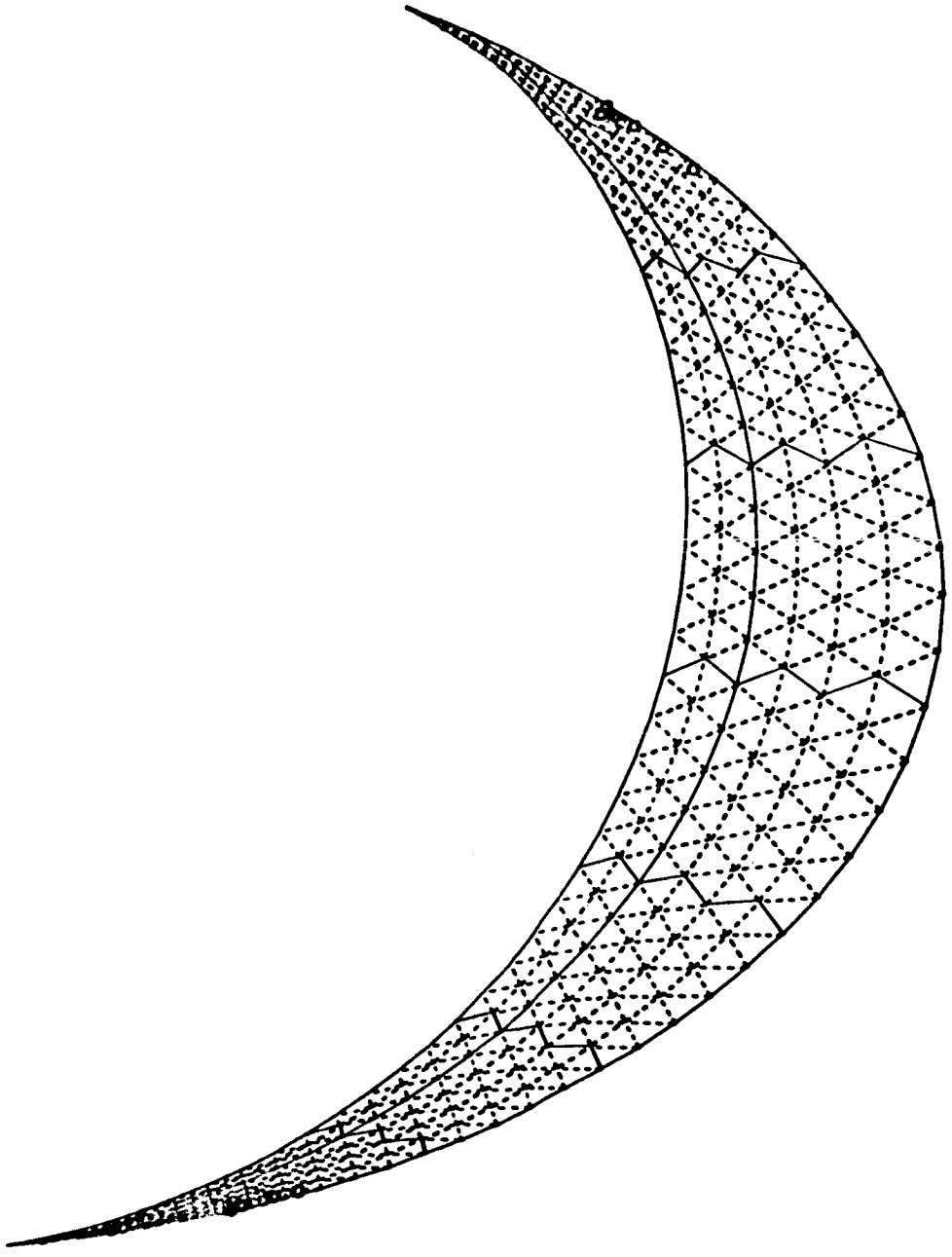

Triangular Mesh Used for $B_\alpha = 1$, $V = 3/8$ and $\epsilon = 0.8$

Figure 6

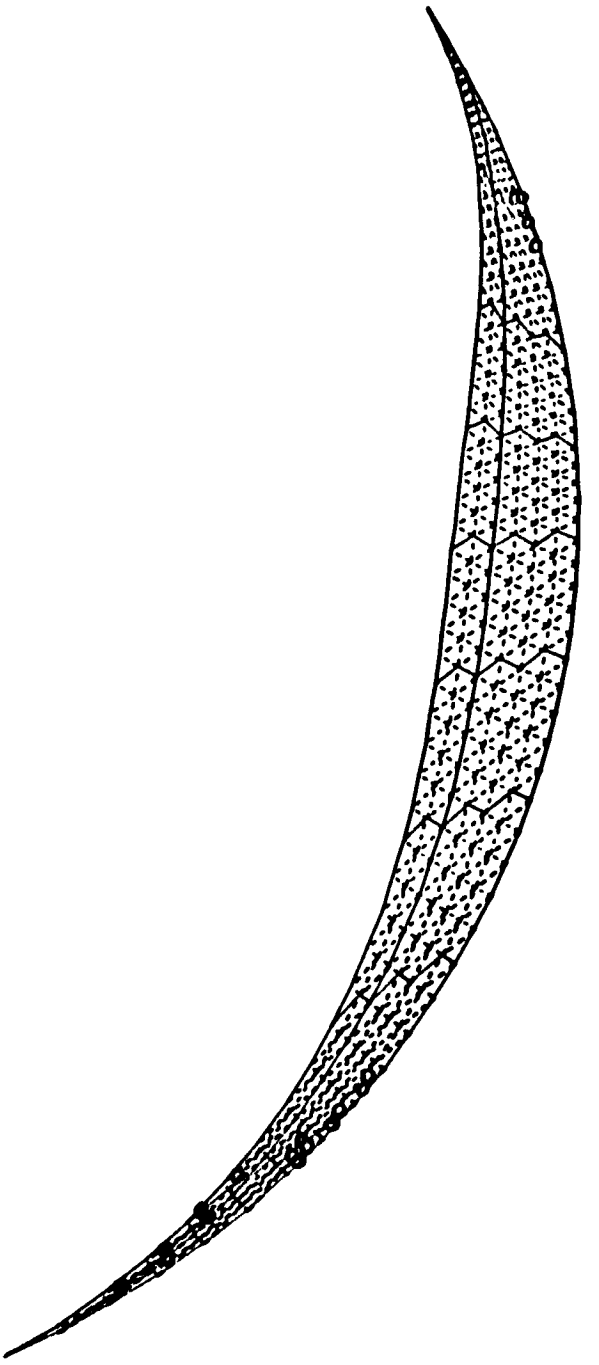

Conformal Map of Figure 6 into the Unit Circle

Figure 7

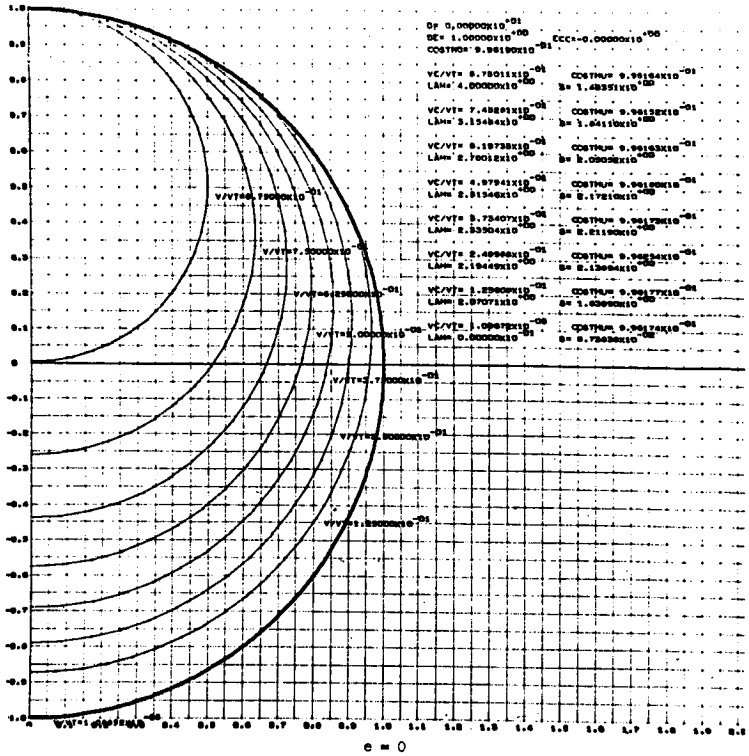

e = 0

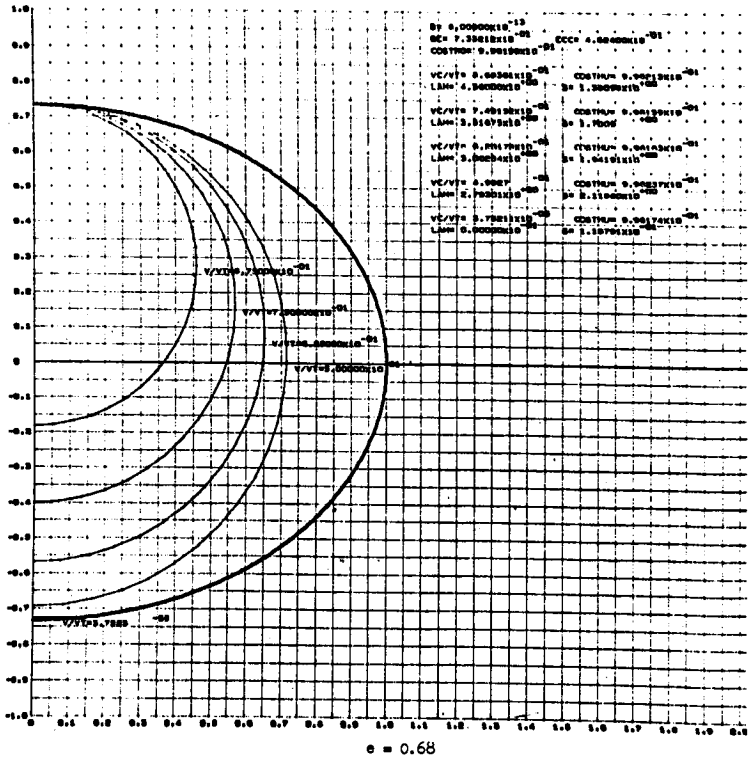

e = 0.68

FOLD-OUT #1

Meniscus Shapes at $B_\alpha = 0$

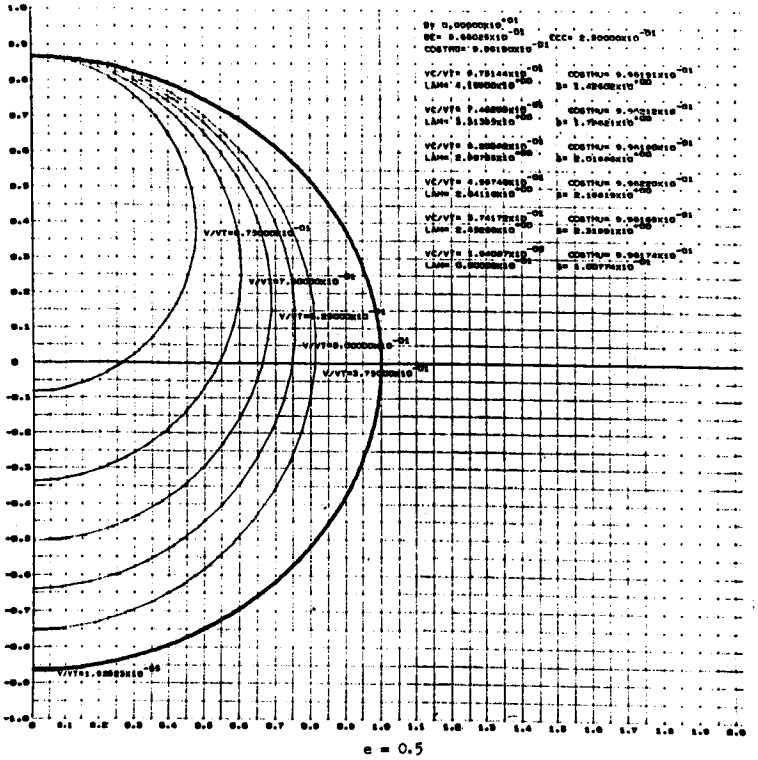

e = 0.5

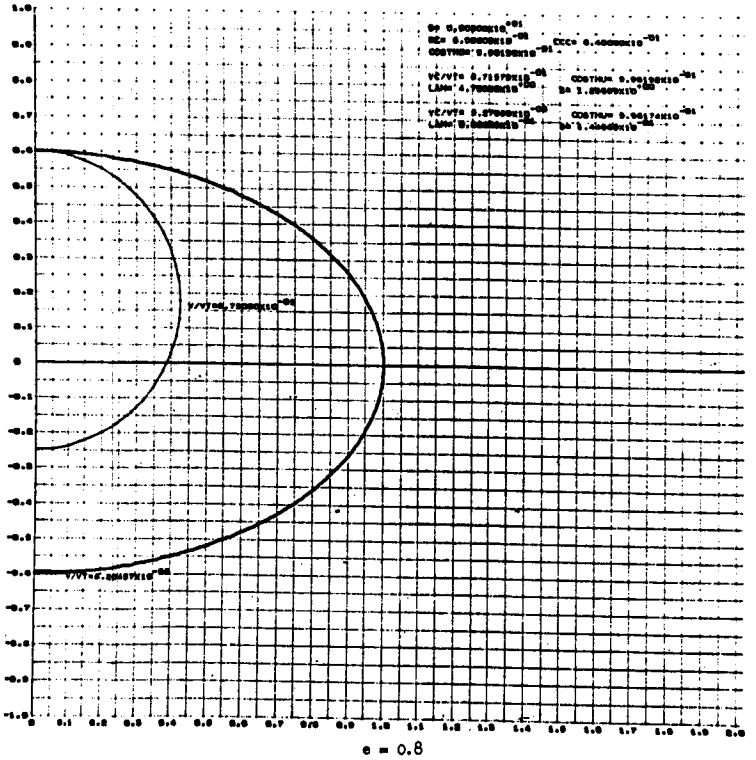

e = 0.8

for Tanks of Eccentricity 0, 0.5, 0.68 and 0.8

Figure 8a

FOLD-OUT #2

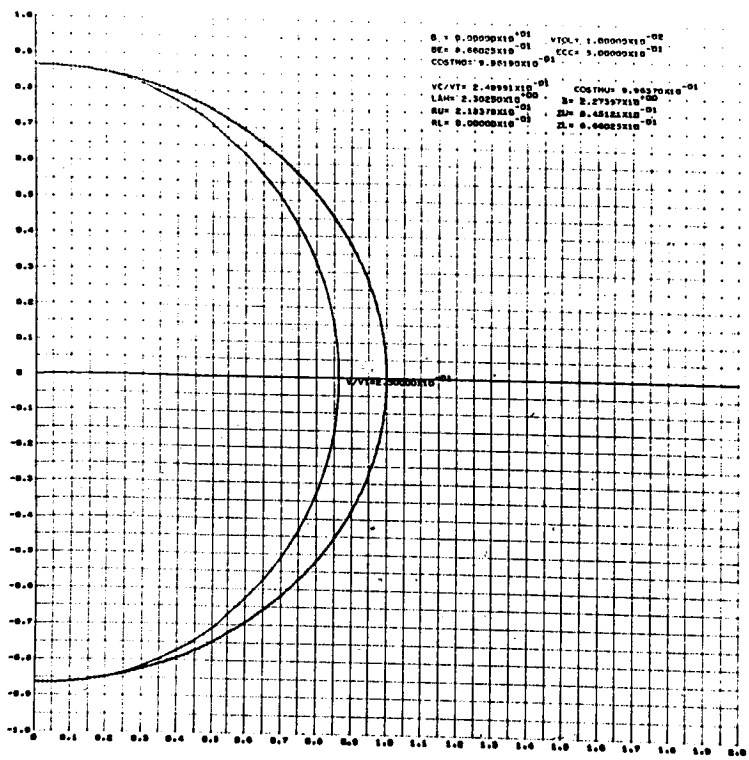

e = 0.5

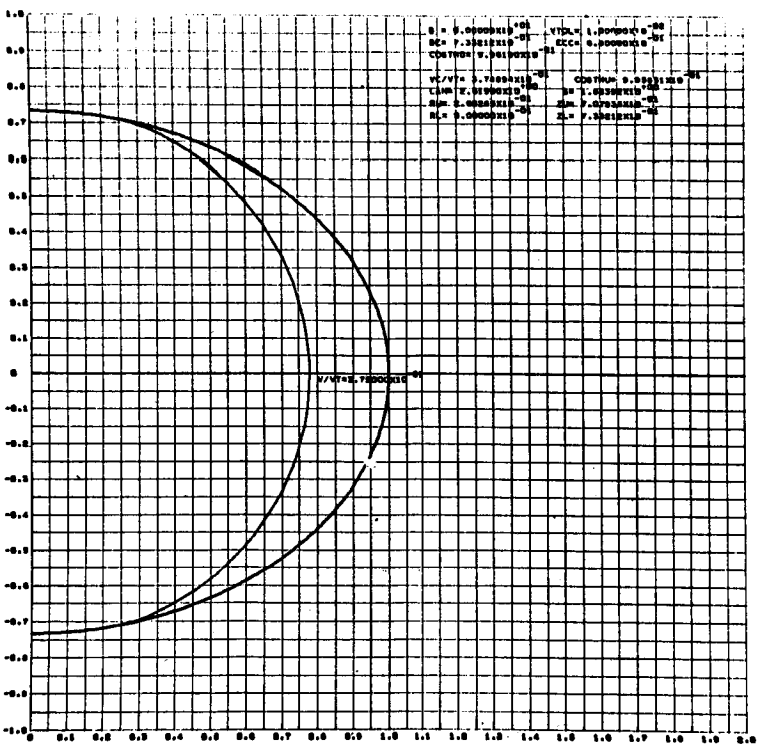

e = 0.68

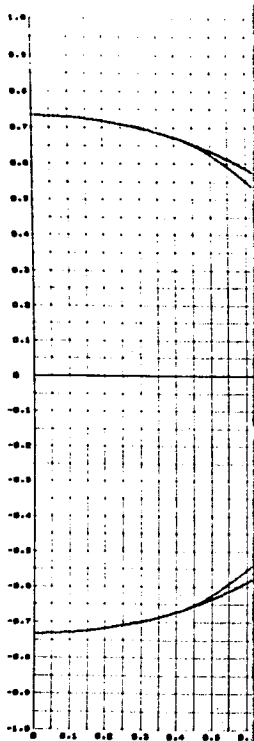

Meniscus Shapes at B_α =

FOLD-OUT #1

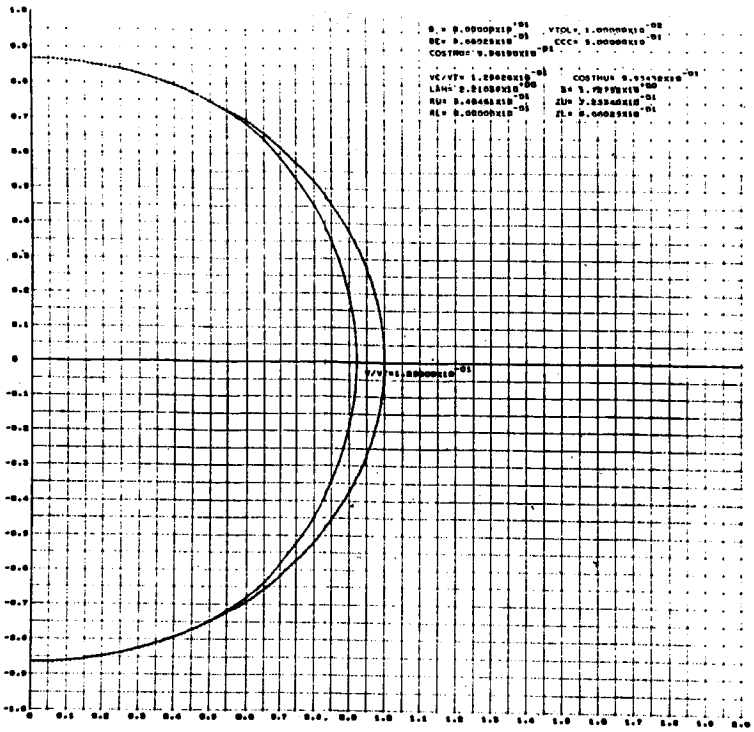

e = 0.5

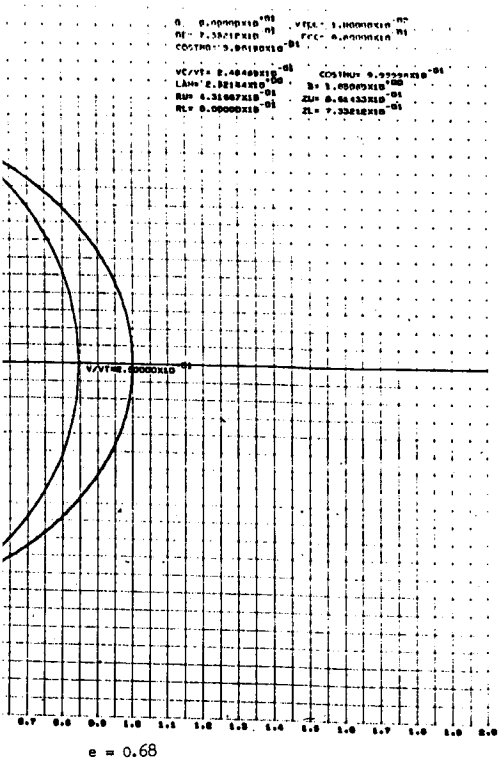

e = 0.68

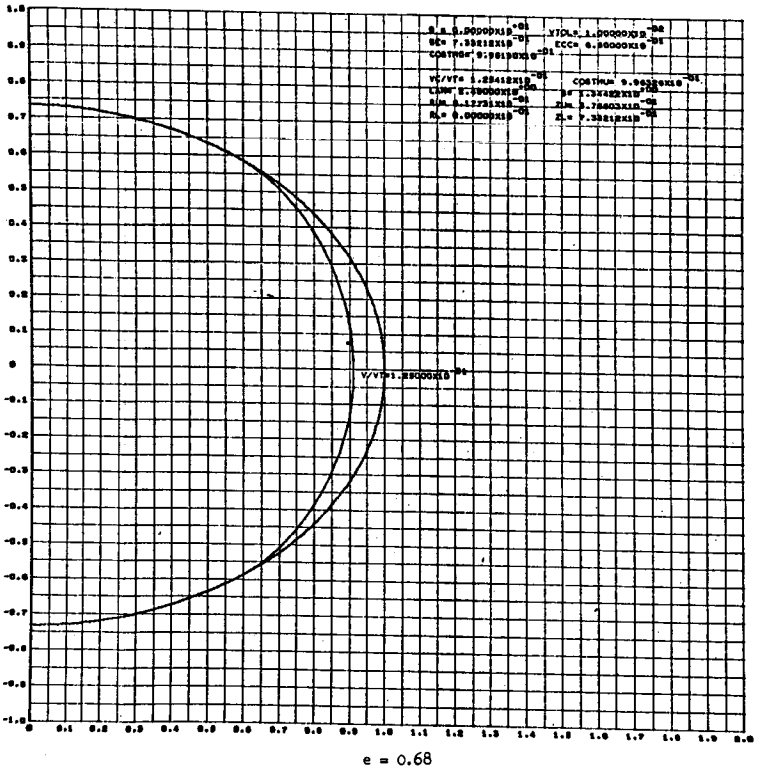

e = 0.68

0 for Tanks of Eccentricity 0.5 and 0.68

Figure 8b

FOLD-OUT #2

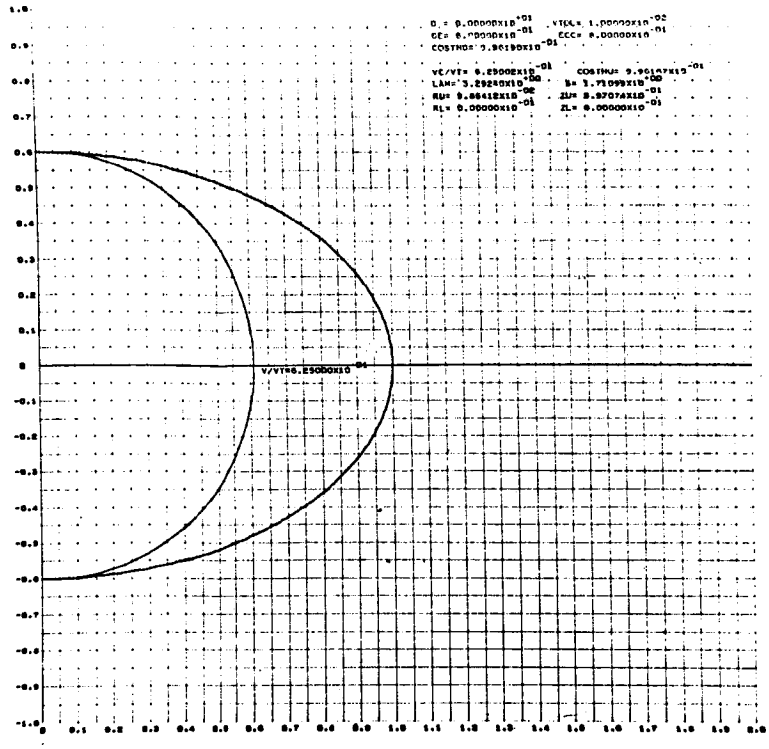

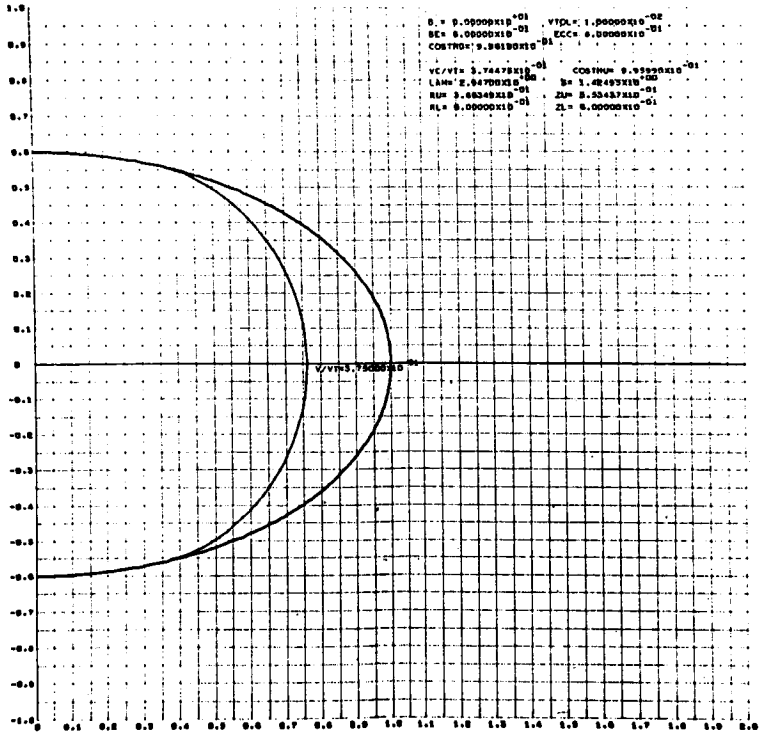

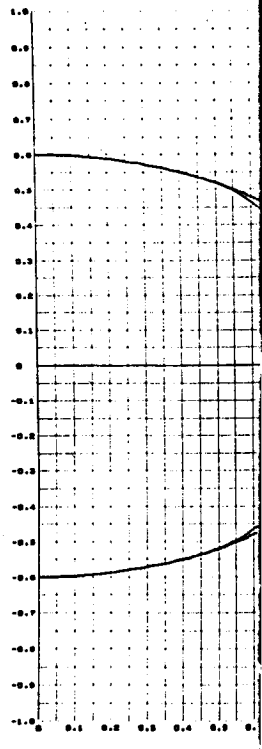

Meniscus Shapes at

FOLD-OUT #1

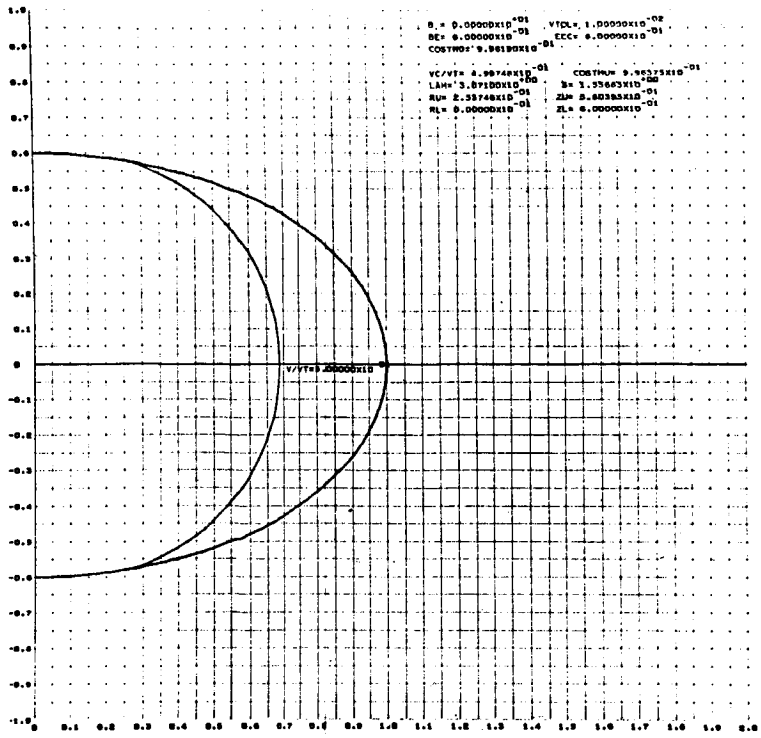

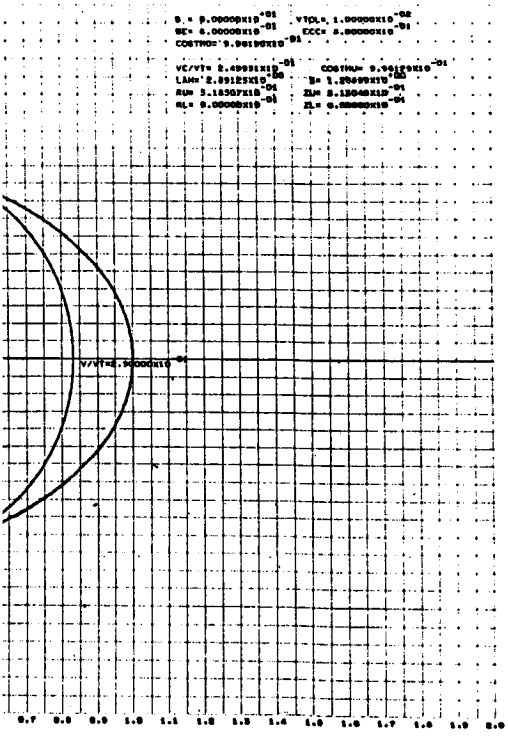

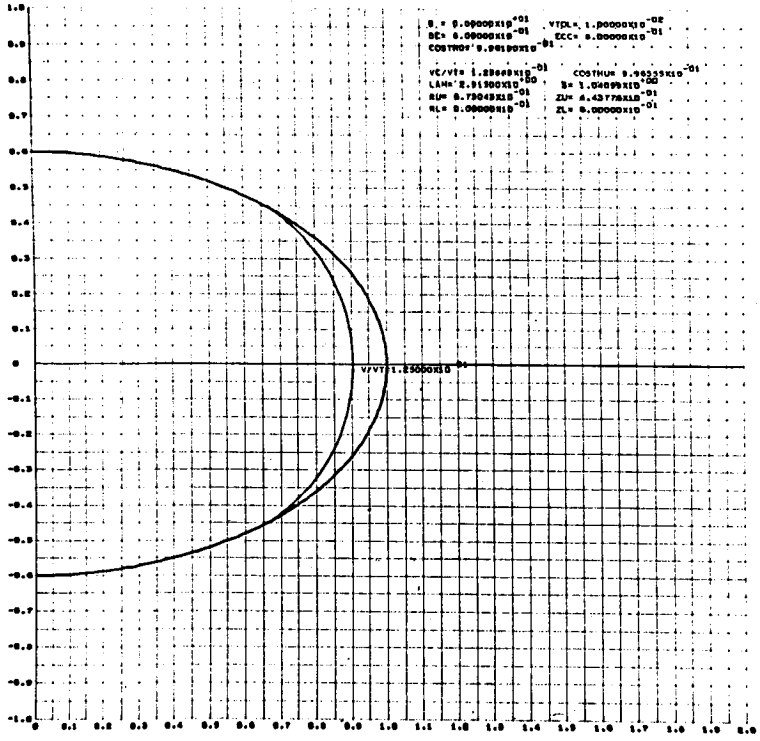

β_α = 0 for Tank of Eccentricity 0.8

Figure 8c

FOLD-OUT #2

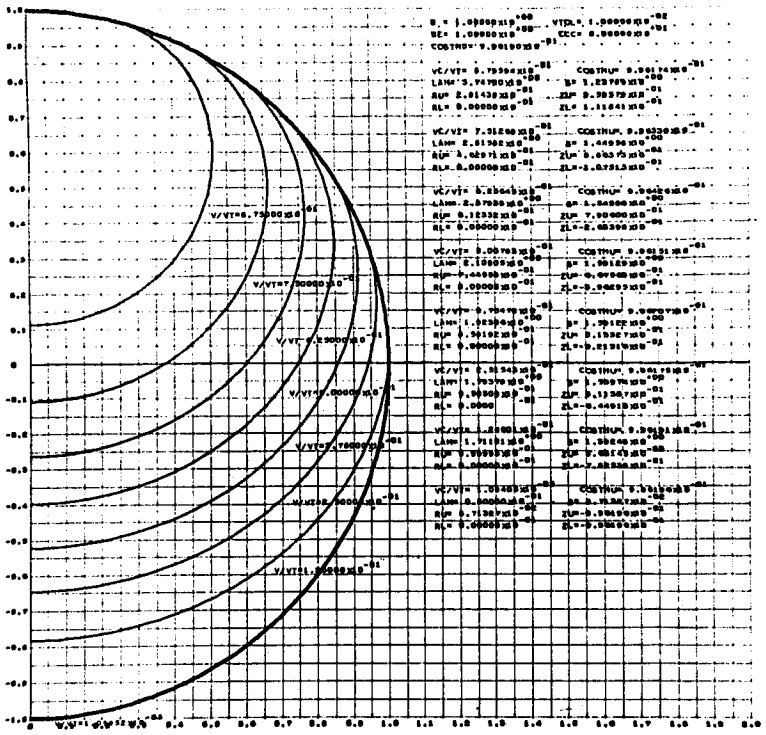

e = 0

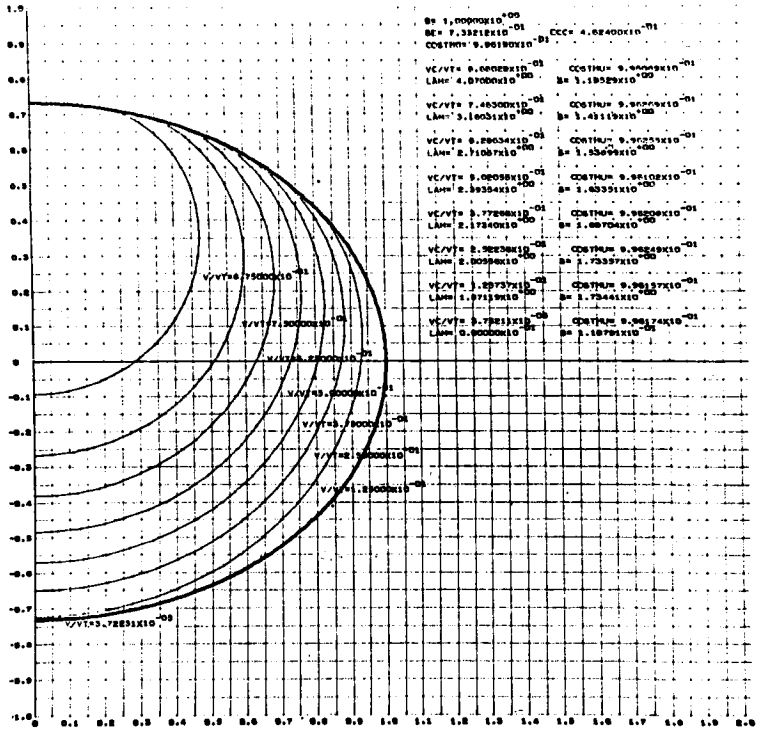

e = 0.68

Meniscus Shapes at B_α =

FOLD-OUT #1

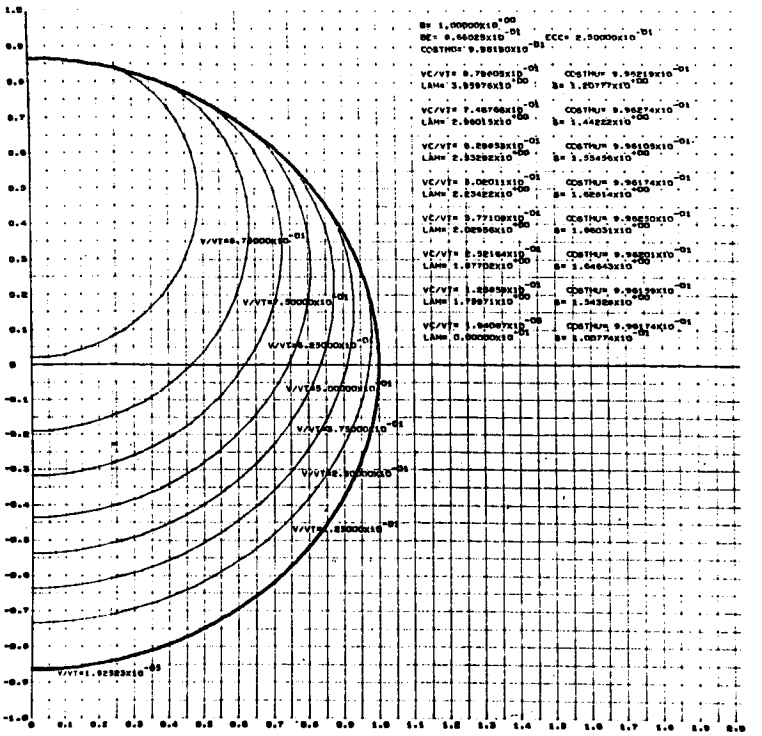

e = 0.5

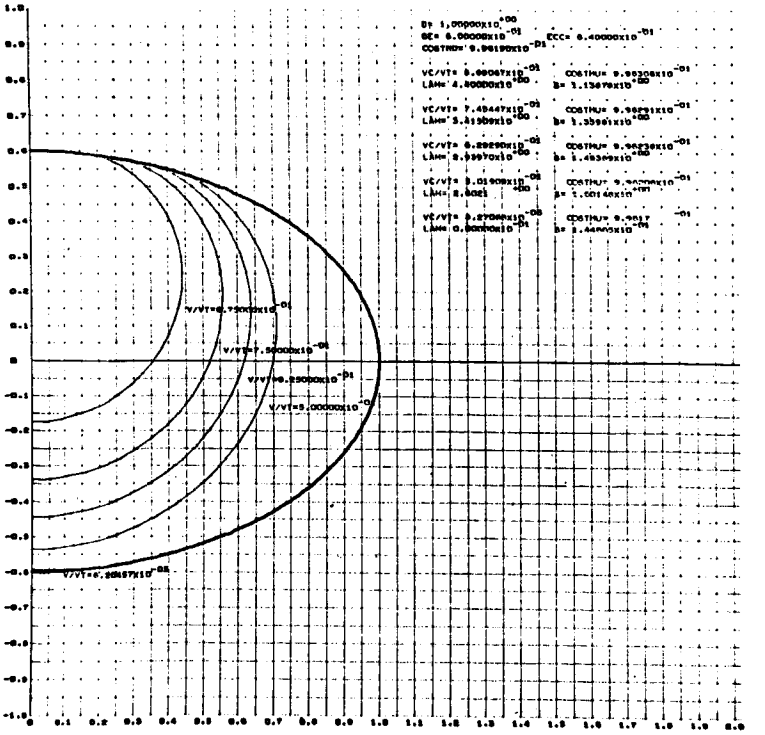

e = 0.8

l for Tanks of Eccentricity 0, 0.5, 0.68 and 0.8

Figure 9a

FOLD-OUT #2

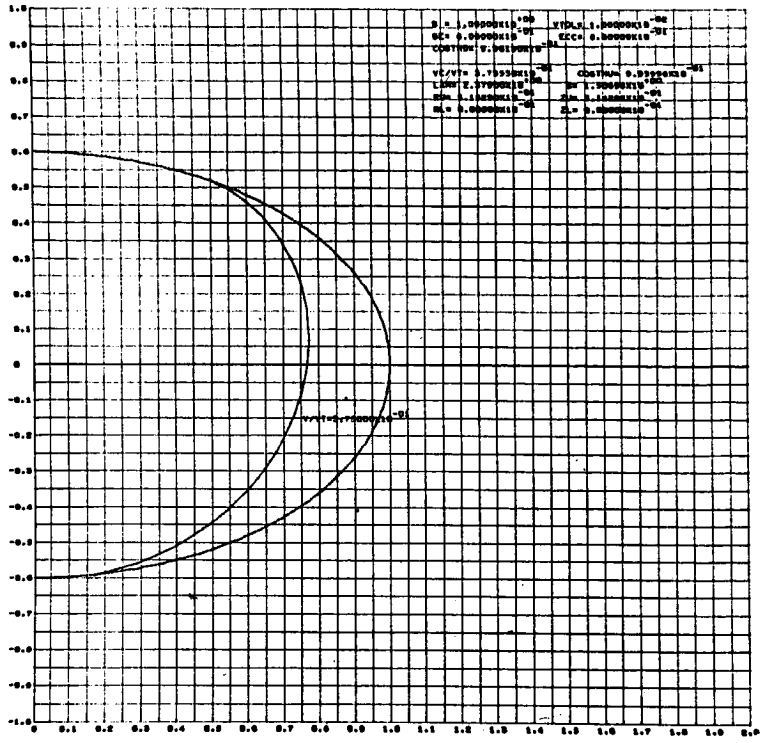

Mensicus Shapes at

FOLD-OUT
#1

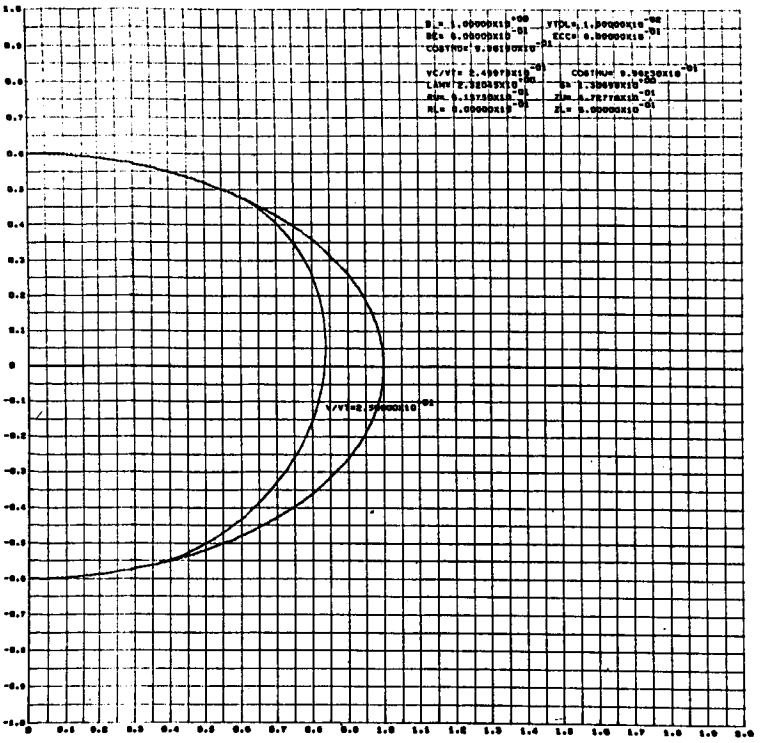

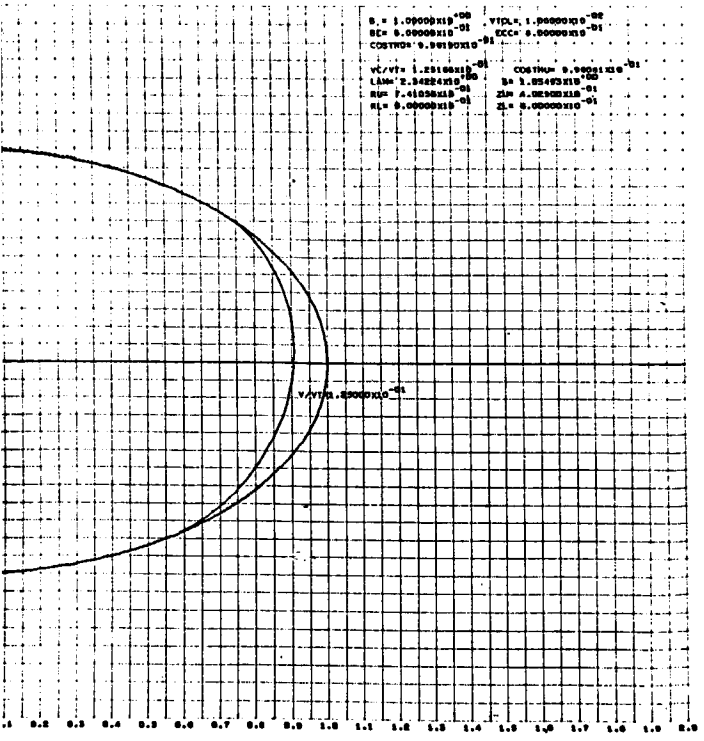

$\beta_\alpha = 1$ for Tank of Eccentricity 0.8

Figure 9b

FOLD-OUT #2

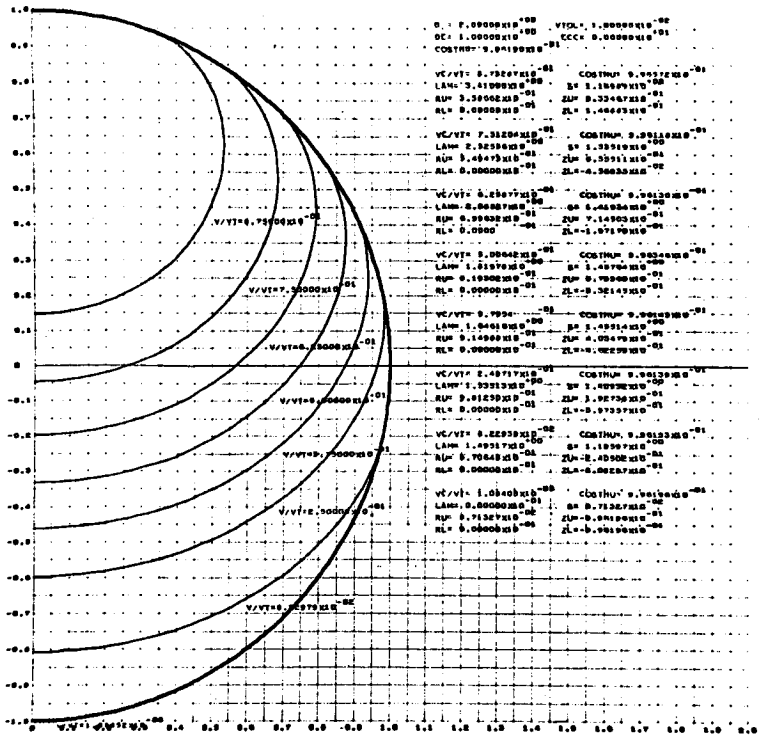

e = 0

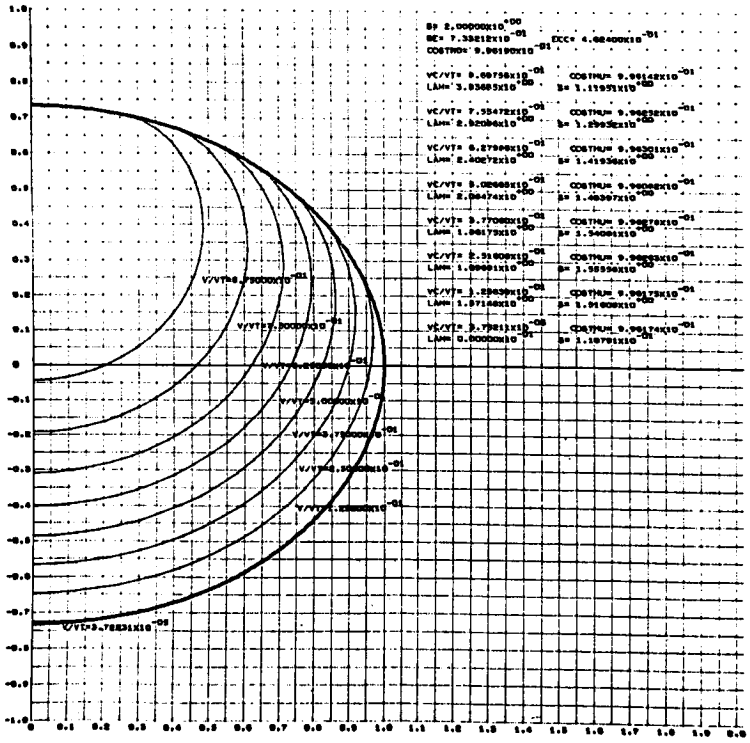

e = 0.68

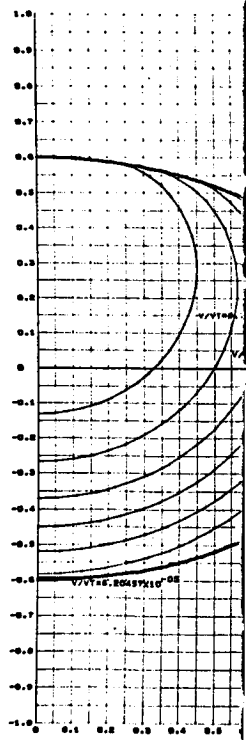

Meniscus Shapes at $B_\alpha = 2$

FOLD-OUT
#1

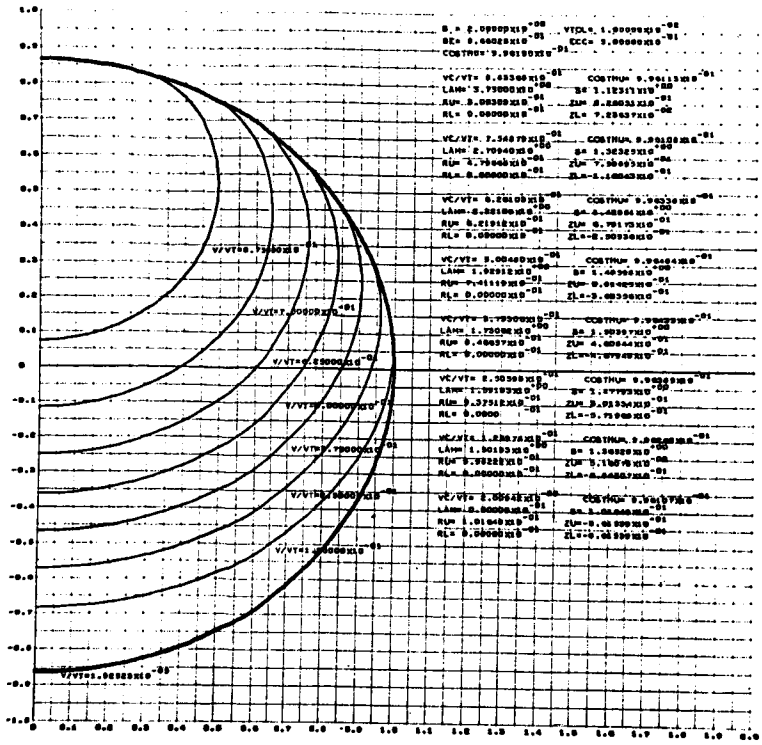

e = 0.5

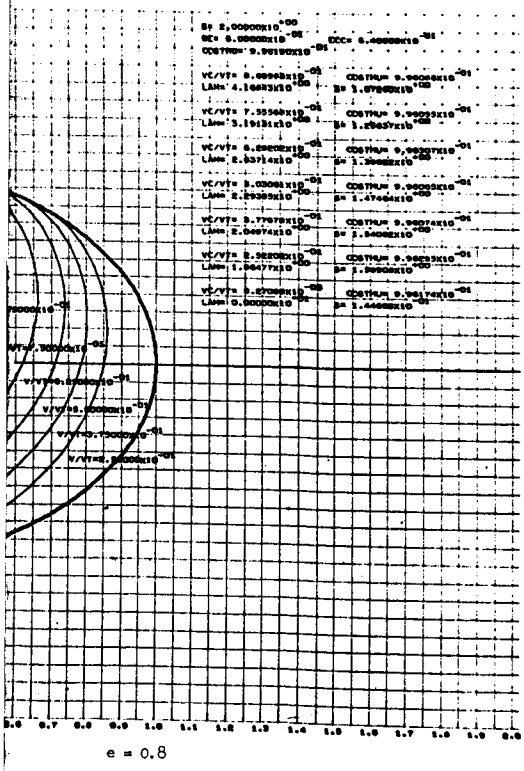

e = 0.8

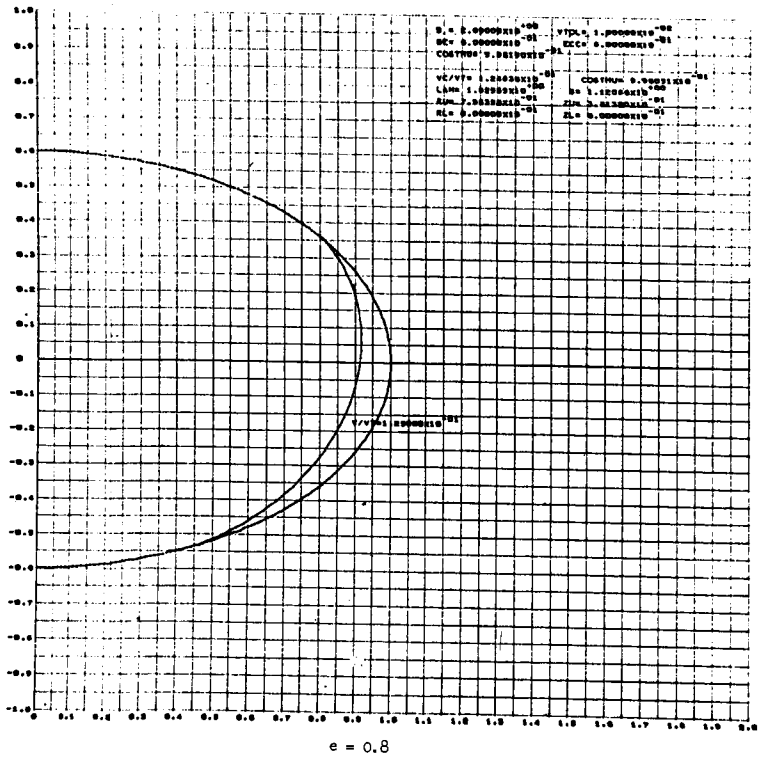

e = 0.8

for Tanks of Eccentricity 0, 0.5, 0.68 and 0.8

Figure 10

FOLD-OUT #2

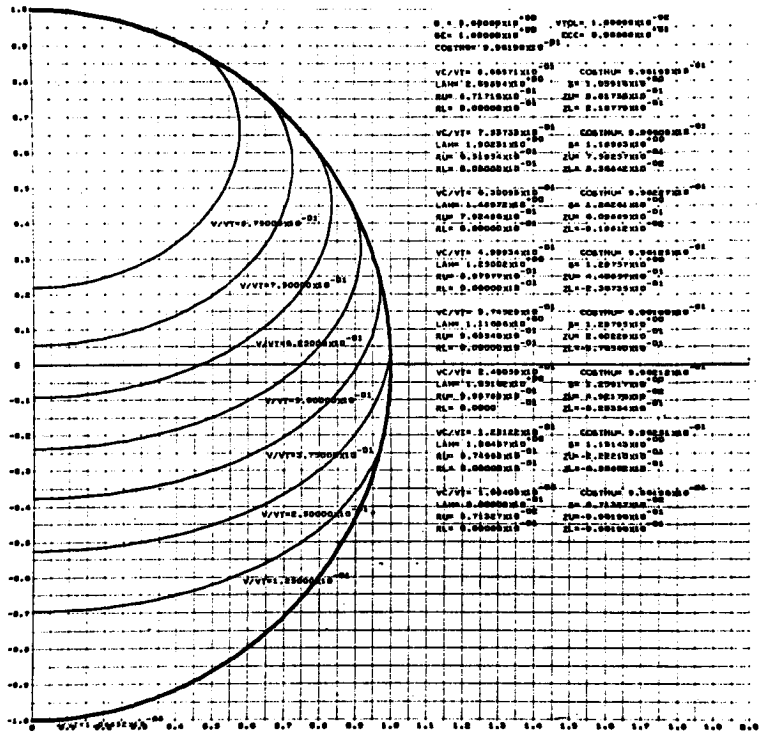

e = 0

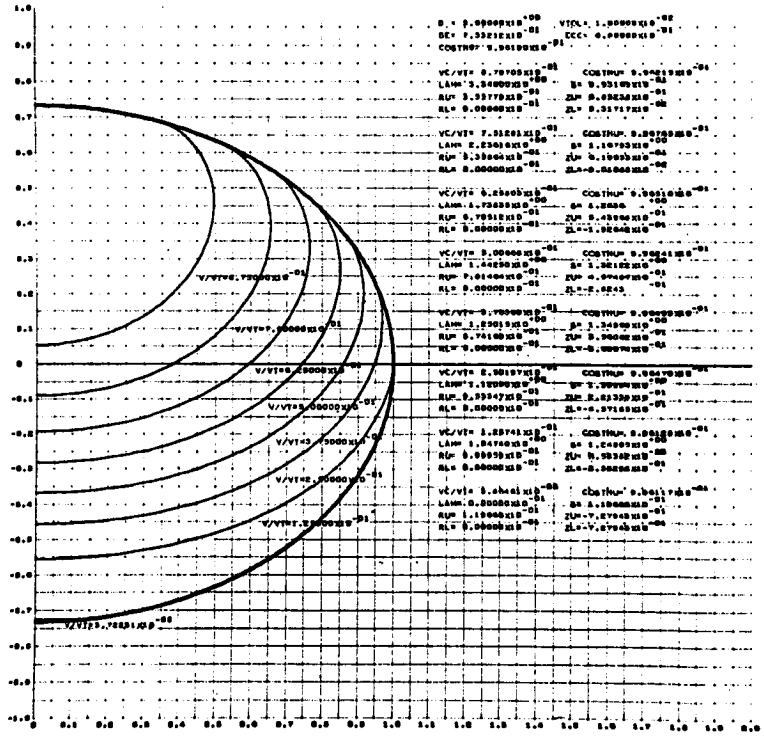

e = 0.68

Meniscus Shapes at $B_\alpha = 5$ for Ta

F

FOLD-OUT
#1

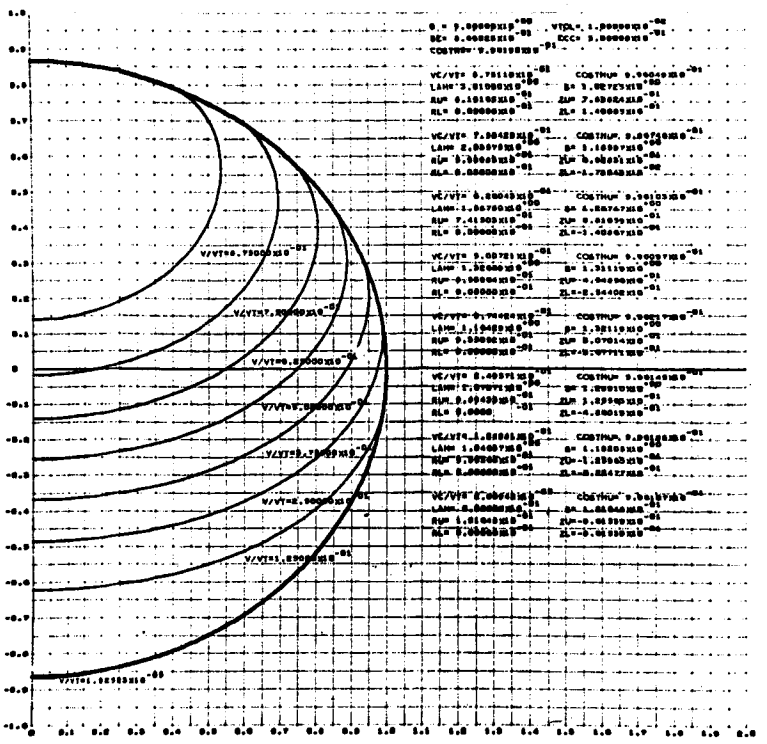

e = 0.5

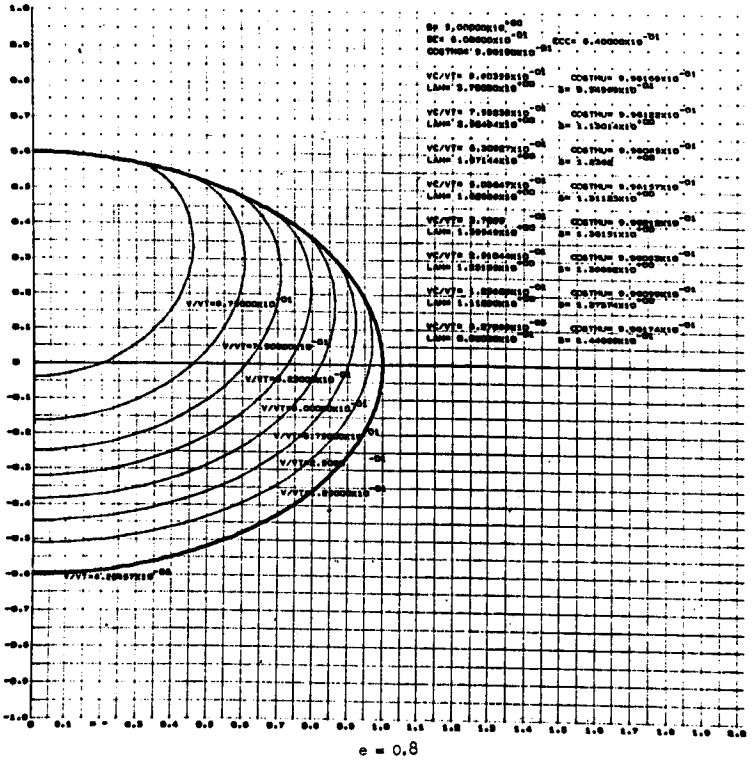

e = 0.8

nks of Eccentricity 0, 0.5, 0.68 and 0.8

igure 11

FOLD-OUT
#2

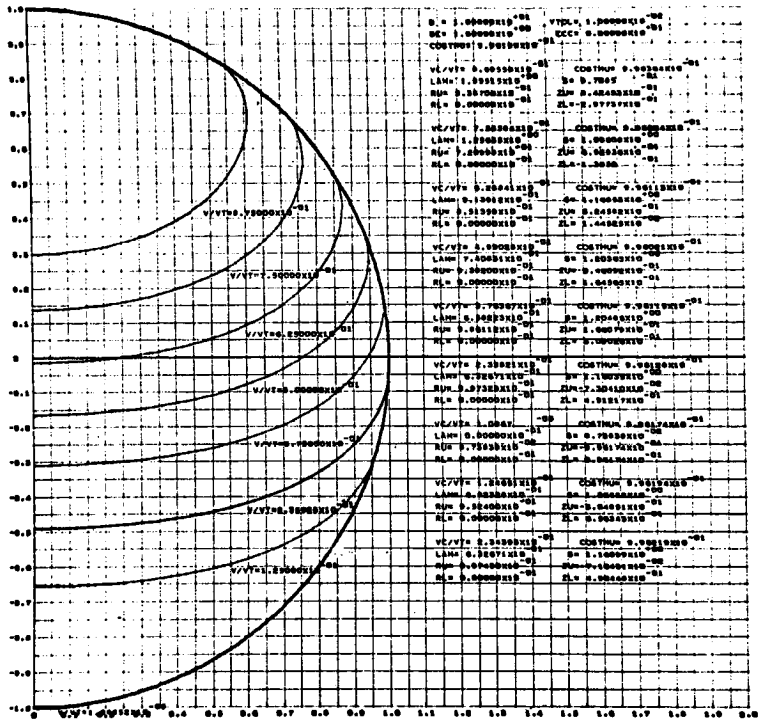

e = 0

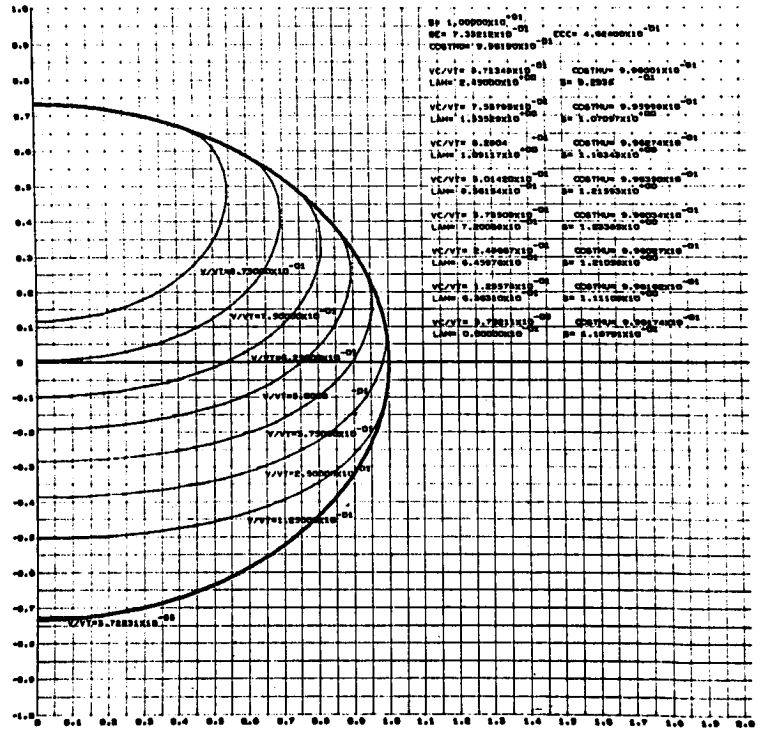

e = 0.68

Meniscus Shapes at B_α = 10 fo

FOLD-OUT
#1

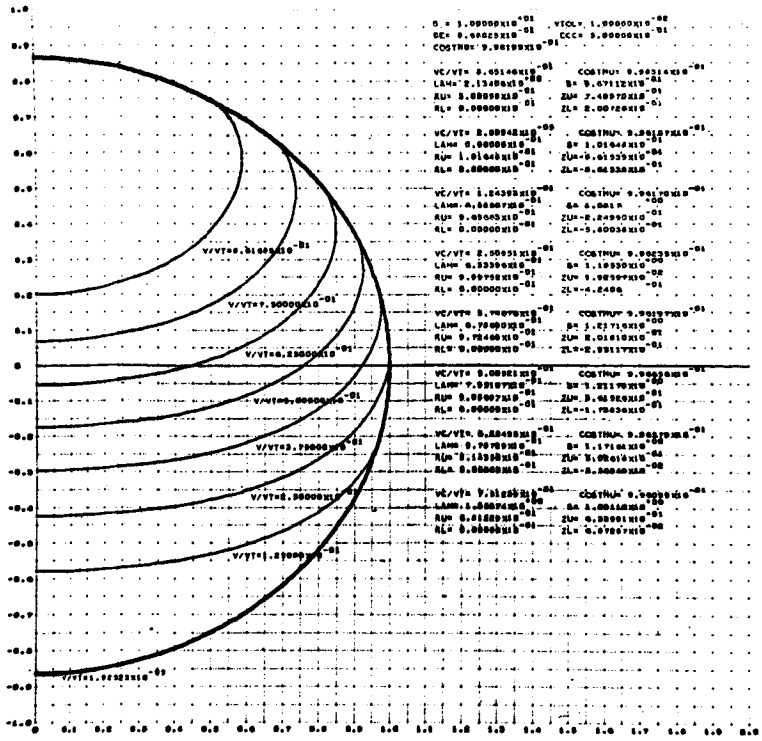

e = 0.5

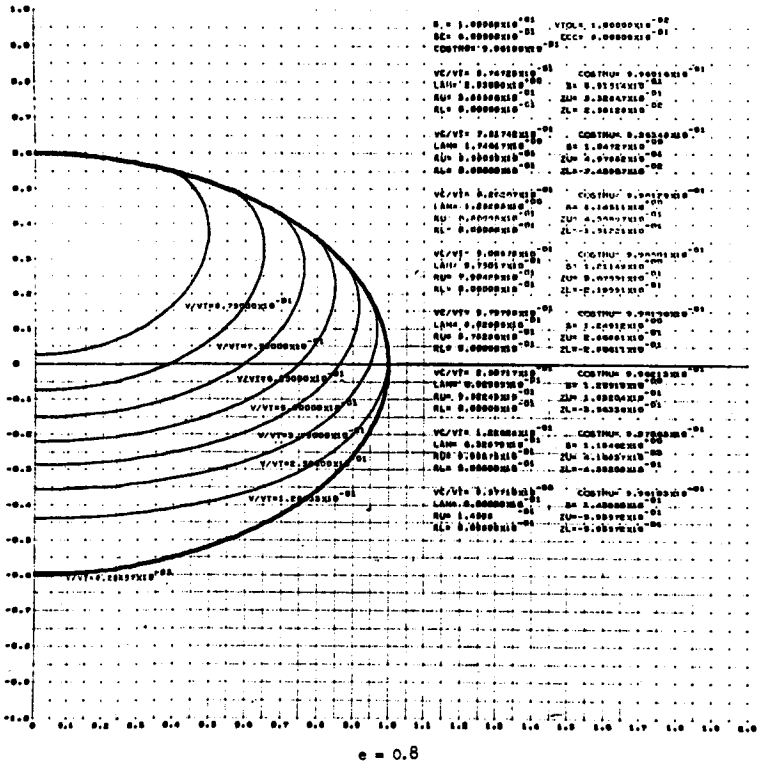

e = 0.8

or Tanks of Eccentricity 0, 0.5, 0.68 and 0.8

Figure 12

FOLD-OUT #2

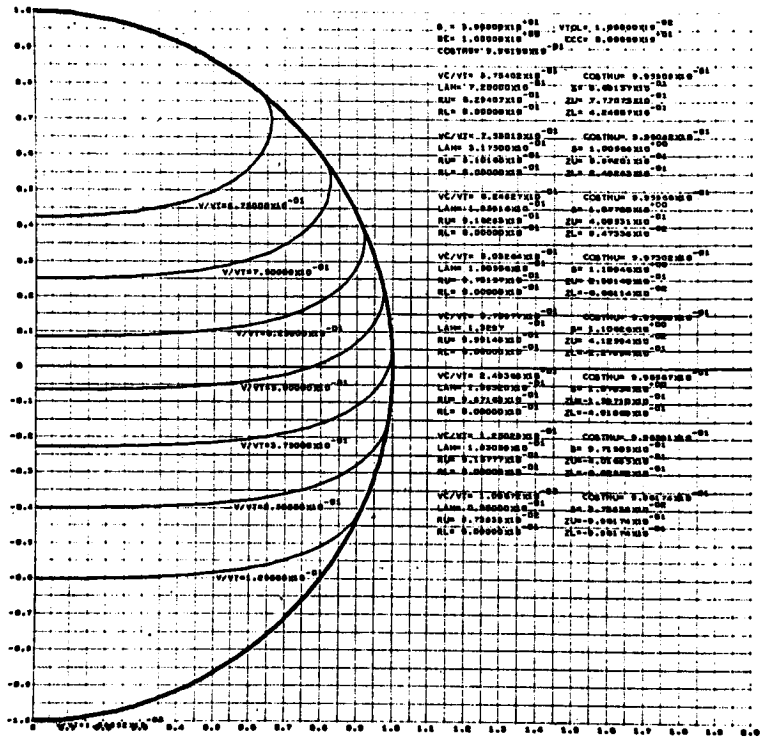

e = 0

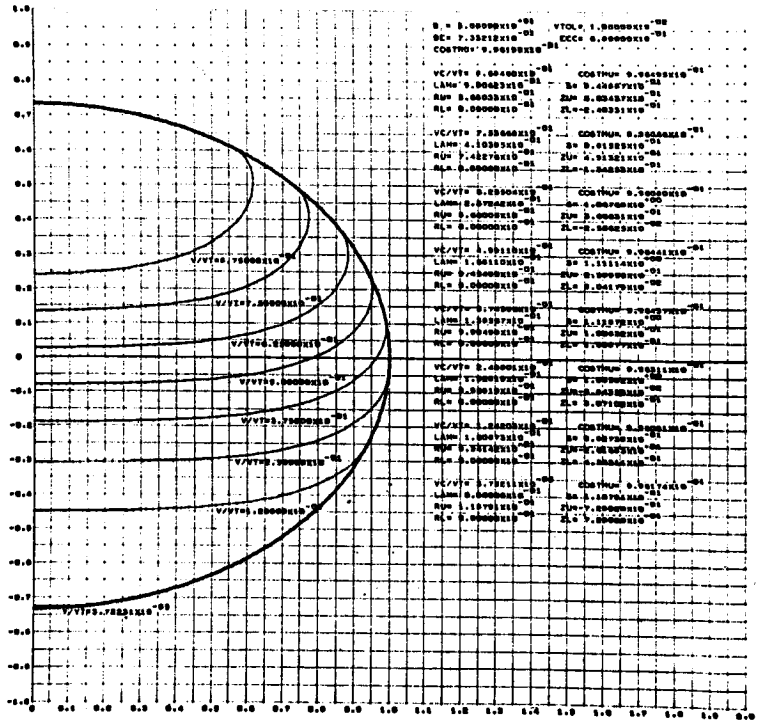

e = 0.68

Meniscus Shapes at $B_\alpha = 30$

FOLD-OUT #1

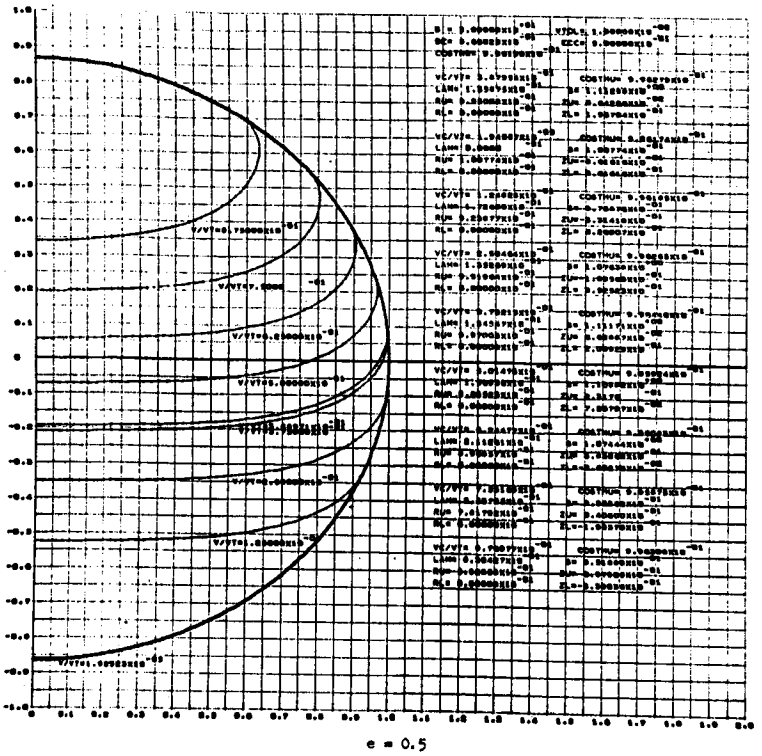

e = 0.5

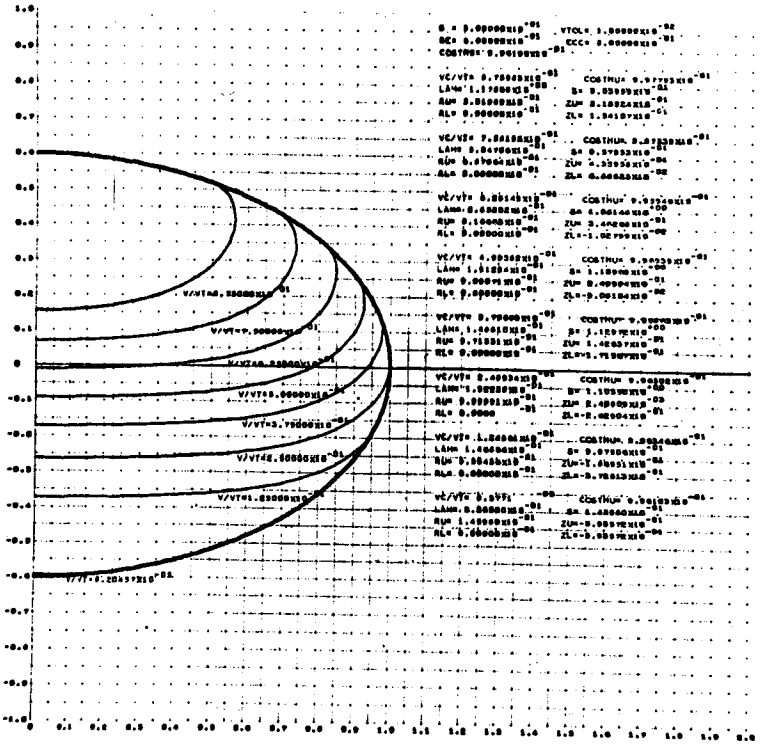

e = 0.8

for Tanks of Eccentricity 0, 0.5, 0.68 and 0.8

Figure 13

FOLD-OUT #2

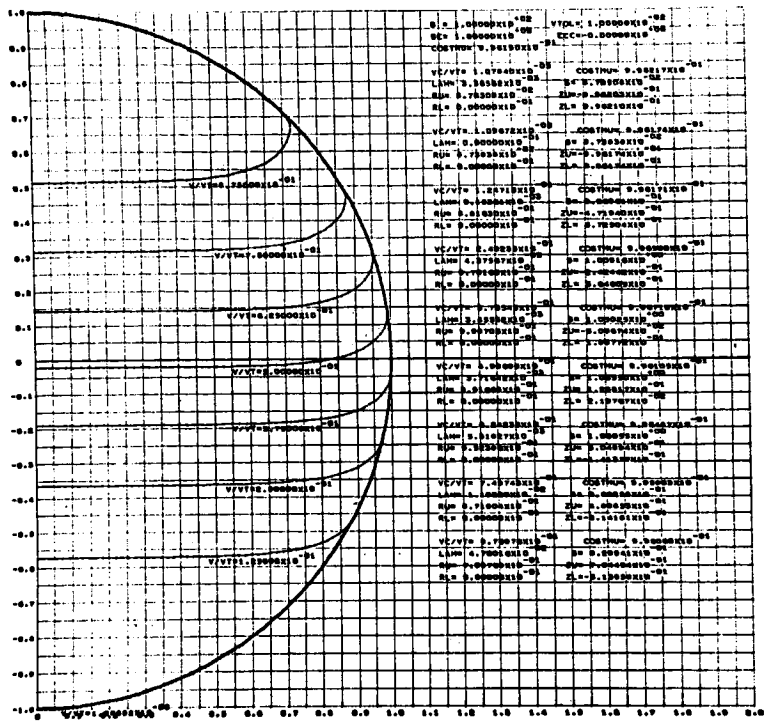

e = 0

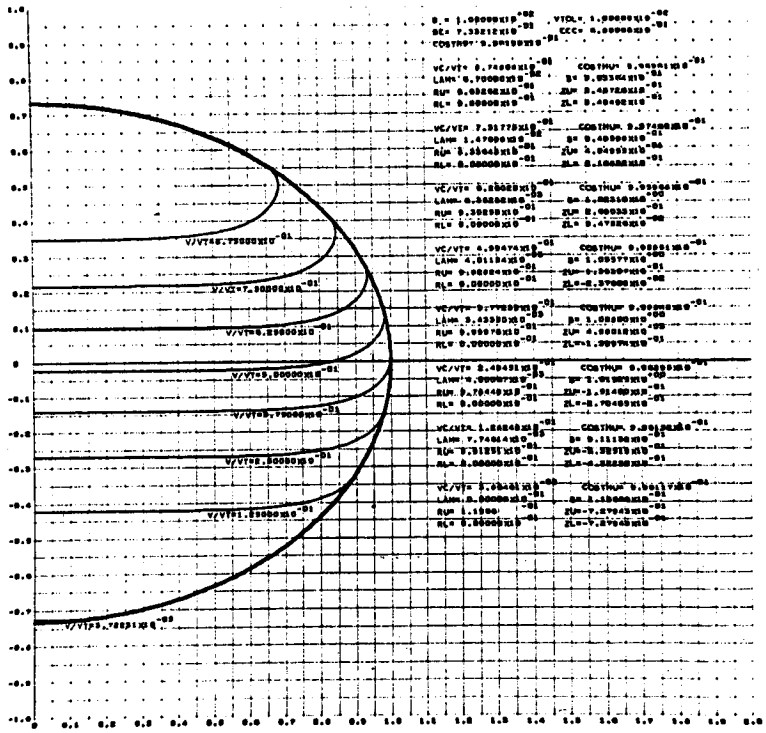

e = 0.68

Meniscus Shapes at B_α = 100

FOLD-OUT #1

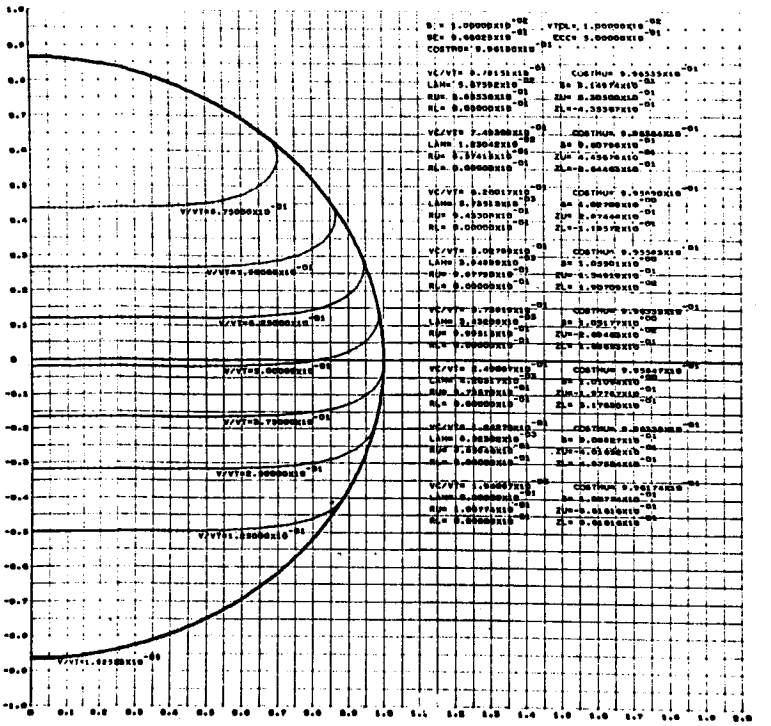

e = 0.5

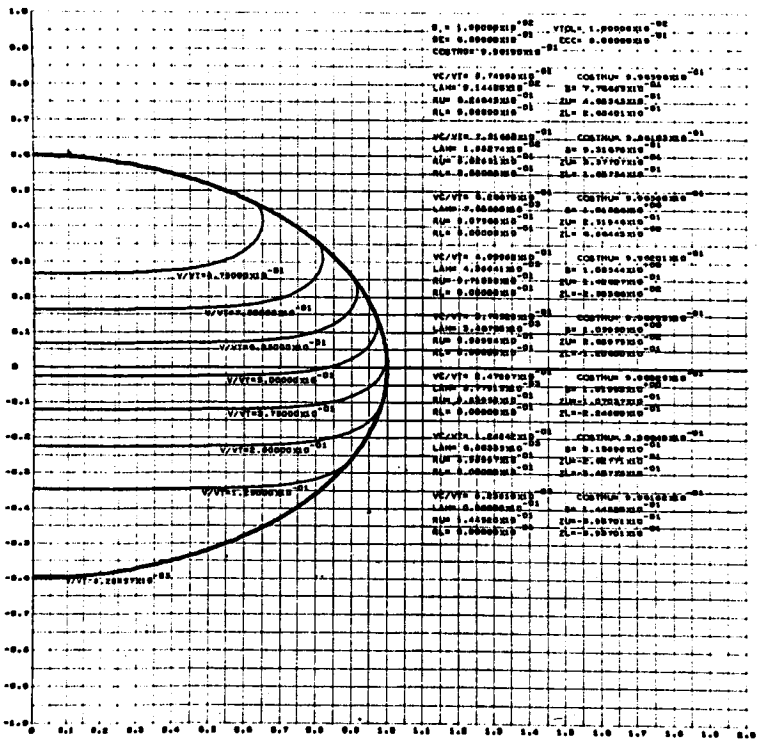

e = 0.8

for Tanks of Eccentricity 0, 0.5, 0.68 and 0.8

Figure 14

FOLD-OUT #2

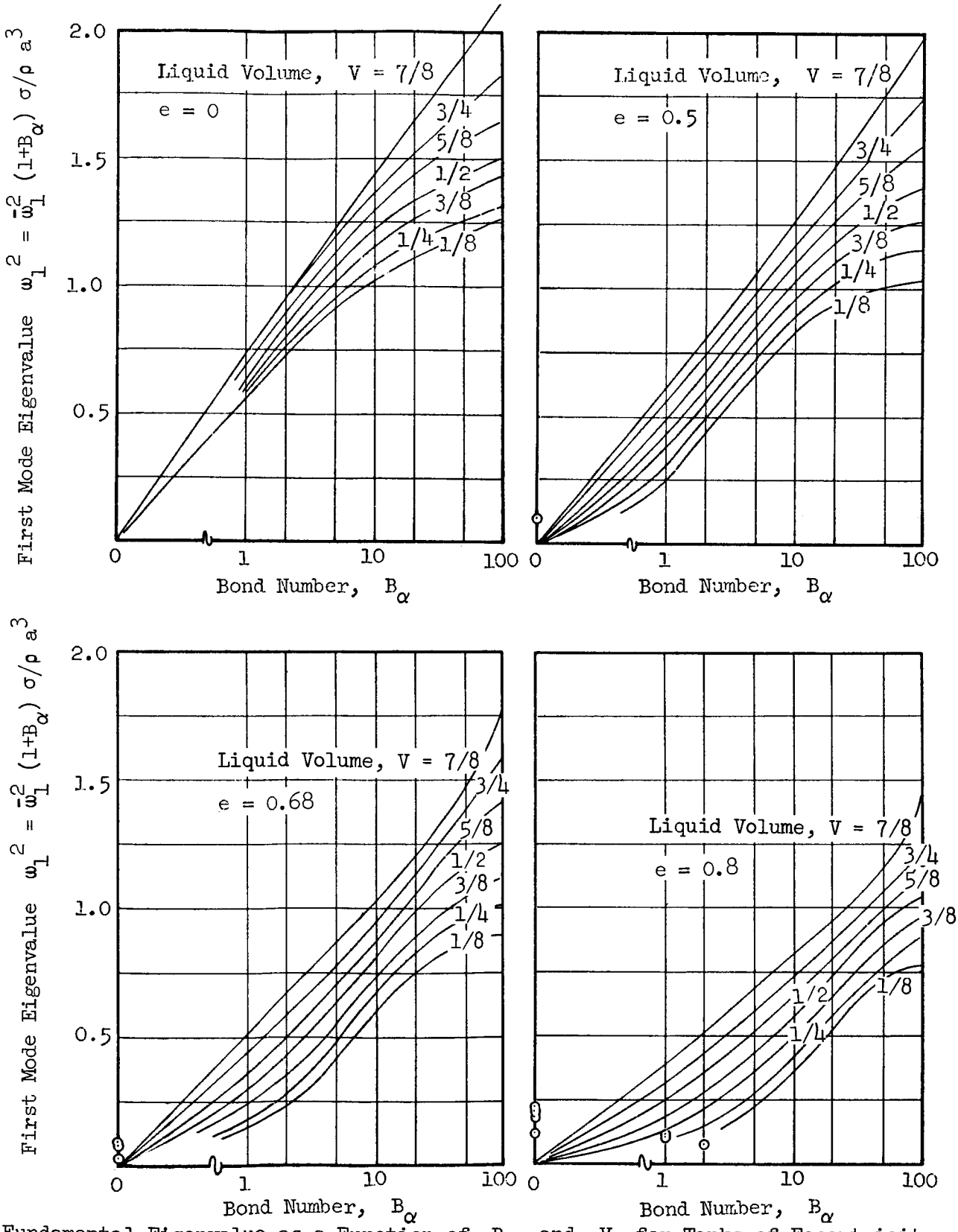

Fundamental Eigenvalue as a Function of B_α and V for Tanks of Eccentricity 0, 0.5, 0.68, and 0.8 (Two circle eigenvalues are circled)

Figure 15

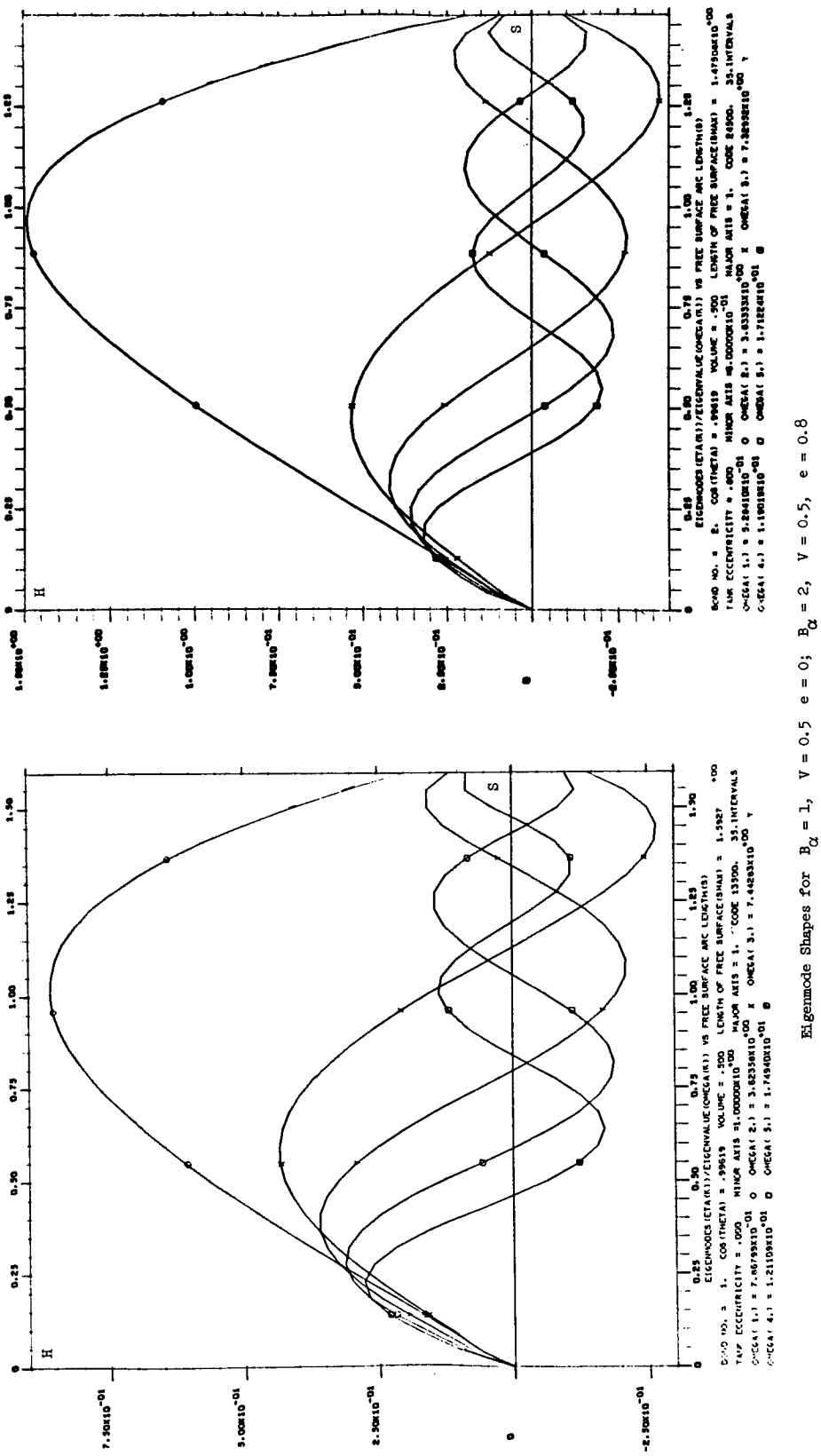

Eigenmode Shapes for $B_\alpha = 1$, V = 0.5 e = 0; $B_\alpha = 2$, V = 0.5, e = 0.8

Figure 16

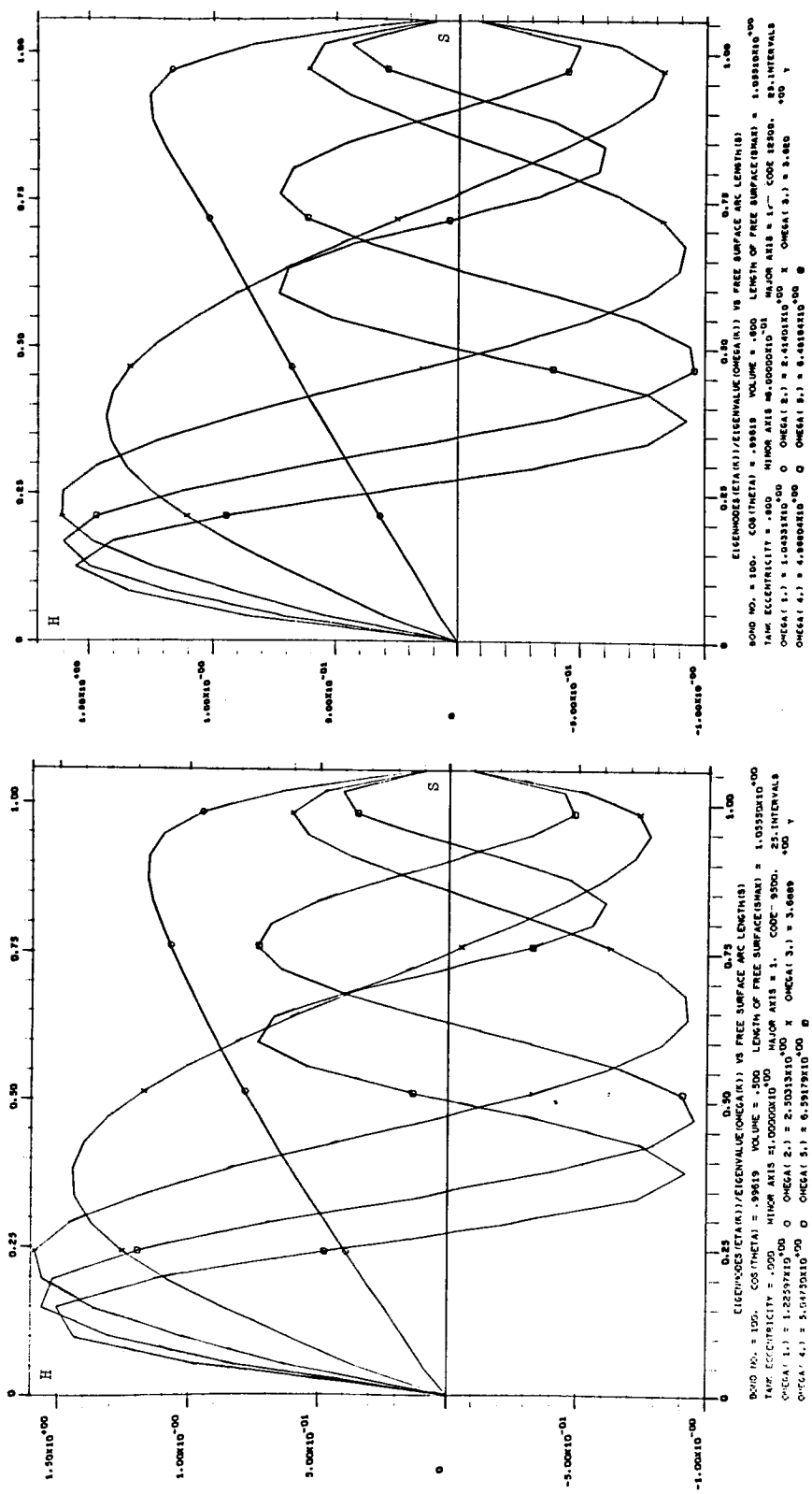

Eigenmode Shapes for $B_\alpha = 100$, V = 0.5, e = 0 and e = 0.8

Figure 17

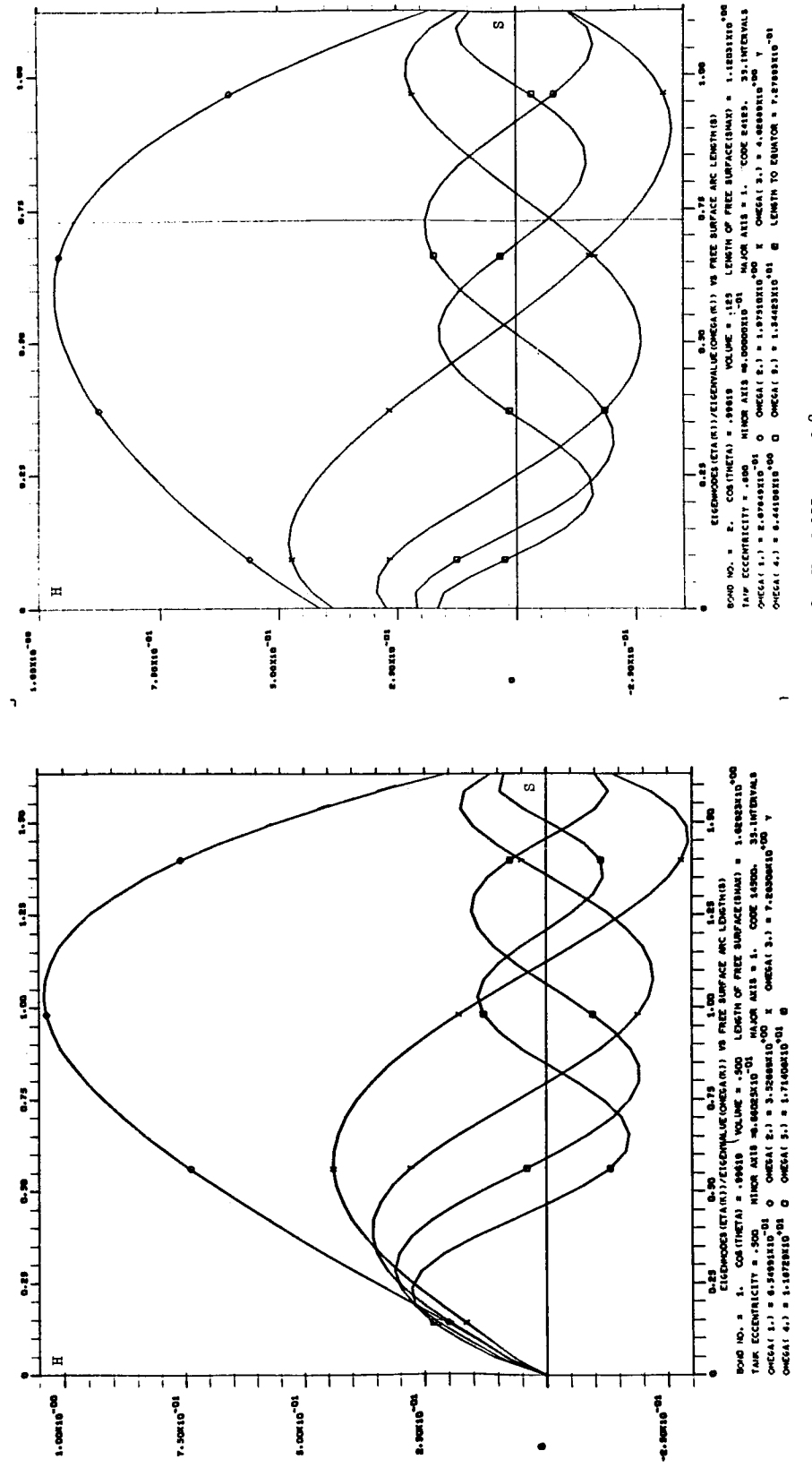

Eigenmode Shapes for $B_\alpha = 1$, V = 0.5, e = 0.5; $B_\alpha = 2$, V = 0.125, e = 0.8

Figure 18

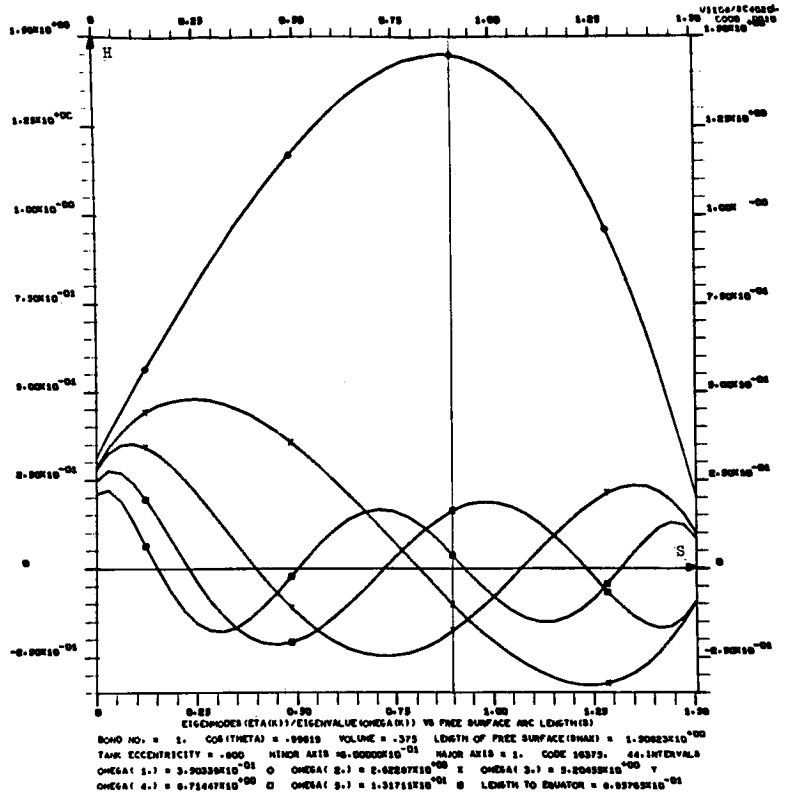

(a)

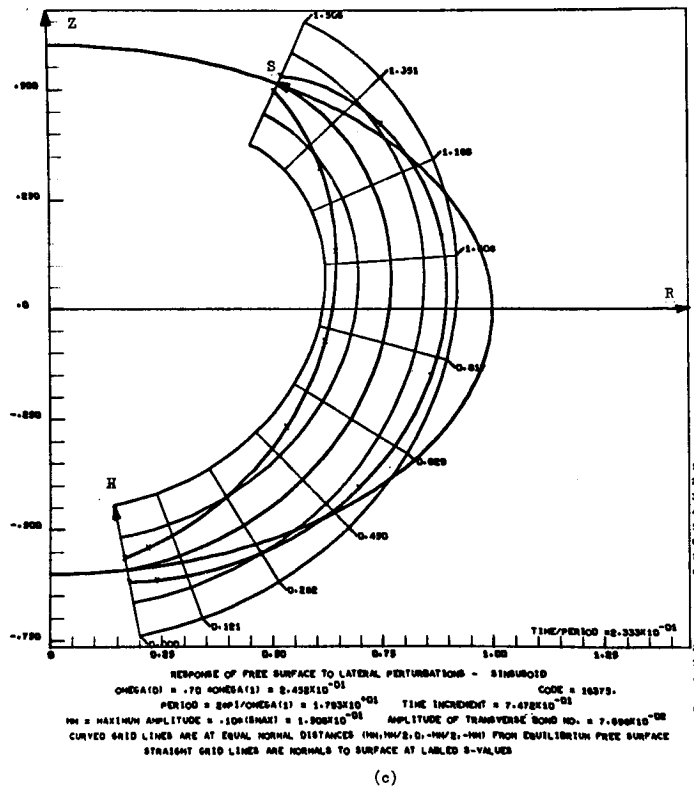

(c)

Liquid Response to Sinuso

$B_\alpha = 1, \quad V = 3/8,$

FOLD-OUT
#1

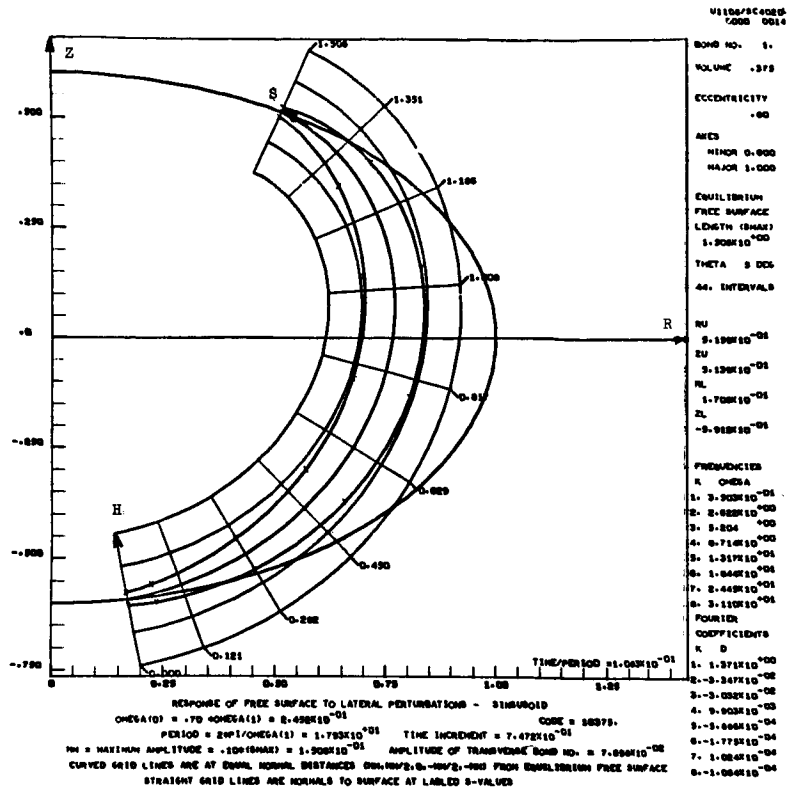

(b)

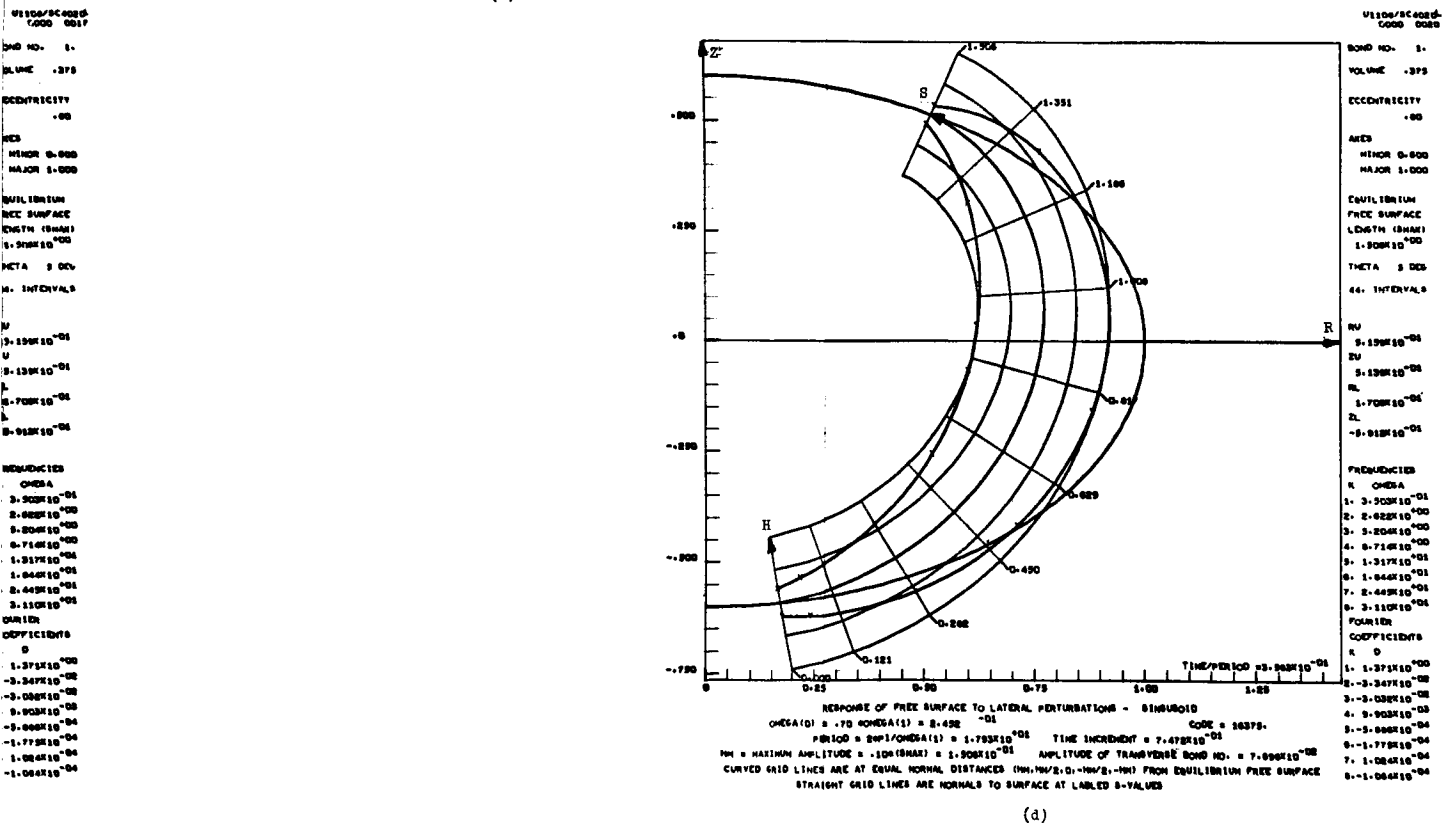

(d)

idal Lateral Perturbing Acceleration for

and $e = 0.8$, for $\omega_o/\omega_1 = 0.7$

Figure 19

FOLD-OUT #2

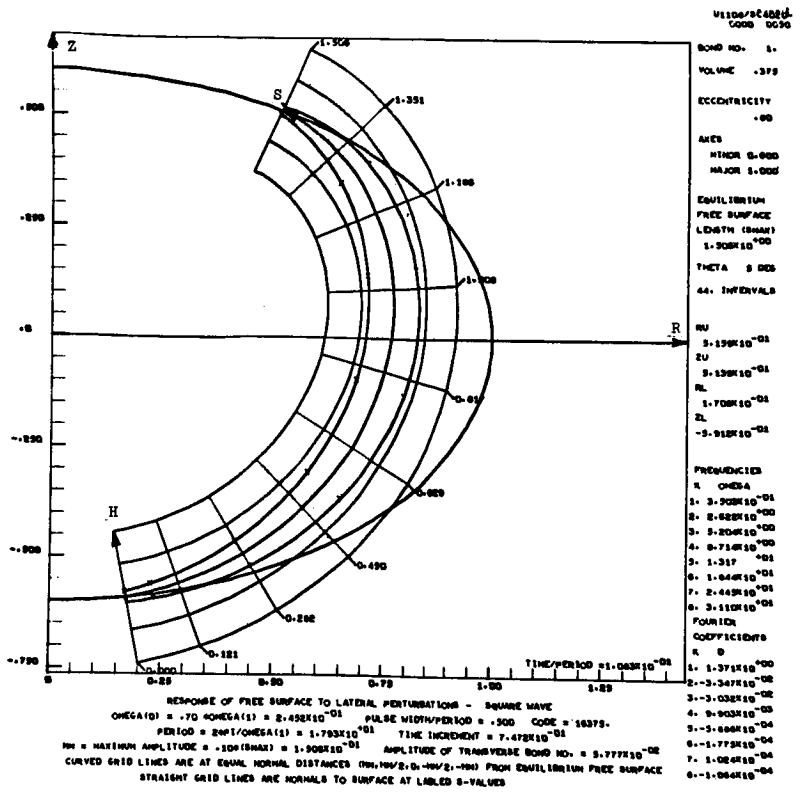

(a)

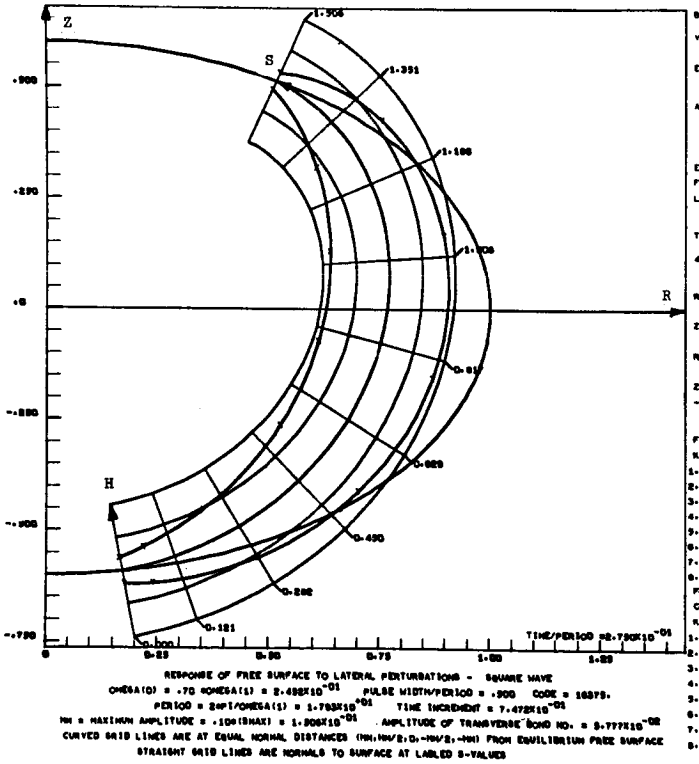

(c)

Liquid Response to Square

$B_\alpha = 1, \quad V = 3/8,$

FOLD-OUT #1

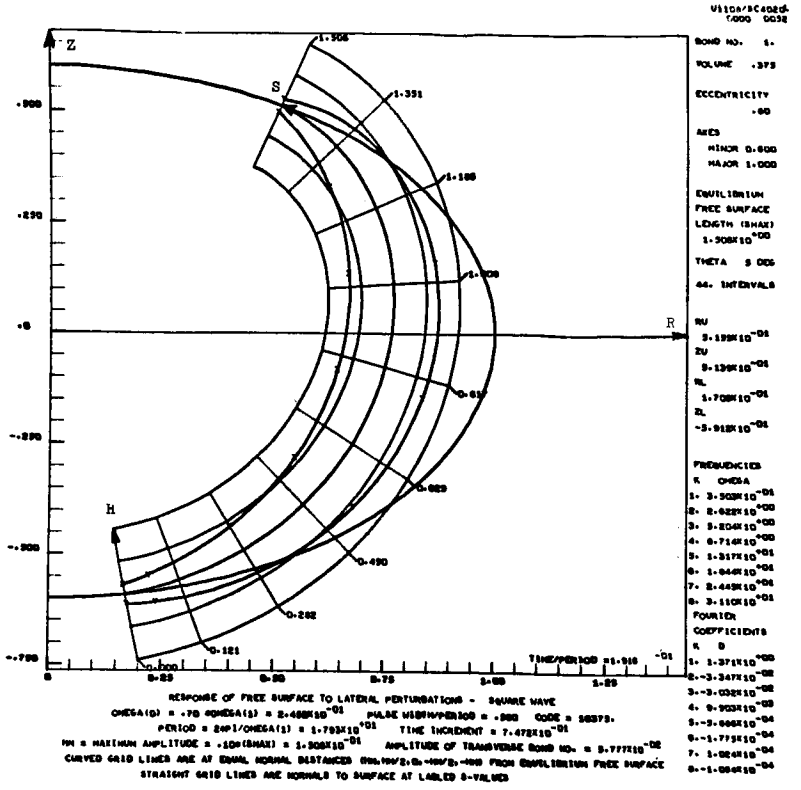

(b)

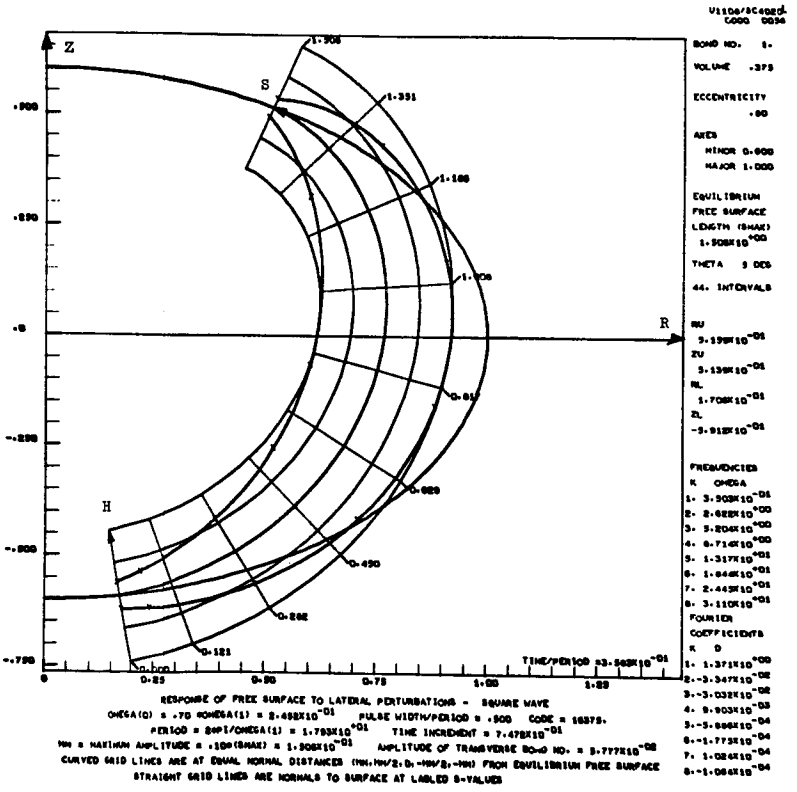

(a)

Wave Lateral Perturbing Acceleration for

and e = 0.8, for $\omega_o/\omega_1 = 0.7$

Figure 20

FOLD-OUT #2

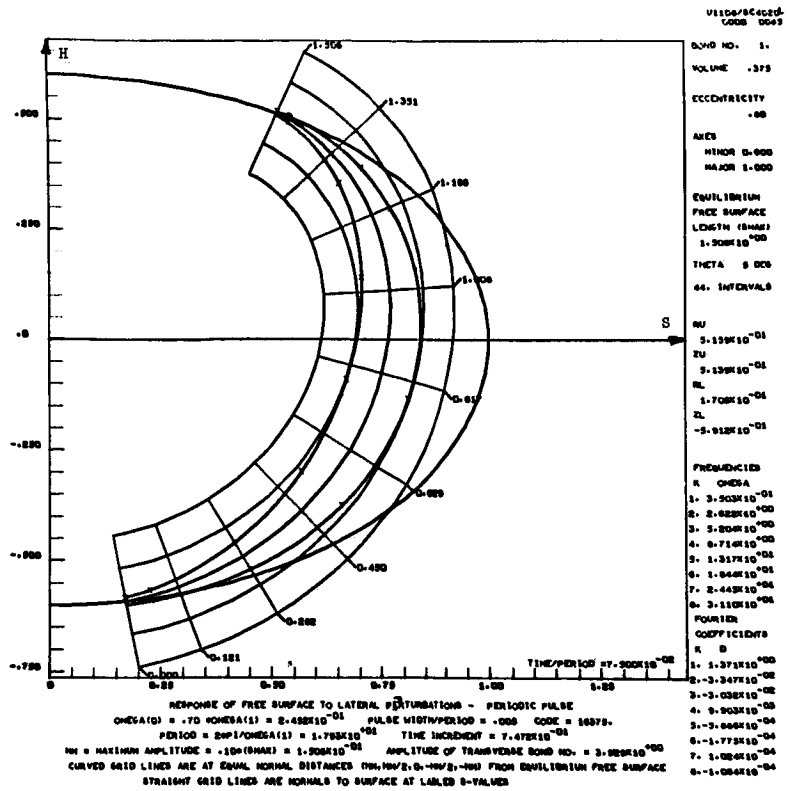

RESPONSE OF FREE SURFACE TO LATERAL PERTURBATIONS - PERIODIC PULSE
OMEGA(0) = .70 *OMEGA(1) = 2.452X10^-01 PULSE WIDTH/PERIOD = .000 CODE = 16379.
PERIOD = 2*PI/OMEGA(1) = 1.793X10^+01 TIME INCREMENT = 7.478X10^-01
MM = MAXIMUM AMPLITUDE = .10*(SMAX) = 1.508X10^-01 AMPLITUDE OF TRANSVERSE BOND NO. = 3.989X10^00
CURVED GRID LINES ARE AT EQUAL NORMAL DISTANCES (MM,MM/2.0,-MM/2.0,-MM) FROM EQUILIBRIUM FREE SURFACE
STRAIGHT GRID LINES ARE NORMALS TO SURFACE AT LABLED S-VALUES

(a)

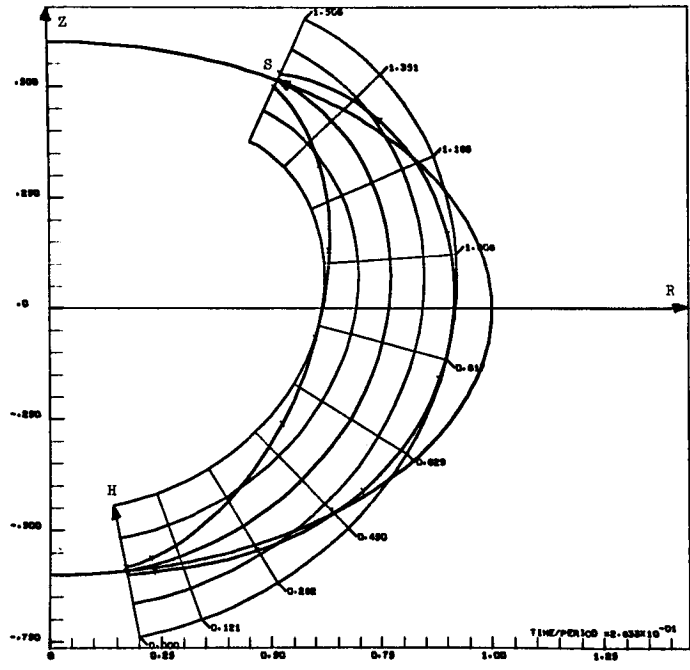

RESPONSE OF FREE SURFACE TO LATERAL PERTURBATIONS - PERIODIC PULSE
OMEGA(0) = .70 *OMEGA(1) = 2.452X10^-01 PULSE WIDTH/PERIOD = .000 CODE = 16379.
PERIOD = 2*PI/OMEGA(1) = 1.793X10^+01 TIME INCREMENT = 7.478X10^-01
MM = MAXIMUM AMPLITUDE = .10*(SMAX) = 1.508X10^-01 AMPLITUDE OF TRANSVERSE BOND NO. = 3.989X10^00
CURVED GRID LINES ARE AT EQUAL NORMAL DISTANCES (MM,MM/2.0,-MM/2.0,-MM) FROM EQUILIBRIUM FREE SURFACE
STRAIGHT GRID LINES ARE NORMALS TO SURFACE AT LABLED S-VALUES

(c)

Liquid Response to Periodic P

$B_\alpha = 1$, V = 3/8, a

FOLD-OUT
#1

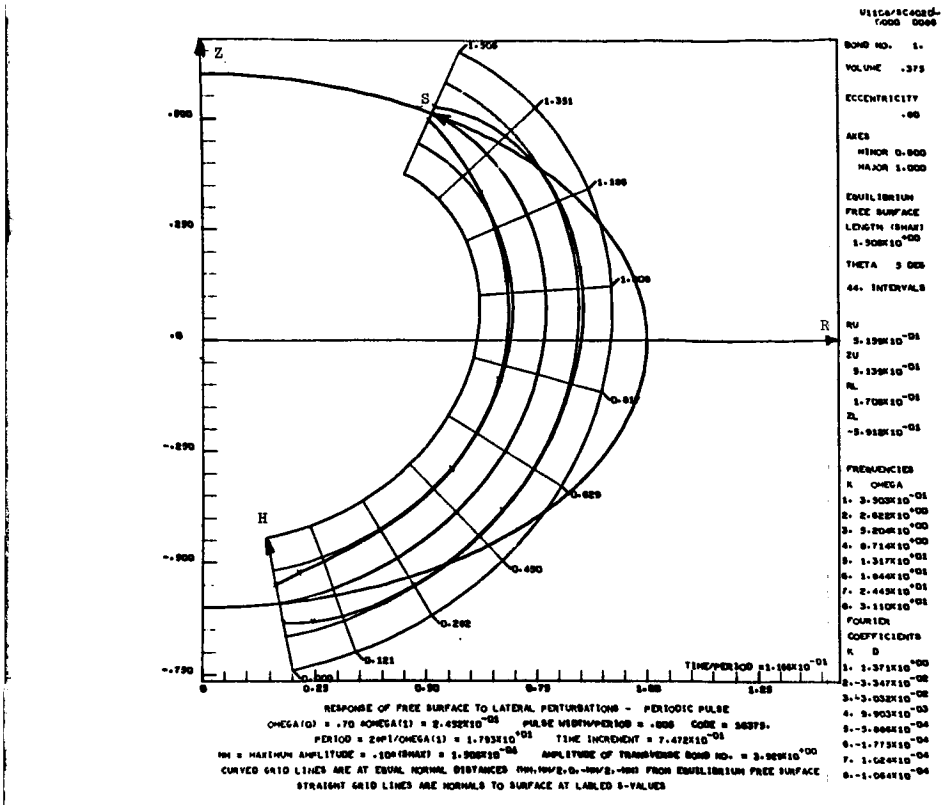

(b)

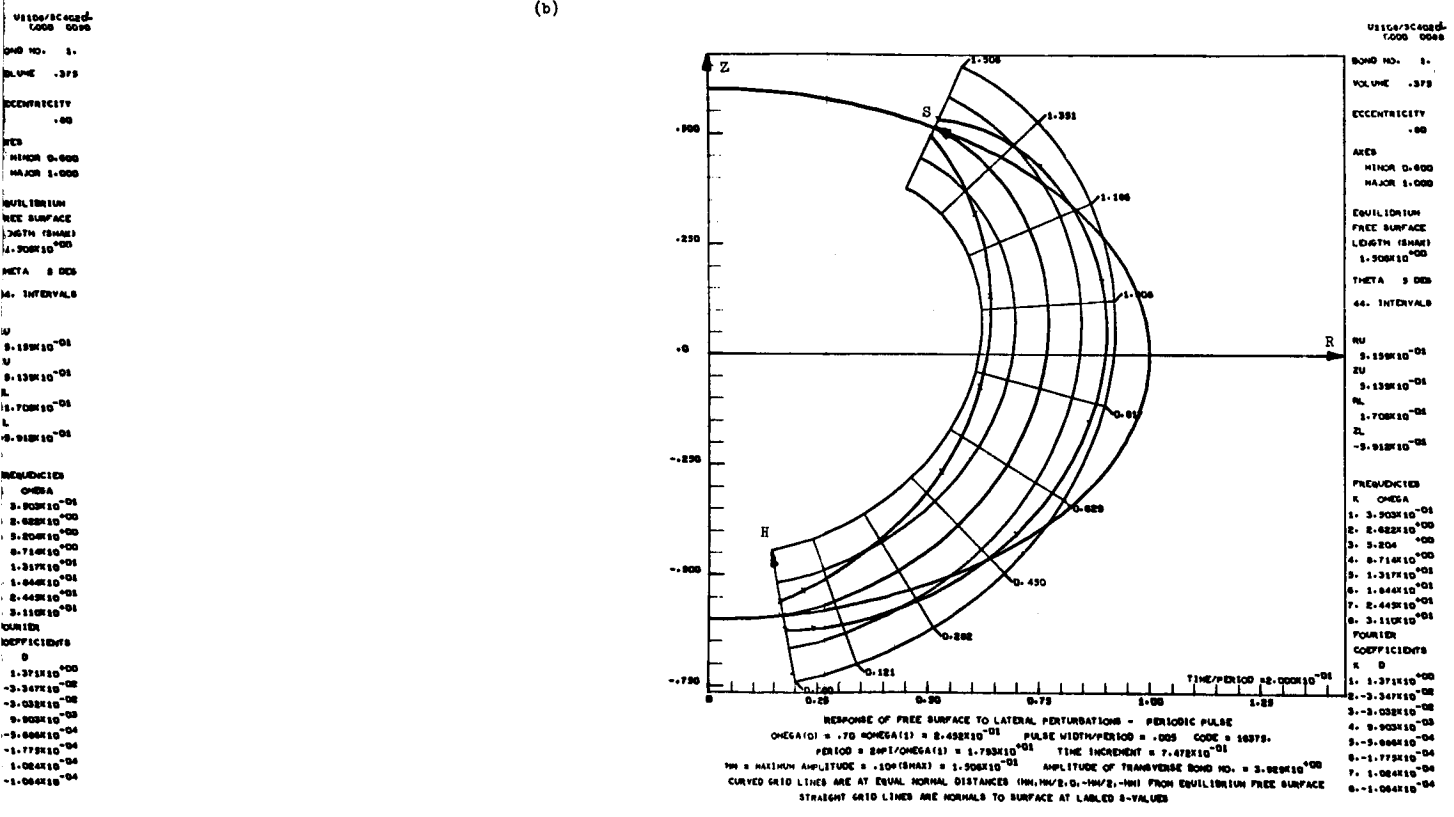

(d)

ulse Lateral Perturbing Acceleration for

nd e = 0.8 for $\omega_o/\omega_1 = 0.7$

Figure 21

FOLD-OUT #2

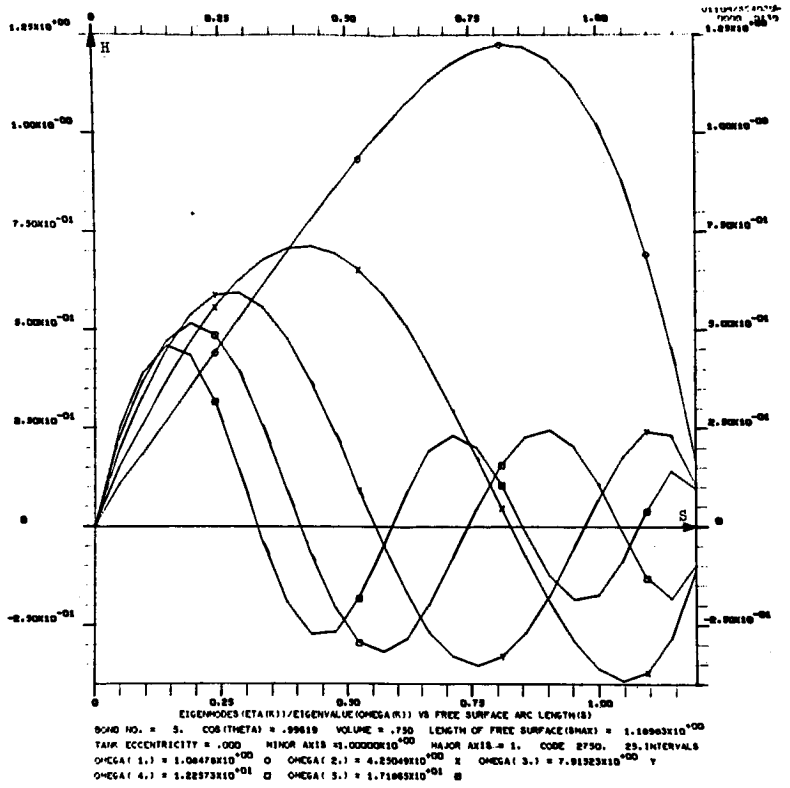

(a)

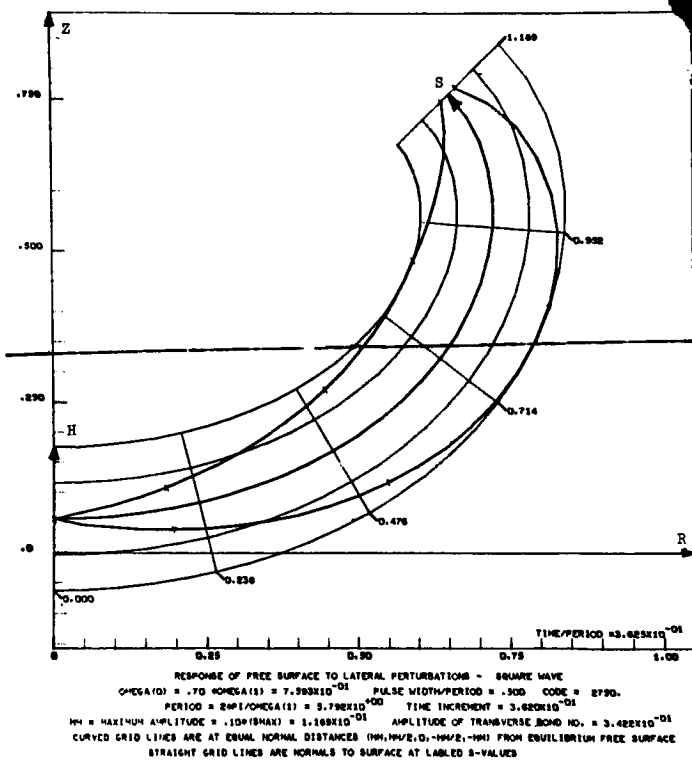

(c)

Maximum Response to Sinus

Perturbing Accele

and e =

FOLD-OUT
#1

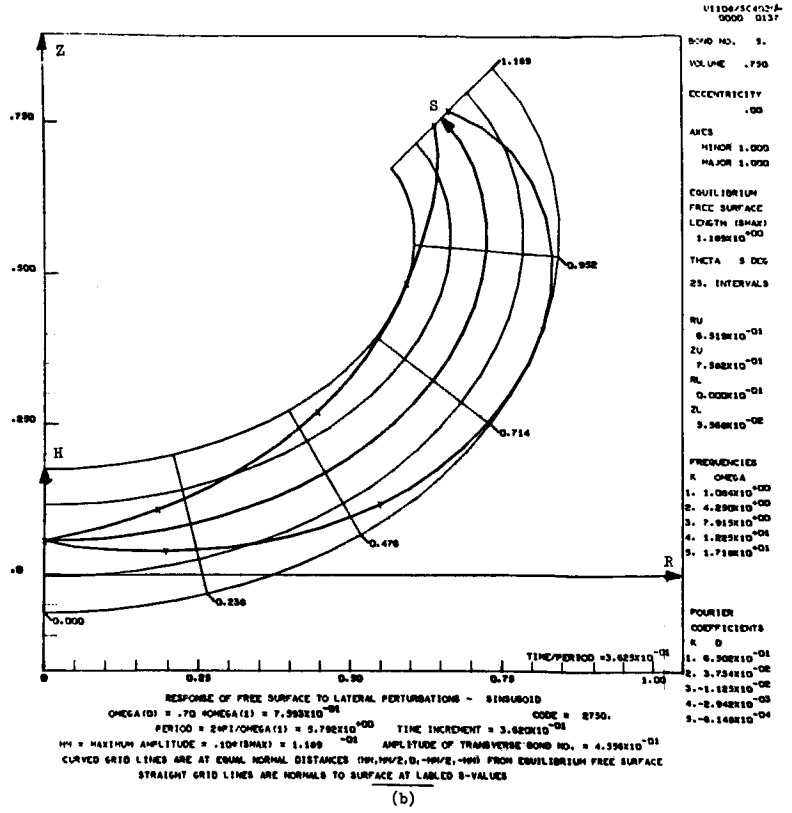

(b)

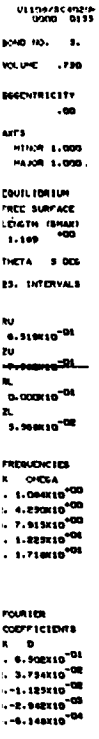

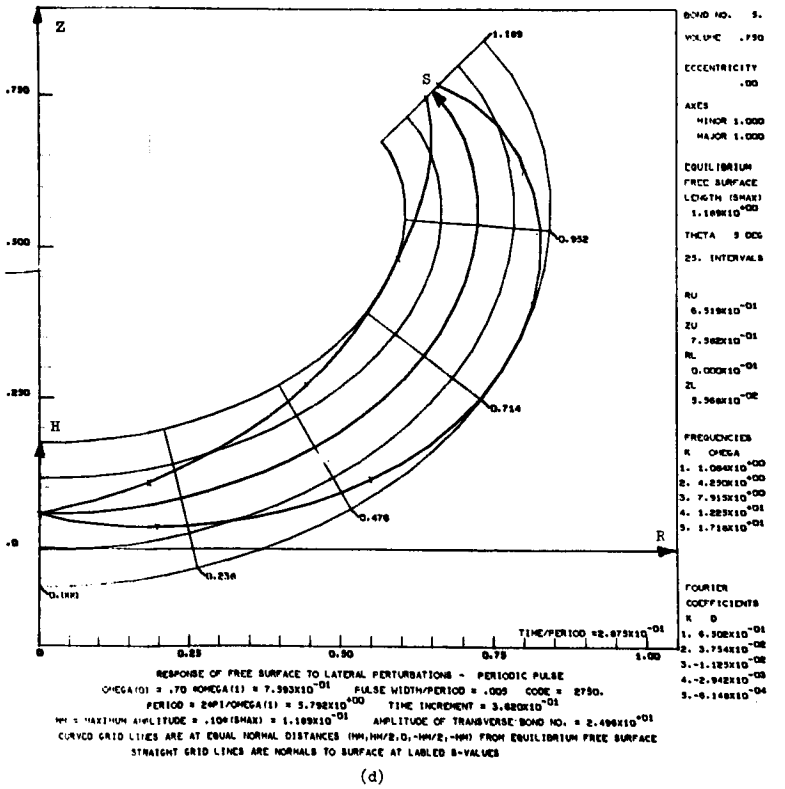

(d)

)idal, Square Wave, and Periodic Pulse

rations for $B_\alpha = 5$, $V = 3/4$,

0 for $\omega_o/\omega_1 = 0.7$

Figure 22

FOLD-OUT #2

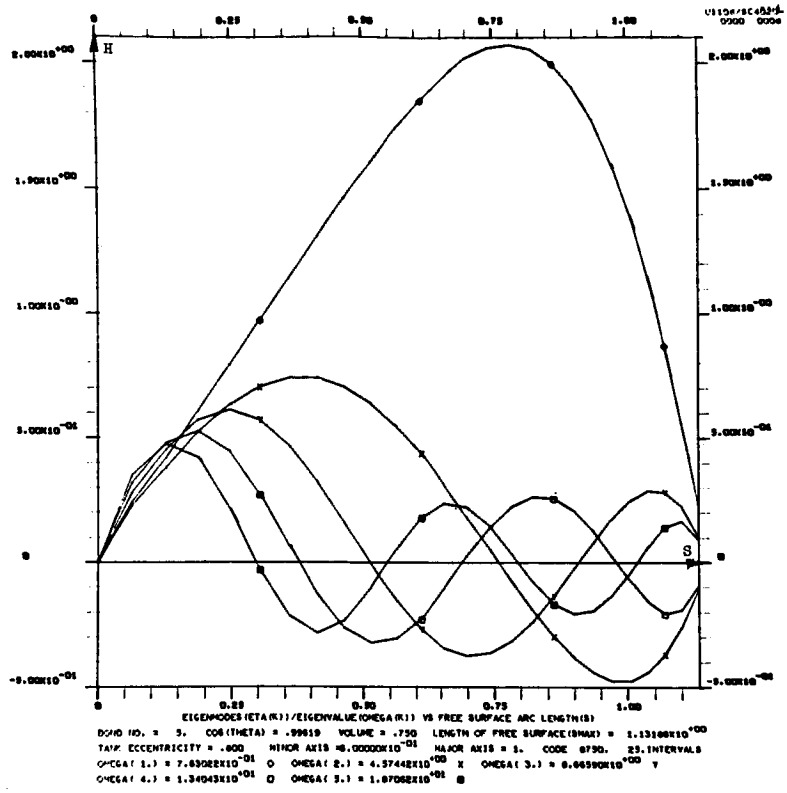

(a)

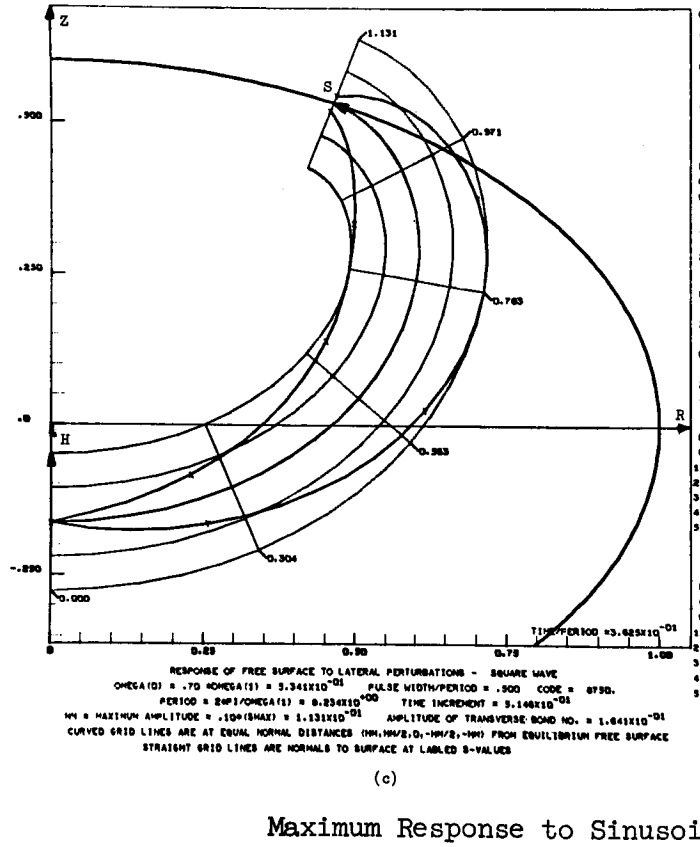

(c)

Maximum Response to Sinusoid
Perturbing Accelera
and e = 0.

FOLD-OUT
#1

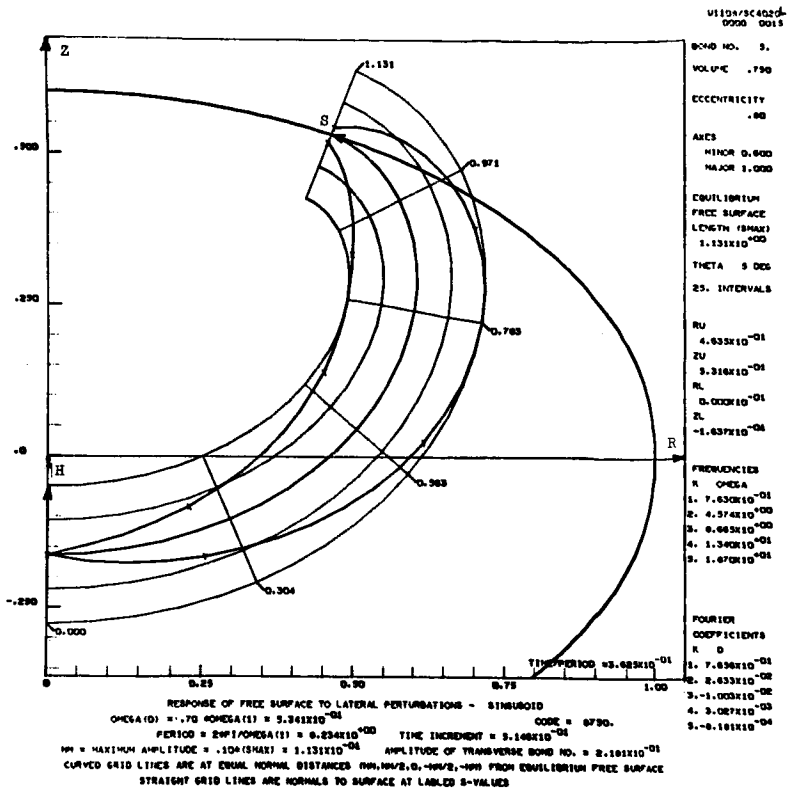

(b)

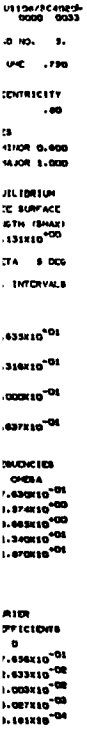

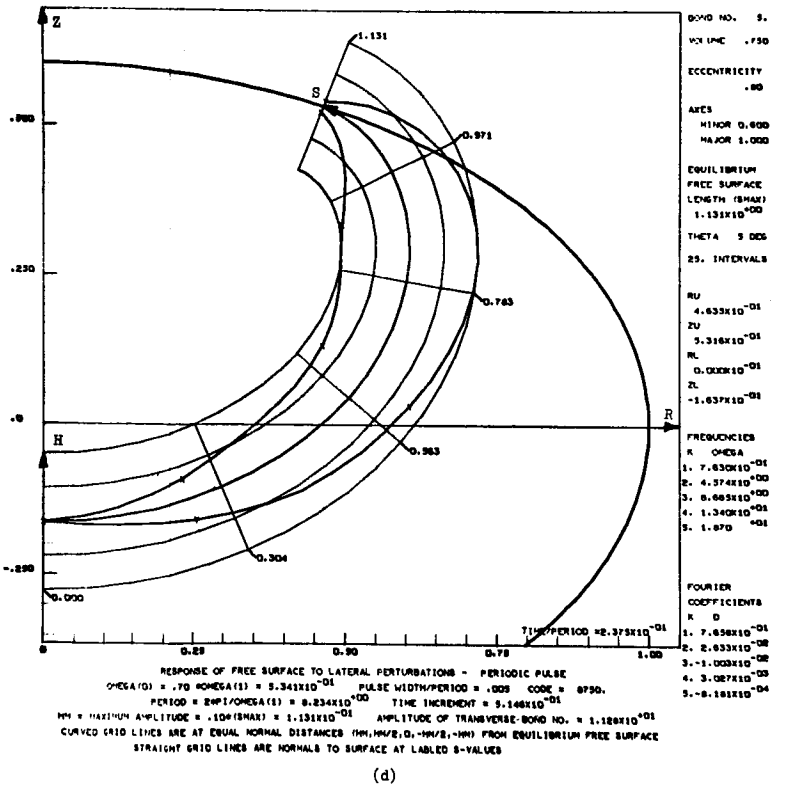

(d)

al, Square Wave, and Periodic Pulse
ions for $B_\alpha = 5$, $V = 3/4$,
8 for $\omega_o/\omega_1 = 0.7$
Figure 23

FOLD-OUT #2

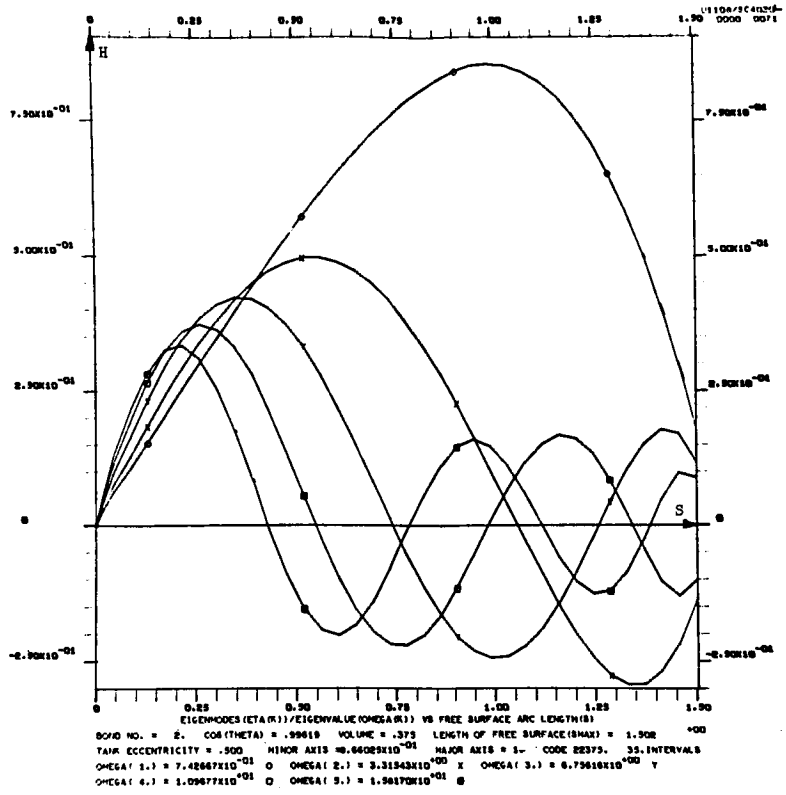

(a)

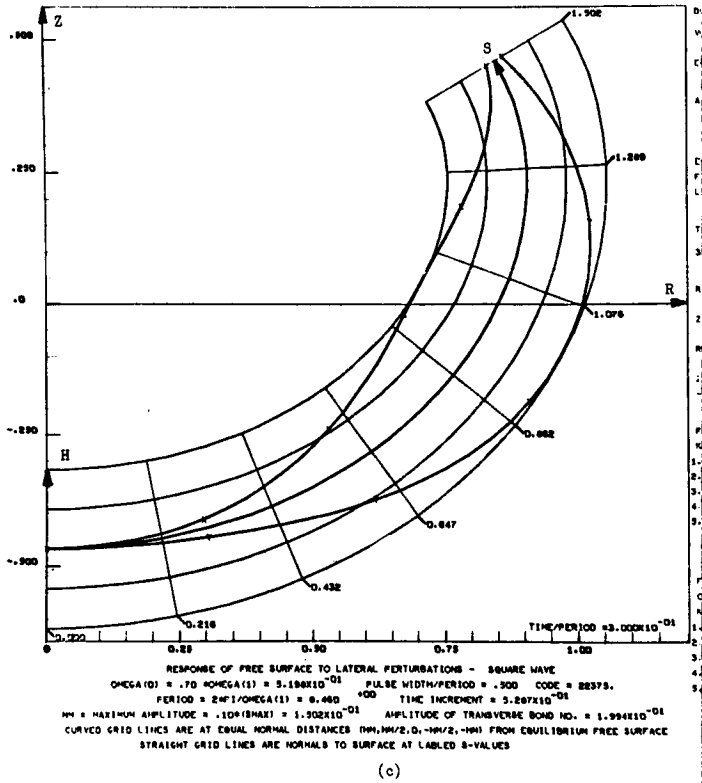

(c)

Maximum Response to Sinusoidal,

Perturbing Accelerations

and e = 0.5 f

Figu

FOLD-OUT
#1

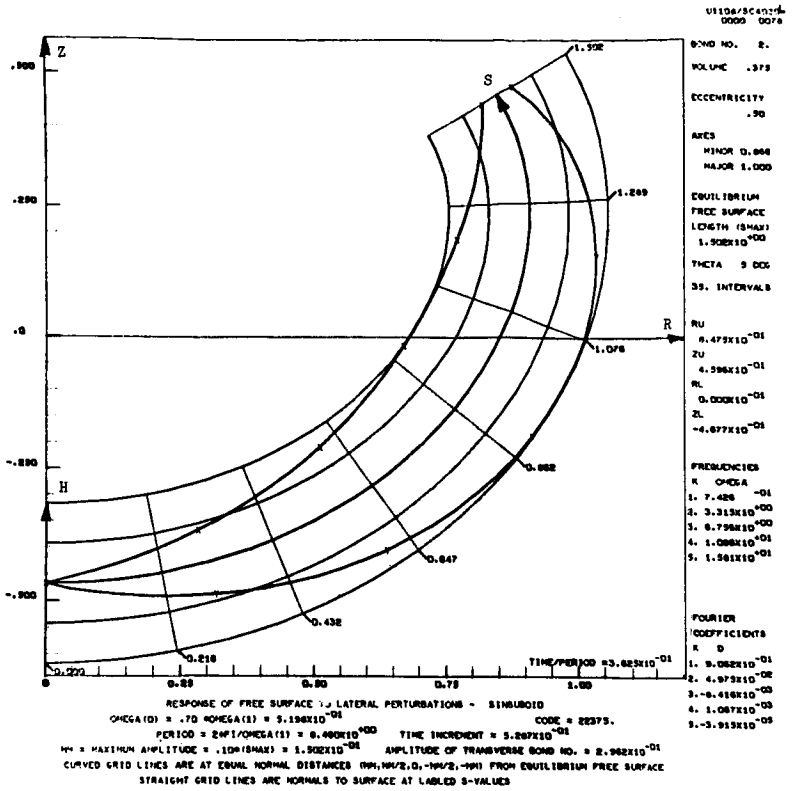

(b)

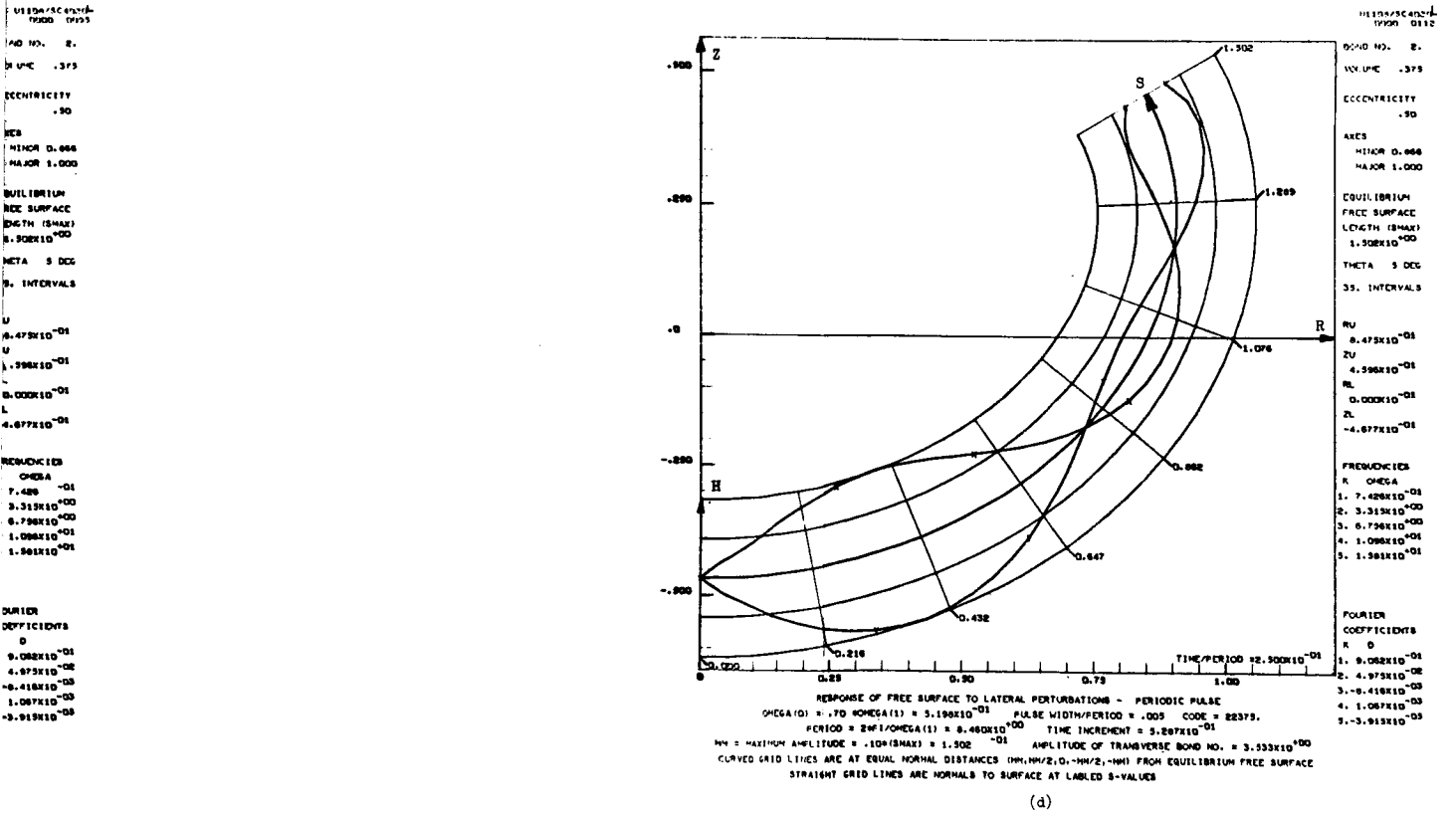

(d)

Square Wave, and Periodic Pulse

for $B_\alpha = 2$, $V = 3/8$,

or $\omega_o/\omega_1 = 0.7$

e 24

FOLD-OUT #2

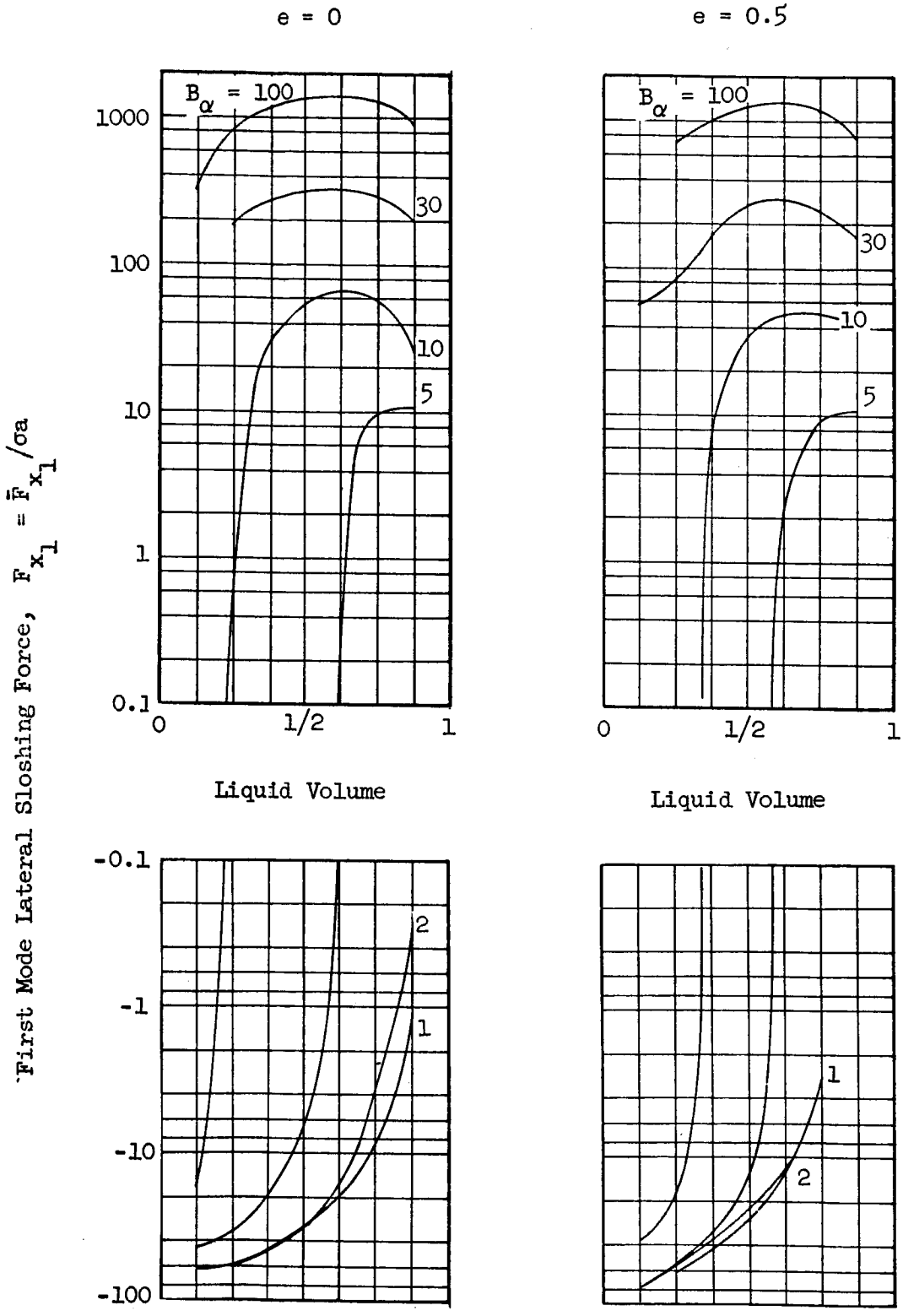

Lateral Force F_{x_1} for First

of Eccentricities

Fi

FOLD-OUT
#1

e = 0.68

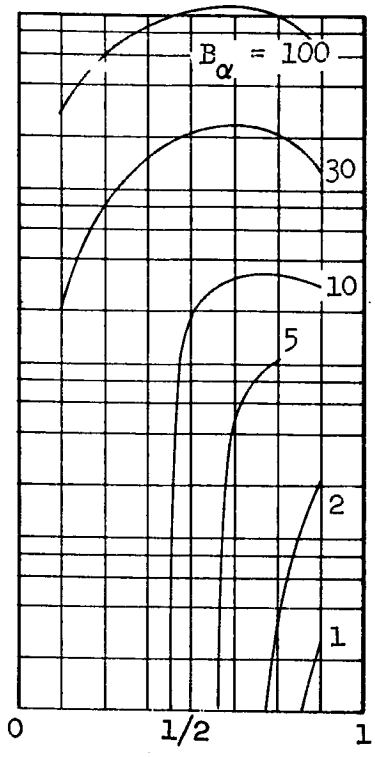

Liquid Volume

e = 0.8

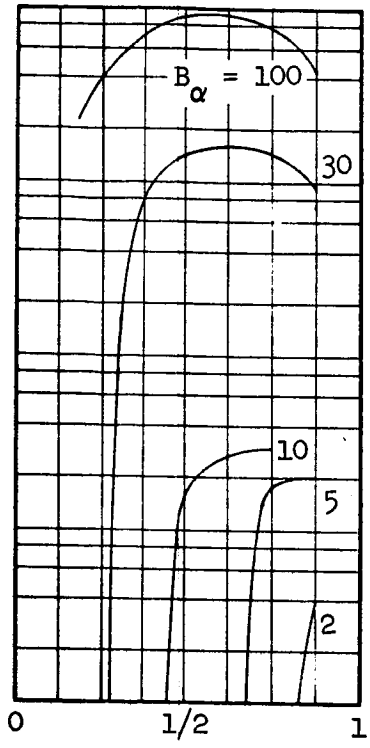

Liquid Volume

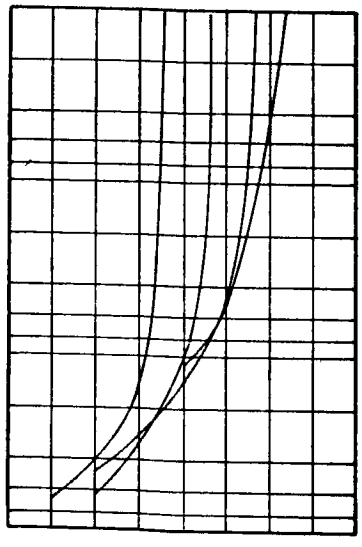

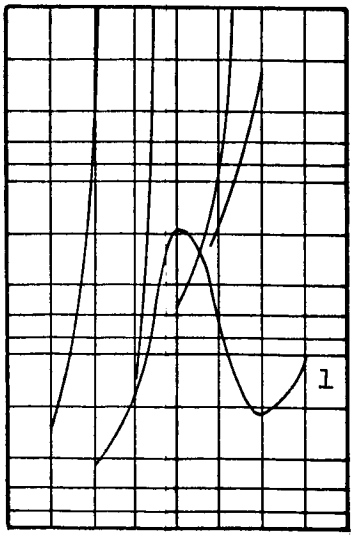

Mode Sloshing in Spheroidal Tanks
0, 0.5, 0.68 and 0.8
gure 25

FOLD-OUT
#2

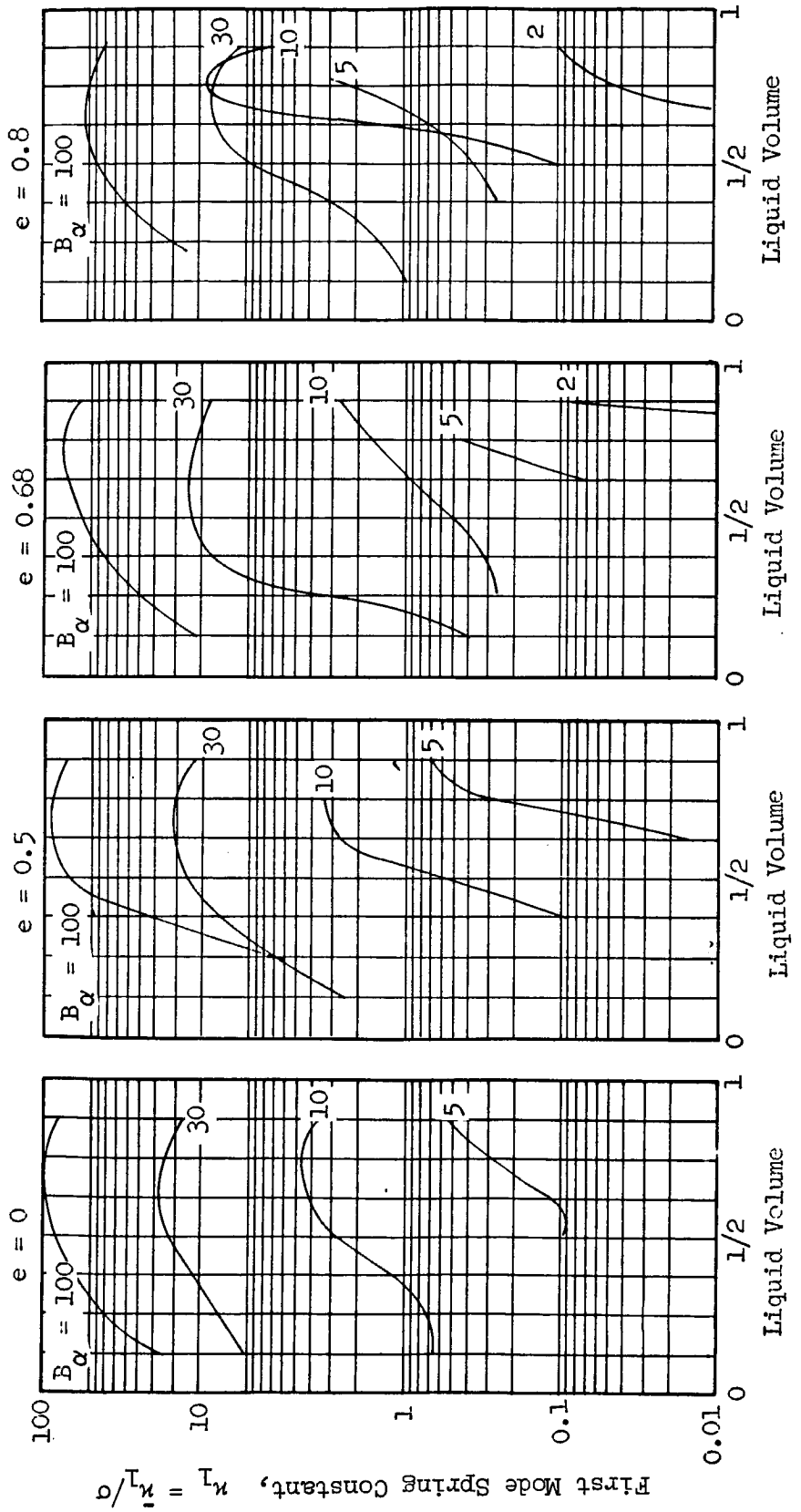

Spring Constant for Spring-Mass Oscillator Analog of First Mode Lateral Sloshing in Spheroidal Tanks of Eccentricities 0, 0.5, 0.68 and 0.8

Figure 26

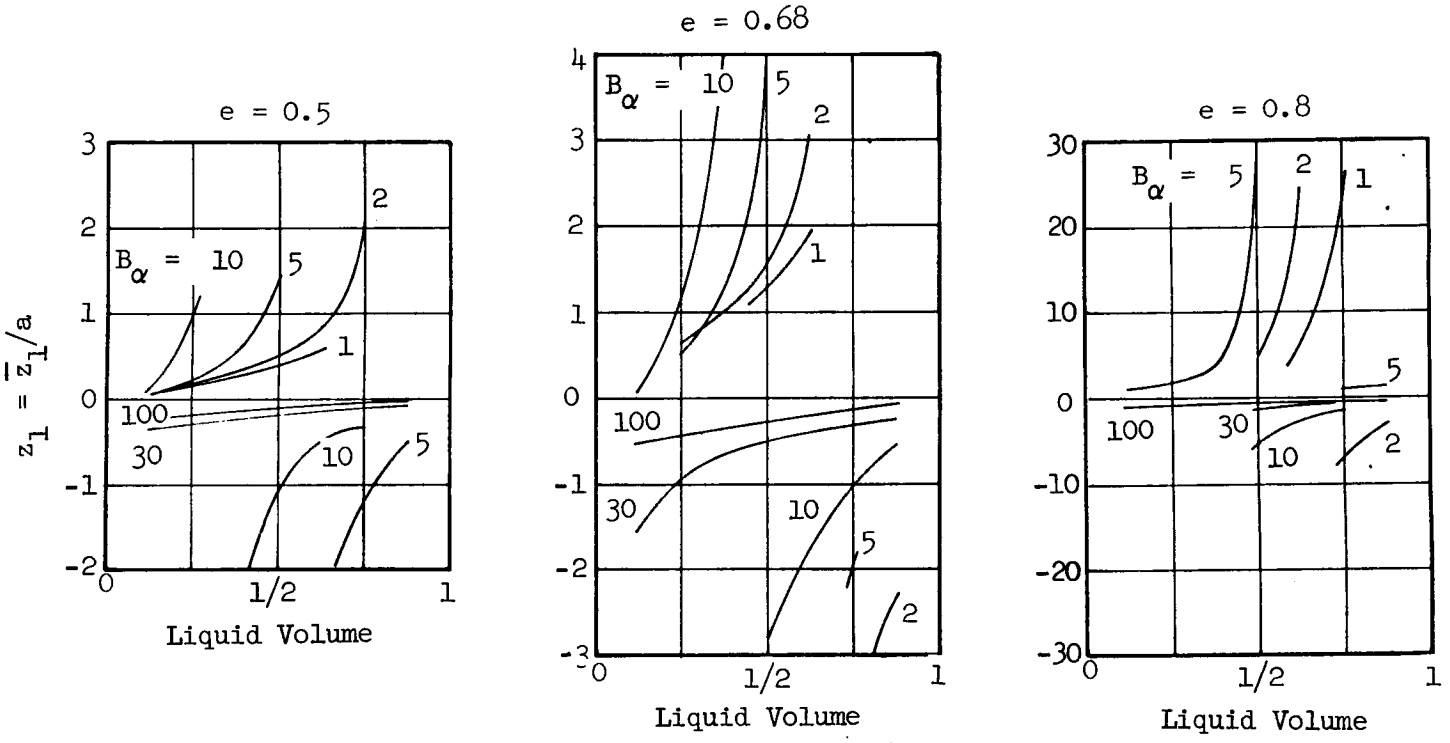

Lateral Force Action Point for First Mode Sloshing in Spheroidal Tanks with Eccentricities 0.5, 0.68, and 0.8

Figure 27

Fold-out #1

e = 0
θ = 5 degrees

Bond No. $B_\alpha=\rho g_\alpha a^2/\sigma$	Liquid Volume in eighths	Eigenvalues $\omega_k^2 = \tilde{\omega}_k^2[(1+B_\alpha)\sigma/\rho a^3]^{-1}$ k = 1	2	3	4	5
0	1	.194-02	.361+01	.238+02	.813+02	.202+03
	7	-.583-01				
1	2	.567-00	.107+02	.491+02	.138+03	.301+03
	4	.619-00	.131+02	.554+02	.147+03	.306+03
	6	.688-00	.212+02	.843+02	.215+03	.439+03
	7	.721-00	.360+02	.138+03	.344+03	.693+03
2	1	.725-00	.119+02	.541+02	.153+03	.334+03
	2	.763-00	.121+02	.507+02	.135+03	.283+03
	3	.798-00	.128+02	.513+02	.133+03	.274+03
	5	.882-00	.163+02	.623+02	.156+03	.315+03
	6	.942-00	.209+02	.786+02	.196+03	.393+03
	7	.970-00	.325+02	.121+03	.299+03	.595+03
5	1	.920-00	.122+02	.487+02	.127+03	.264+03
	3	.103+01	.126+02	.444+02	.108+03	.214+03
	4	.108+01	.135+02	.468+02	.113+03	.223+03
	6	.118+01	.181+02	.627+02	.150+03	.295+03
	7	.125+01	.253+02	.892+02	.215+03	.422+03
10	1	.102+01	.112+02	.402+02	.989+02	.199+03
	3	.115+01	.110+02	.353+02	.818+02	.158+03
	4	.123+01	.116+02	.369+02	.853+02	.165+03
	6	.137+01	.151+02	.487+02	.113+03	.219+03
	7	.144+01	.209+02	.695+02	.164+03	.319+03
30	2	.121+01	.831+01	.231+02	.497+02	.923+02
	4	.137+01	.822+01	.223+02	.477+02	.884+02
	5	.150+01	.881+01	.240+02	.512+02	.942+02
	7	.176+01	.138+02	.412+02	.921+02	.174+03
100	2	.126+01	.631+01	.139+02	.258+02	.432+02
	4	.150+01	.627+01	.136+02	.255+02	.435+02
	6	.183+01	.700+01	.158+02	.304+02	.526+02
	7	.211+01	.871+01	.214+02	.431+02	.769+02

e = 0.5
θ = 5 degrees

Bond No. $B_\alpha=\rho g_\alpha a^2/\sigma$	Liquid Volume in eighths	Eigenvalues $\omega_k^2 = \tilde{\omega}_k^2[(1+B_\alpha)\sigma/\rho a^3]^{-1}$ k = 1	2	3	4	5
0	1	.103-01	.180+01	.103+02	.369+02	.992+02
	2	-.147-01				
	7	-.537-01				
1	1	.224+00	.580+01	.301+02	.936+02	.220+03
	2	.309+00	.771+01	.365+02	.106+03	.237+03
	3	.375+00	.987+01	.441+02	.122+03	.260+03
	4	.429+00	.124+02	.530+02	.141+03	.294+03
	5	.491+00	.164+02	.673+02	.174+03	.357+03
2	2	.484-00	.923+01	.404+02	.111+03	.237+03
	3	.552-00	.110+02	.456+02	.120+03	.250+03
	4	.604-00	.130+02	.515+02	.131+03	.265+03
	5	.673-00	.162+02	.628+02	.157+03	.315+03
	6	.751-00	.220+02	.834+02	.206+03	.410+03
5	1	.681-00	.971+01	.405+02	.109+03	.231+03
	3	.805-00	.113+02	.412+02	.101+03	.201+03
	4	.866-00	.126+02	.446+02	.107+03	.212+03
	5	.929-00	.147+02	.515+02	.124+03	.244+03
	7	.107+01	.279+02	.989+02	.238+03	.467+03
10	1	.835-00	.974+01	.362+02	.905+02	.182+03
	2	.905-00	.980+01	.334+02	.795+02	.156+03
	3	.974-00	.103+02	.337+02	.787+02	.152+03
	5	.110+01	.125+02	.402+02	.931+02	.180+03
	6	.118+01	.153+02	.499+02	.116+03	.225+03
30	1	.974-00	.823+01	.252+02	.569+02	.108+03
	2	.126+01	.954+01	.275+02	.601+02	.112+03
	4	.127+01	.815+01	.223+02	.480+02	.891+02
	6	.145+01	.101+02	.290+02	.637+02	.119+03
	7	.158+01	.143+02	.434+02	.974+02	.185+03
100	1	.115+01	.620+01	.139+02	.262+02	.445+02
	4	.141+01	.618+01	.134+02	.251+02	.425+02
	5	.157+01	.644+01	.141+02	.266+02	.454+02
	7	.199+01	.882+01	.220+02	.448+02	.805+02

FOLD-OUT #2

e = 0.68
Θ = 5 degrees

Bond No. $B_\alpha=\rho g_\alpha a^2/\sigma$	Liquid Volume in eighths	Eigenvalues $\omega_k^2=\bar{\omega}_k^2[(1+B_\alpha)\sigma/\rho a^3]^{-1}$ k = 1	2	3	4	5
0	1	.902+01	.594+01	.312+02	.106+03	.273+03
	2	.834-01	.591+01	.268+02	.833+02	.203+03
	3	.370-01	.641+01	.251+02	.704+02	.161+03
	6	-.210-01				
1	4	.293-00	.128+02	.544+02	.145+03	.305+03
	5	.363-00	.180+02	.732+02	.189+03	.386+03
	6	.427+00	.261+02	.102+02	.255+03	.513+03
	7	.508-00	.493+02	.184+03	.451+03	.897+03
2	2	.272-00	.730+01	.326+02	.920+02	.202+03
	3	.349-00	.987+01	.416+02	.111+03	.231+03
	4	.424-00	.129+02	.520+02	.133+03	.270+03
	5	.496-00	.168+02	.656+02	.165+03	.331+03
	6	.588-00	.241+02	.915+02	.225+03	.447+03
	7	.678-00	.403+02	.150+03	.365+03	.721+03
5	2	.483-00	.814+01	.327+02	.847+02	.174+03
	3	.564-00	.100+02	.382+02	.954+02	.191+03
	4	.640-00	.120+02	.439+02	.107+03	.211+03
	5	.709-00	.147+02	.529+02	.127+03	.250+03
	6	.775-00	.190+02	.675+02	.161+03	.316+03
10	1	.610-00	.762+01	.297+02	.766+02	.157+03
	3	.735-00	.918+01	.312+02	.732+02	.142+03
	4	.820-00	.106+02	.354+02	.827+02	.160+03
	7	.123+01	.234+02	.796+02	.188+03	.365+03
30	1	.818-00	.729+01	.232+02	.530+02	.101+03
	2	.903-00	.720+01	.209+02	.457+02	.855+02
	4	.108+01	.782+01	.218+02	.471+02	.874+02
	5	.118+01	.867+01	.244+02	.528+02	.980+02
	7	.131+01	.144+02	.440+02	.995+02	.189+03
100	1	.894-00	.603+01	.152+02	.299+02	.521+02
	2	.102+01	.593+01	.136+02	.258+02	.438+02
	4	.127+01	.603+01	.132+02	.246+02	.416+02
	6	.159+01	.692+01	.161+02	.313+02	.545+02
	7	.177+01	.883+01	.224+02	.460+02	.826+02

e = 0.8
Θ = 5 degrees

Bond No. $B_\alpha=\rho g_\alpha a^2/\sigma$	Liquid Volume in eighths	Eigenvalues $\omega_k^2=\bar{\omega}_k^2[(1+B_\alpha)\sigma/\rho a^3]^{-1}$ k = 1	2	3	4	5
0	1	.210+00	.176+02	.882+02	.289+03	.719+03
	2	.215+00	.153+02	.692+02	.213+03	.508+03
	3	.190+00	.148+02	.620+02	.182+03	.418+03
	4	.124+00	.157+02	.600+02	.165+03	.362+03
	5	.174-02	.199+02	.670+02	.162+03	.327+03
	7	-.806-01				
1	1	.106+00	.809+01	.416+02	.137+03	.343+03
	2	.114+00	.676+01	.308+02	.944+02	.226+03
	3	.123+00	.688+01	.271+02	.759+02	.173+03
	5	.248+00	.201+02	.804+02	.209+03	.431+03
	6	.306+00	.304+02	.117+03	.293+03	.588+03
	7	.371+00	.589+02	.217+03	.527+03	.104+04
2	1	.717+01	.390+01	.214+02	.712+02	.181+03
	4	.279+00	.132+02	.537+02	.142+03	.293+03
	5	.356+00	.185+02	.726+02	.184+03	.371+03
	6	.442+00	.274+02	.104+03	.258+03	.513+03
	7	.516+00	.471+02	.174+03	.421+03	.828+03
5	2	.266+00	.659+01	.279+02	.756+02	.161+03
	3	.352+00	.919+01	.368+02	.944+02	.191+03
	4	.430+00	.118+02	.449+02	.111+03	.219+03
	5	.510+00	.155+02	.573+02	.139+03	.274+03
	6	.582+00	.209+02	.751+02	.180+03	.350+03
	7	.695+00	.343+02	.123+03	.293+03	.571+03
10	3	.494+00	.829+01	.300+02	.722+02	.141+03
	4	.569+00	.101+02	.355+02	.839+02	.163+03
	6	.736+00	.166+02	.561+02	.131+03	.252+03
	7	.831+00	.263+02	.906+02	.214+03	.416+03
30	1	.634+00	.596+01	.198+02	.467+02	.906+02
	3	.755+00	.661+01	.195+02	.419+02	.775+02
	4	.834+00	.738+01	.213+02	.459+02	.847+02
	6	.997+00	.106+02	.316+02	.701+02	.131+03
	7	.102+01	.159+02	.498+02	.113+03	.215+03
100	2	.844+00	.539+01	.128+02	.243+02	.414+02
	4	.109+01	.583+01	.131+02	.247+02	.420+02
	5	.122+01	.614+01	.139+02	.262+02	.445+02
	7	.145+01	.905+01	.237+02	.489+02	.883+02

Table I

Lateral Sloshing Eigenvalues for Spheroidal Tanks

of Eccentricity 0, 0.5, 0.68 and 0.8 .

Θ = 5 degrees

fold-out #1

$$D_k = \left(\int_0^s u R^2 H_k \, ds \Big/ \int_0^s u_k H_k \, ds\right)$$

For Spheroidal Tanks
e = 0
θ = 5 degrees

Bond No. $B_\alpha = \rho g a^2/\sigma$	Liquid Volume in eighths	k = 1	2	3	4	5
0	1	.976+01	-.987-01	-.215-02	.569-03	-.185-03
1	2	-.817-00	-.536-01	.330-02	.671-04	-.600-05
	4	-.911-00	-.735-01	.539-02	-.225-03	-.237-03
	6	-.791-00	.605-01	-.556-02	-.245-03	.392-03
	7	-.636-00	.386-01	-.419-02	-.103-03	-.320-03
2	1	-.573-00	-.231-01	-.229-02	-.212-03	.375-04
	2	-.724-00	-.382-01	.462-02	.387-03	.146-05
	3	-.795-00	-.492-01	.685-02	-.618-03	-.505-04
	5	-.781-00	-.566-01	.907-02	-.926-03	.154-03
	6	-.697-00	-.507-01	.835-02	-.902-03	.154-03
	7	-.553-00	.357-01	-.586-02	.587-03	.168-03
5	1	-.523+00	-.140-01	.296-02	.476-03	.632-04
	3	-.731+00	.286-01	.876-02	.214-02	-.430-03
	4	-.748+00	.337-01	.107-01	.283-02	-.621-03
	6	-.650+00	.375-01	-.113-01	.294-02	-.615-03
	7	-.517+00	.307-01	-.850-02	-.209-02	-.386-03
10	1	-.507+00	-.885+01	.327-02	.854-03	-.188-03
	3	-.710+00	-.153-01	.885-02	.338-02	-.116-02
	4	.727+00	.187-01	-.107-01	.429-02	-.158-02
	6	.632+00	.247-01	-.118-01	.462-02	-.171-02
	7	-.499+00	.236-01	-.942-02	.337-02	-.113-02
30	2	-.627+00	.354-02	.385-02	-.257-02	-.133-02
	4	-.720+00	-.188-02	-.743-02	.518-02	-.300-02
	5	-.693+00	-.103-02	-.790-02	.564-02	-.340-02
	7	-.486+00	.118-01	-.859-02	.480-02	-.255-02
100	2	-.625+00	.171-01	.242-03	.176-02	-.167-02
	4	-.707+00	-.304-01	.266-02	.161-02	.205-02
	6	-.625+00	.211-01	-.171-02	.379-02	-.332-02
	7	-.486+00	-.487-02	-.463-02	.416-02	-.309-02

$$D_k = \left(\int_0^s u R^2 H_k \, ds \Big/ \int_0^s u_k H_k \, ds\right)$$

For Spheroidal Tanks
e = 0.5
θ = 5 degrees

Bond No. $B_\alpha = \rho g a^2/\sigma$	Liquid Volume in eighths	k = 1	2	3	4	5
0	1	.355+01	.101-02	.499-01	-.209-04	-.406-03
1	1	-.930+00	-.365-01	-.522-02	.691-03	-.149-03
	2	-.103+01	-.552-01	.728-02	.579-03	.252-04
	3	-.106+01	-.645-01	-.806-02	.430-03	.974-04
	4	-.105+01	-.678-01	+.819-02	.286-03	-.231-03
	5	.973+00	.635-01	-.769-02	-.216-03	.310-03
2	2	-.857+00	-.411-01	-.637-02	.791-03	.830-04
	3	-.906+00	-.498-01	.842-02	.107-02	.392-04
	4	-.909+00	.548-01	-.978-02	.124-02	.123-04
	5	-.855+00	.534-01	-.979-02	.137-02	.733-05
	6	-.746+00	.457-01	-.857-02	.124-02	.297-04
5	1	-.575+00	-.142-01	-.305-02	.542-03	-.100-03
	3	-.789+00	-.299-01	.913-02	.235-02	-.943-03
	4	-.801+00	-.352-01	-.113-01	.310-02	-.762-03
	5	-.767+00	.375-01	-.120-01	.339-02	-.830-03
	7	-.522+00	.276-01	-.776-02	.199-02	.394-03
10	1	-.530+00	-.729-02	.288-02	.712-03	.145-03
	2	-.676+00	-.124-01	.618-02	.208-02	.647-03
	3	-.742+00	-.184-01	.875-02	.336-02	-.119-02
	5	-.737+00	-.248-01	-.122-01	.494-02	-.189-02
	6	-.656+00	.258-01	-.117-01	-.463-02	.175-02
30	1	-.500+00	.114-02	.209-02	.101-02	-.390-03
	2	-.539+00	-.173-01	-.272-02	.556-03	+.134-03
	4	.727+00	-.206-02	-.645-02	.458-02	.272-02
	6	-.642+00	-.105-01	-.972-02	.585-02	.331-02
	7	-.492+00	.138-01	.853-02	.465-02	.246-02
100	2	-.625+00	.172-01	.101-02	.106-02	-.111-02
	4	-.712+00	-.281-01	-.211-02	.176-02	-.212-02
	5	-.691+00	.281-01	.170-02	.190-02	-.216-02
	7	-.488+00	-.269-03	.543-02	.420-02	-.298-02

FOLD-OUT #2

$D_k = \left(\int_o^{S_u} R^2 H_k \, ds \Big/ \int_o^{S_u} \Phi_k H_k \, ds \right)$

For Spheroidal Tanks
e = 0.68
Θ = 5 degrees

Bond No. $B_\alpha = \rho g a^2/\sigma$	Liquid Volume in eighths	k = 1	2	3	4	5
0	1	.110+01	-.211-03	.241-01	.767-04	-.363-03
	2	.155+01	.189-02	.376-01	.557-03	.108-02
	3	.278+01	.105-03	.456-01	.523-04	.223-02
1	4	-.118+01	.492-01	.131-01	-.926-03	.221-03
	5	-.107+01	.486-01	-.101-01	.716-03	.236-03
	6	-.926+00	.412-01	-.750-02	.614-03	-.204-03
	7	.694+00	.252-01	-.439-02	.414-03	.139-03
2	2	-.105+01	-.282-01	.119-01	.230-02	-.299-03
	3	-.105+01	-.384-01	.127-01	-.223-02	-.228-03
	4	-.101+01	.437-01	-.123-01	.208-02	-.174-03
	5	.936+00	.443-01	-.110-01	.186-02	.119-03
	6	-.797+00	.381-01	.866-02	.152-02	-.104-03
	7	-.609+00	.258-01	-.552-02	.950-03	-.350-04
5	2	-.837+00	-.228-01	.762-02	.205-02	-.530-03
	3	-.884+00	-.279-01	.102-01	-.300-02	-.823-03
	4	-.875+00	-.319-01	.118-01	-.362-02	-.102-02
	5	-.826+00	-.340-01	-.120-01	.368-02	-.103-02
	6	-.728+00	.332-01	-.108-01	-.313-02	-.779-03
10	1	-.581+00	-.837-02	-.288-02	.719-03	.167-03
	3	-.806+00	.186-01	-.938-02	.372-02	-.140-02
	4	-.810+00	.207-01	-.107-01	.455-02	-.184-02
	7	-.531+00	-.216-01	-.833-02	.305-02	-.106-02
30	1	-.512+00	.122-02	.172-02	.790-03	-.285-03
	2	-.658+00	.181-02	-.361-02	.220-02	-.112-02
	4	-.752+00	-.186-02	-.690-02	.462-02	-.274-02
	5	-.727+00	-.567-02	.807-02	.529-02	-.318-02
	7	-.526+00	-.161-01	-.866-02	-.459-02	-.241-02
100	1	-.495+00	.760-02	.169-03	-.573-03	-.376-03
	2	-.629+00	-.164-01	-.125-02	.638-03	-.747-03
	4	-.720+00	-.243-01	-.121-02	-.193-02	-.212-02
	6	-.646+00	.926-02	-.422-02	.423-02	-.328-02
	7	.563+00	-.713-02	.671-02	-.451-02	-.307-02

$D_k = \left(\int_o^{S_u} R^2 H_k \, ds \Big/ \int_o^{S_u} \Phi_k H_k \, ds \right)$

For Spheroidal Tanks
e = 0.8
Θ = 5 degrees

Bond No. $B_\alpha = \rho g a^2/\sigma$	Liquid Volume in eighths	k = 1	2	3	4	5
0	1	.652+00	-.128-03	.123-01	.382-04	.256-03
	2	-.868+00	.138-03	.201-01	.272-04	.611-03
	3	.107+01	-.364-03	-.253-01	.996-04	.892-03
	4	-.145+01	-.802-04	-.278-01	-.339-04	.110-02
	5	-.128+02	.769-04	-.248-01	.289-04	.134-02
1	1	.915+00	.194-01	-.163-01	-.244-02	.985-04
	2	-.120+01	.319-01	.261-01	.582-02	.107-03
	3	-.137+01	.335-01	-.303-01	.990-02	-.589-03
	5	-.116+01	.283-01	-.134-01	.911-03	.769-04
	6	-.999+00	.285-01	-.837-02	.670-03	.112-03
	7	-.753+00	.190-01	-.418-02	.485-03	.748-04
2	1	.111+01	.557-01	.157-01	.609-02	-.959-03
	4	-.111+01	.211-01	-.162-01	.300-02	.401-03
	5	-.996+00	.284-01	-.125-01	.216-02	-.281-03
	6	-.840+00	.281-01	-.864-02	.151-02	-.151-03
	7	-.644+00	.210-01	.504-02	-.950-03	-.916-04
5	2	-.999+00	.495-02	.986-02	.418-02	-.135-02
	3	-.998+00	-.128-01	-.118-01	.446-02	.144-02
	4	-.961+00	.202-01	-.127-01	.440-02	-.136-02
	5	-.884+00	.252-01	-.118-01	.386-02	-.117-02
	6	-.766+00	.263-01	-.100-01	.303-02	.818-03
	7	-.565+00	.199-01	-.636-02	.177-02	-.425-03
10	3	-.896+00	.128-01	-.899-02	.429-02	.187-02
	4	-.887+00	.161-01	-.104-01	.491-02	-.217-02
	6	-.721+00	.219-01	-.105-01	-.435-02	.172-02
	7	-.539+00	-.182-01	-.719-02	.269-02	-.965-03
30	1	-.535+00	-.718-04	-.164-02	.646-03	.207-03
	3	-.778+00	-.332-02	-.581-02	.371-02	.218-02
	4	-.797+00	-.609-02	-.738-02	.485-02	.297-02
	6	-.689+00	-.161-01	.955-02	.554-02	-.317-02
	7	-.538+00	-.167-01	-.811-02	.418-02	-.214-02
100	2	-.641+00	.136-01	-.233-03	.981-03	.879-03
	4	-.733+00	.204-01	.820-03	.150-02	.160-02
	5	-.718+00	.136-01	-.239-02	.332-02	-.261-02
	7	-.522+00	-.154-01	-.798-02	.473-02	-.307-02

Table II

Fourier Coefficients $D_k = \left(\int_o^{S_u} R^2 H_k \, ds \Big/ \int_o^{S_u} \Phi_k H_k R \, ds \right)$ For Spheroidal Tanks of Eccentricity 0, 0.5, 0.68 and 0.8 .

Θ = 5 degrees

Fold-out 1 #

$H_k = \bar{H}_k a$

For Spheroidal Tanks
e = 0
θ = 5 degrees

Bond No. $B_\alpha = \rho g_\alpha a^2/\sigma$	Liquid Volume in eighths	k = 1	2	3	4	5
0	1	.228+00	-.522+00	.767+00	-.990+00	.120+01
1	2	.168+00	-.534+00	.867+00	-.114+01	.138+01
	4	.159+00	-.519+00	.869+00	-.118+01	.148+01
	6	.192+00	-.630+00	.108+01	-.151+01	.192+01
	7	.248+00	-.824+00	.144+01	-.202+01	.256+01
2	1	.200+00	-.634+00	.103+01	-.137+01	.167+01
	2	.164+00	-.531-00	.885+00	-.121+01	.152+01
	3	.155+00	-.493+00	.822+00	-.112+01	.139+01
	5	.166+00	-.510+00	.864+00	-.121+01	.154+01
	6	.189+00	-.576+00	.990+00	-.141+01	.182+01
	7	.245+00	-.752+00	.131+01	-.188+01	.246+01
5	1	.197+00	-.635+00	.105+01	-.143+01	.179+01
	3	.150+00	-.447+00	.759+01	-.109+01	.144+01
	4	.151+00	-.430+00	.734+01	-.106+01	.141+01
	6	.183+00	-.491+00	.849+01	-.124+01	.165+01
	7	.234+00	-.627+00	.109+01	-.159+01	.213+01
10	1	.196+00	-.610+00	.102+01	-.141+00	.179+01
	3	.148+00	-.396+00	.669+00	-.966+00	.129+01
	4	.149+00	-.375+00	.636+00	-.928+00	.125+01
	6	.183+00	-.420+00	.722+00	-.106+01	.142+01
	7	.237+00	-.548+00	.952+00	-.140+01	.189+01
30	2	.157+00	-.381+00	.617+00	-.888+00	.119+01
	4	.147+00	-.294+00	.474+00	-.687+00	.925+00
	5	.160+00	-.297+00	.475+00	-.683+00	.908+00
	7	.249+00	-.424+00	.707+00	-.104+01	.139+01
100	2	.154+00	-.323+00	.467+00	-.632+00	.810+00
	4	.144+00	-.252+00	.357+00	-.484+00	.631+00
	6	.185+00	-.275+00	.377+00	-.508+00	.662+00
	7	.261+00	-.346+00	.485+00	-.671+00	.886+00

$H_k = \bar{H}_k a$

For Spheroidal Tanks
e = 0.5
θ = 5 degrees

Bond No. $B_\alpha = \rho g_\alpha a^2/\sigma$	Liquid Volume in eighths	k = 1	2	3	4	5
0	1	.933-01	-.362+00	.661+00	-.941+00	.120+01
1	1	.165+00	-.514+00	.839+00	-.113+01	.140+01
	2	.135+00	-.463+00	.794+00	-.108+01	.134+01
	3	.131+00	-.462+00	.808+00	-.112+01	.141+01
	4	.137+00	-.482+00	.845+00	-.118+01	.149+01
	5	.153+00	-.531+00	.928+00	-.130+01	.165+01
2	2	.143+00	-.483+00	.829+00	-.114+01	.142+01
	3	.136+00	-.459+00	.796+00	-.111+01	.140+01
	4	.138+00	-.459+00	.792+00	-.110+01	.139+01
	5	.151+00	-.491+00	.858+00	-.123+01	.163+01
	6	.180+00	-.570+00	.998+00	-.144+01	.191+01
5	1	.193+00	-.625+00	.104+01	-.141+01	.176+01
	3	.141+00	-.434+00	.746+00	-.107+01	.141+01
	4	.143+00	-.420+00	.715+00	-.102+01	.131+01
	5	.154+00	-.434+00	.747+00	-.108+01	.142+01
	7	.243+00	-.660+00	.115+01	-.167+01	.220+01
10	1	.194+00	-.621+00	.105+01	-.147+01	.191+01
	2	.154+00	-.459+00	.773+00	-.110+01	.143+01
	3	.143+00	-.395+00	.668+00	-.966+00	.129+01
	5	.155+00	-.376+00	.640+00	-.937+00	.126+01
	6	.181+00	-.422+00	.725+00	-.106+01	.143+01
30	1	.195+00	-.565+00	.929+00	-.132+01	.175+01
	2	.223+00	-.567+00	.909+00	-.128+01	.167+01
	4	.146+00	-.297+00	.475+00	-.687+00	.926+00
	6	.187+00	-.322+00	.523+00	-.762+00	103+01
	7	.259+00	-.437+00	.730+00	-.107+01	.144+01
100	2	.152+00	-.335+00	.486+00	-.663+00	.860+00
	4	.144+00	-.257+00	.360+00	-.485+00	.628+00
	5	.153+00	-.248+00	.339+00	-.452+00	.584+00
	7	.274+00	-.349+00	.489+00	-.678+00	.896+00

FOLD-OUT #2

$H_k = \bar{H}_k\, a$

For Spheroidal Tanks
e = 0.68
Θ = 5 degrees

Bond No. $B_\alpha = \rho g_\alpha a^2/\sigma$	Liquid Volume in eighths	k = 1	2	3	4	5
0	1	.723-01	-.381+00	.741+00	-.110+01	.144+01
	2	.802-01	-.363+00	.712+00	-.107+01	.141+01
	3	.917-01	-.392+00	.782+00	-.119+01	.158+01
1	4	.115+00	-.439+00	.806+00	-.116+01	.147+01
	5	.138+00	-.512+00	.923+00	-.132+01	.169+01
	6	.172+00	-.615+00	.110+01	-.158+01	.205+01
	7	.248+00	-.867+00	.156+01	-.226+01	.295+01
2	2	.102+00	-.377+00	.704+00	-.102+01	.130+01
	3	.107+00	-.390+00	.717+00	-.103+01	.131+01
	4	.119+00	-.421+00	.760+00	-.108+01	.139+01
	5	.138+00	-.471+00	.841+00	-.122+01	.160+01
	6	.174+00	-.570+00	.101+01	-.147+01	.197+01
	7	.243+00	-.778+00	.139+00	-.203+01	.272+01
5	2	.129+00	-.430+00	.762+00	-.108+01	.138+01
	3	.121+00	-.392+00	.700+00	-.102+01	.136+01
	4	.128+00	-.393+00	.688+00	-.990+00	.129+01
	5	.143+00	-.419+00	.733+00	-.107+01	.144+01
	6	.174+00	-.490+00	.853+00	-.124+01	.163+01
10	1	.194+00	-.623+00	.106+01	-.148+01	.190+01
	3	.132+00	-.377+00	.641+00	-.916+00	.119+01
	4	.135+00	-.358+00	.611+00	-.894+00	.120+01
	7	.248+00	-.585+00	.102+01	-.150+01	.203+01
30	1	.198+00	-.596+00	.986+00	-.140+01	.184+01
	2	.152+00	-.403+00	.651+00	-.933+00	.124+01
	4	.142+00	-.295+00	.467+00	-.675+00	.907+00
	5	.157+00	-.293+00	.464+00	-.669+00	.896+00
	7	.259+00	-.434+00	.724+00	-.106+01	.144+01
100	1	.193+00	-.524+00	.793+00	-.110+01	.144+01
	2	.150+00	-.349+00	.505+00	-.690+00	.900+00
	4	.142+00	-.260+00	.359+00	-.480+00	.619+00
	6	.196+00	-.278+00	.371+00	-.497+00	.645+00
	7	.290+00	-.353+00	.494+00	-.684+00	.903+00

$H_k = \bar{H}_k\, a$

For Spheroidal Tanks
e = 0.8
Θ = 5 degrees

Bond No. $B_\alpha = \rho g a^2/\sigma$	Liquid Volume in eighths	k = 1	2	3	4	5
0	1	.639-01	-.440+00	.885+00	-.135+01	.181+01
	2	.701-01	-.394+00	.794+00	-.122+01	.165+01
	3	.807-01	-.396+00	.792+00	-.122+01	.164+01
	4	.968-01	-.433+00	.868+00	-.135+01	.182+01
	5	.131+00	-.580+00	.123+01	-.197+01	.271+01
1	1	.552-01	-.330+00	.732+00	-.116+01	.159+01
	2	.600-01	-.261+00	.580+00	-.926+00	.129+01
	3	.720-01	-.245+00	.510+00	-.804+00	.113+01
	5	.127+00	-.495+00	.923+00	-.136+01	.178+01
	6	.166+00	-.626+00	.114+01	-.165+01	.211+01
	7	.252+00	-.908+00	.165+01	-.242+01	.318+01
2	1	.487-01	-.227+00	.556+00	-.922+00	.130+01
	4	.102+00	-.382+00	.728+00	-.108+01	.144+01
	5	.129+00	-.463+00	.850+00	-.125+00	.164+01
	6	.171+00	-.588+00	.106+01	-.154+01	.203+01
	7	.248+00	-.819+00	.147+01	-.216+01	.291+01
5	2	.873-01	-.307+00	.608+00	-.922+00	.123+01
	3	.957-01	-.325+00	.621+00	-.929+00	.125+01
	4	.111+00	-.360+00	.658+00	-.957+00	.125+01
	5	.135+00	-.414+00	.739+00	-.109+01	.147+01
	6	.174+00	-.509+00	.890+00	-.129+01	.170+01
	7	.256+00	-.725+00	.127+01	-.185+01	.243+01
10	3	.111+00	-.328+00	.585+00	-.852+00	.112+01
	4	.119+00	-.330+00	.579+00	-.851+00	.114+01
	6	.180+00	-.443+00	.761+00	-.111+01	.147+01
	7	.260+00	-.632+00	.110+01	-.162+01	.219+01
30	1	.209+00	-.643+00	.107+01	-.150+01	.196+01
	3	.131+00	-.316+00	.502+00	-.716+00	.943+00
	4	.136+00	-.288+00	.454+00	-.650+00	.862+00
	6	.196+00	-.338+00	.546+00	-.793+00	.108+01
	7	.282+00	-.481+00	.808+00	-.119+00	.160+01
100	2	.149+00	-.375+00	.543+00	-.736+00	.949+00
	4	.136+00	-.255+00	.346+00	-.459+00	.591+00
	5	.161+00	-.262+00	.343+00	-.451+00	.574+00
	7	.315+00	-.365+00	.516+00	-.717+00	.947+00

Table III

Eigenmode at Wall $H_k = \bar{H}_k/a$ For Spheroidal Tanks of Eccentricity 0, 0.5, 0.68 and 0.8.. Θ = 5 degrees

APPENDIX A
SYMBOL LIST

Quantities are nondimensional unless otherwise designated. When appropriate, the relation between a dimensionless variable and the physical dimensional one, which is topped by a bar, is given. Underlined variables are generally vectors.

English Alphabet

a	-Dimensional semi-major axis of container. The characteristic length with respect to which the variables are made nondimensional.
A	-Diagonal matrix whose entries are areas of zones on free surface; -Matrix in generalized eigenvalue-vector problem.
A_k	-Coefficient of Φ_k in Fourier expansion of perturbed velocity potential.
$A_k^{(m)}$	-Coefficient of $\Phi_k \cos(m\omega_o t)$ in Fourier expansion of perturbed velocity potential.
b	-Semi-minor container axis $= \bar{b}/a$.
B	-Matrix in generalized eigenvalue-vector problem.
B_{tr}	-Transverse time-varying Bond number $= \rho g_{tr} a^2/\sigma$.
$\hat{B}_{tr}$	-Amplitude of B_{tr}.
B_α	-Axial Bond number $= \rho g_\alpha a^2/\sigma$ (assumed non-negative).
C	-Curvature of meridian of equilibrium free-surface.
C_ℓ	-Contribution of lower intersection to F_x.
C_m	-Coefficient of $\sin(m\omega_o t)$ in Fourier expansion of periodic perturbation.
C_u	-Contribution of upper intersection to F_x.
D	-Matrix approximating the Laplace equation within the liquid with zero normal derivative on the equilibrium free-surface and w and zero potential on the center line.
D_k	-Fourier coefficient in the expansion of R in terms of Φ_k.

e -Eccentricity of an ellipse.

$\underline{e}_n$ -Unit vector in η direction.

$\underline{e}_r$ -Unit vector in r direction.

$\underline{e}_s$ -Unit vector in s direction.

$\underline{e}_\theta$ -Unit vector in θ direction.

$\underline{e}_\tau$ -Unit vector in τ direction.

f -Arbitrary function of time = $[\sigma/(\rho a)]^{1/2} \bar{f}$.

F -A generic function of convenience.

F_x -Lateral force = $\bar{F}_x/\sigma a$.

g_i -i^{th} component of $\underline{G}$ in surface polar normal coordinates.

g_{tr} -Dimensional time-varying lateral acceleration (positive when acting in direction of increasing x).

g_α -Dimensional steady axial acceleration (positive when acting downward).

$\underline{G}$ -A vector function.

$\mathcal{H}$ -Mean curvature of free surface = $a\bar{\mathcal{H}}$.

h_i -Signed scalar magnitude of derivative of position vector with respect to i^{th} coordinate direction, $i = 1,2,3$.

H -See capital eta.

k -Modulus ($k^2 = m$, where m is the parameter of a Jacobian elliptic function).

K -Real quarter period of a Jacobian elliptic function.

$\underline{k}$ -Unit vector in z direction.

L -Left triangular factor of the matrix S.

m -Index, particularly in Fourier sine expansion of perturbing acceleration.

M_y -Moment of lateral force = $\bar{M}_y/\sigma a^2$.

$\mathcal{M}_k$ -Equivalent mass for mechanical analogue for k^{th} mode = $(1+B_\alpha)\bar{\mathcal{M}}_k(a^3\rho)$.

$\underline{n}_H$ -Unit vector normal to free surface.

$\underline{n}_w$ -Unit vector normal to container wall.

p -Pressure = $\bar{p}a/\sigma$.

p_g -Gas pressure = $\bar{p}_g a/\sigma$.

p_o -Static liquid pressure at a fixed point on equilibrium free surface = $\bar{p}_o a/\sigma$.

P Distance from (R,Z) to upper branch of ellipse along r = R.

P_m -$P_m = \max(P: 0 \le s \le s - \delta,\ 0 < \delta < \Delta s)$.

Q -Distance from (R,Z) to lower branch of ellipse along r = R;

-Coefficient of Φ_n in the free-surface boundary condition;

-A function of convenience.

r -Radial coordinate = $\bar{r}/a$.

R -Radial coordinate of point on equilibrium free-surface meridian = $\bar{R}/a$;

-Right triangular factor of the matrix S.

R_1 -Principal radii of curvature of equilibrium free-surface

R_2 = $\bar{R}_1/a$, $\bar{R}_2/a$.

$\underline{r}$ -Radius vector from origin of tank fixed coordinate system = $\underline{\bar{r}}/a$.

s -Arc length along equilibrium free surface meridian = $\bar{s}/a$.

s_{max} -Symbol for s_u on plotted output.

S -Tridiagonal matrix $S = \frac{1}{2} A^{-1} T A^{-1}$.

sn -A Jacobian elliptic function.

t -Time = $[(1+B_\alpha)\sigma/(\rho a^3)]^{1/2}\ \bar{t}$;

-Dummy variable.

t_1

t_2 -s-coordinates of mid-points of two adjacent mesh intervals.

T -Tridiagonal matrix approximating the free-surface boundary operator $\underline{L}$;

-As superscript denotes transposition;

-Period of B_{tr} = $[(1+B_\alpha)\sigma/(\rho a^3)]^{1/2}\ \bar{T}$.

U -R_s in system of first order differential equations for meridian of equilibrium free-surface.

$\underline{v}$ -Fluid velocity = $\nabla\Phi$ = $[(1+B_\alpha)\sigma/(\rho a)]^{-1/2}\ \underline{\bar{v}}$.

V -Volume = $\bar{V}/(4\pi\bar{a}^2\bar{b}/3)$.

V_k -Energy amplitude of k^{th} mode = $\bar{V}_k/(\sigma a^2)$.

w -Denotes container wall;
-Complex variable.

w_j -Weight in integration formula.

W -Z_s in system of first order differential equations for meridian of tank wall.

x -Cartesian coordinate = $r\cos\theta = \bar{x}/a$

$\hat{x}$ -Maximum lateral mass displacement of mechanical analogue = $\hat{\bar{x}}/a$.

X -Radial coordinate of point on container wall meridian = $\bar{X}/a$ (measured from polar axis).

$\underline{y}$ -Vector of approximations to Φ for mesh points not on free-surface.

$\underline{y}^{(1)}$ -Improved approximation for $\underline{y}$.

Y -Axial coordinate of point on container wall meridian = $\bar{Y}/a$ (measured from equatorial plane).

z -Axial coordinate = $\bar{z}/a$.

$\underline{z}$ -Vector of approximations to Φ on the free-surface.

z_k -Axial coordinate of action point of mechanical analog = $\bar{z}_k/a$ (measured from the tank center).

$\underline{z}^{(0)}$ -Initial guess for $\underline{z}$.

$\underline{z}^{(1)}$ -Improved approximation for $\underline{z}$.

Z -Axial coordinate of point on equilibrium free surface meridian = $\bar{Z}/a$.

Greek Alphabet

δ -Ratio of periodic pulse width to half period to the perturbing acceleration.

δ_{jk} -Kronecker delta = 1 if $j = k$, otherwise = 0.

Δs -Mesh spacing on s.

Δt -Perturbing pulse width.

$\Delta\tau$ -Mesh spacing on w.

ζ -A complex variable.

η -Normal coordinate = $\bar{\eta}/a$.

H -Normal coordinate of free surface = $\bar{H}/a$.

θ -Angular coordinate

Θ -Contact angle.

$\varkappa_k$ -Spring constant for mechanical analogue for k^{th} mode $= \bar{\varkappa}_k/\sigma$.

λ -Pressure difference across a fixed point on the equilibrium free surface $= p_g - p_o$;
-Approximation to the eigenvalue ω^2.

$\lambda^{(0)}$ -Guessed λ in Wielandt inverse-iteration.

$\lambda^{(1)}$ -Improved λ in Wielandt inverse-iteration.

μ -Integer index.

ν -Integer index.

ρ -Dimensional liquid density.

σ -Dimensional surface tension.

τ -Arc length along container wall meridian $= \bar{\tau}/a$.

τ_L -The length of a container meridian from pole to pole $= \bar{\tau}_L/a$.

φ_j -Approximation to Φ at the j^{th} mesh point.

$\underline{\varphi}$ -Vector of approximation to Φ.

$\underline{\varphi}_1$ -Vector component of $\underline{\varphi}$ for points on equilibrium free-surface.

$\underline{\varphi}_2$ -Vector component of φ for points not on equilibrium free-surface.

Φ -Velocity potential $= [(1+B_\alpha)\sigma a/\rho]^{-1/2}\,\bar{\Phi}$.

Φ_k -Φ for k^{th} normal mode.

Φ_n -$\partial\Phi/\partial n$.

χ -Angle between radial direction and container wall meridian.

ψ -Angle between radial direction and equilibrium free surface meridian.

ω -Frequency $= [(1+B_\alpha)\sigma/(\rho a^3)]^{-1/2}\,\bar{\omega}$.

ω_k -ω of k^{th} normal mode.

ω_o -ω of periodic B_{tr}.

$\underline{\Omega}$ -Angular rotation rate of tank-fixed coordinate system $= [(1+B_\alpha)\sigma/(\rho a^3)]^{-1/2}\,\bar{\underline{\Omega}}$.

$\| \|$ -Euclidean vector norm

Combining Subscripts

j	-Index, usually for points and values belonging to boundaries.
k	-Index denoting k^{th} normal mode.
ℓ	-Denotes lower circle of intersection, if any, of equilibrium free-surface and container wall.
m	-Index, particularly in Fourier sine expansion of perturbing acceleration;
	-Also denotes mean or maximum.
n	-Denotes differentiation in the exterior normal direction.
tr	-Denotes transverse (lateral) direction.
u	-Denotes uppermost intersection of equilibrium free-surface and container wall.
w	-Denotes container wall.
α	-Denotes the axial direction.

REFERENCES

1. Abramson, H. H. (ed.): The Dynamic Behavior of Liquids in Moving Containers. NASA SP-106, U. S. Gov't Printing Ofc., Washington, D. C. 1966.

2. Satterlee, H. M. and Reynolds, W. C.: "The Dynamics of the Free Liquid Surface in Cylindrical Containers Under Strong Capillary and Weak Gravity Conditions." Tech. rpt. no. LG-2, Stanford Univ. Dept. Mech. Engr., Stanford, Calif. May 1964.

3. Dodge, F. T. and Garza, L. R.: "Experimental and Theoretical Studies of Liquid Sloshing at Simulated Low Gravities." Trans. A.S.M.E., Ser. E. vol. 34, no. 3, pp. 555-562.

4. Concus, P., Crane, G. E. and Satterlee, H. M.: "Small Amplitude Lateral Sloshing in a Cylindrical Tank With a Hemispherical Bottom Under Low Gravitational Conditions." NASA CR-54700 prepared by Lockheed Missiles and Space Co. under Contract NAS 3-7119, Jan. 1967.

5. Concus, P., Crane, G. E. and Satterlee, H. M.: "Low-Gravity Lateral Sloshing in a Hemispherically Bottomed Cylindrical Tank." Proc. 1968 Heat Transfer and Fluid Mech. Inst., Stanford Univ. Press, pp. 80-97, June 1968.

6. Salzman, J. A., Labus, T. L. and Masica, W. J.: "An Experimental Investigation of the Frequency and Viscous Damping of Liquids During Weightlessness." NASA TN D-4132, Aug. 1967.

7. Dodge, F. T. and Garza, L. R.: "Simulated Low-Gravity Sloshing in Cylindrical Tanks Including Effects of Damping and Small Liquid Depth." Proc. 1968 Heat Transfer and Fluid Mech. Inst., Stanford Univ. Press, pp. 67-79, June 1968.

8. Salzman, J. A., Coney, T. A. and Masica, W. J.: "Effects of Liquid Depth on Lateral Sloshing Under Weightless Conditions." NASA TN D-4458, May 1968.

9. Bogoriad, I. B.: "On the Solution by a Variational Method of the Problem of the Oscillations of a Liquid Partially Filling a Cavity." Applied Math. and Mechanics, vol. 26, no. 6, 1962, pp. 1704-1713.

10. Budiansky, B.: "Sloshing of Liquids in Circular Canals and Spherical Tanks." Jour. Aero/Space Sciences, vol. 27, no. 3, Mar. 1960, pp. 161-173.

11. Rattayya, J. V.: "Sloshing of Liquids in Axisymmetric Ellipsoidal Tanks." AIAA paper no. 65-114, 2nd Aerospace Sciences Meeting, New York, Jan. 25-7, 1965.

12. Dodge, F. T. and Garza, L. R.: "Simulated Low-Gravity Sloshing in Spherical Tanks and Cylindrical Tanks with Inverted Ellipsoidal Bottoms." Tech. rpt. no. 6, Contract NAS 8-20290 prepared by Southwest Research Inst., San Antonio, Tex. for NASA Marshall Space Flight Center, Feb. 1968.

13. Weatherburn, C. E.: Differential Geometry of Three Dimensions. Vol. I, Cambridge Univ. Press, 1955, Section 116.

14. Bakker, G.: "Kapillarität und Oberflächenspannung." Handbuch der Experimental Physik, Wien, W., Harms, F., and Lenz, H. (eds.), vol. VI, Akademische Verlagsgesellshaft, Leipzig, 1928.

15. Kober, H.: Dictionary of Conformal Representation. Dover, New York, 1957.

16. Ostrowski, A. M.: "Conformal Mapping of a Special Ellipse of the Unit Circle." Experiments in the Computation of Conformal Maps, John Todd (ed.), National Bureau of Standards, Applied Mathematics Series, No. 42, U. S. Govt. Printing Ofc., Washington, D. C., 1955.

17. Szegö, Gabor: "Conformal Mapping of the Interior of an Ellipse onto a Circle." Amer. Math Monthly, vol. 57, 1950, pp. 474-478.

18. Abramowitz, M. and Stegun, I. A. (eds.): Handbook of Mathematical Functions with Formulas, Graphs, and Mathematical Tables. National Bureau of Standards Applied Mathematics Series, No. 55, U. S. Govt. Printing Ofc., Washington, D. C., 1965.

19. Bulirsch, Roland: "Numerical Calculation of Elliptic Integrals and Elliptic Functions." Numerische Math., vol. 7, 1965, pp. 78-90.

20. Wynn, P.: "An Arsenal of Algol Procedures for Complex Arithmetic." B.I.T., vol. 2, 1962, pp. 232-255.

21. Winslow, A. M.: "Numerical Solutions of the Quasilinear Poisson Equation in a Nonuniform Triangle Mesh." J. Comp. Physics, vol. 1, 1966/67, pp. 149-172.

22. Kellogg, R. B.: "Difference Equations on a Mesh Arising from a General Triangulation." Math. Comp., vol. 18, 1964, pp. 203-210.

23. Varga, R. S.: Matrix Iterative Analysis. Prentice-Hall, Inc., Englewood, Cliffs, N. J., 1962, pp. 161-173.

24. Gantmacher, F. R.: The Theory of Matrices, vol. I, Chelsea Publishing Co., New York, 1959, pp. 310-326.

25. Wilkinson, J. H.: The Algebraic Eigenvalue Problem. Oxford Univ. Press, Oxford, 1965, pp. 221-232 and 619-629.

DISTRIBUTION LIST FOR NASA CR 72500

CONTRACT NAS 3-9704

Address	Number of Copies
NASA Headquarters FOB -10B 600 Independence Ave., S.W. Washington, D.C. 20546 Attention: Warren Keller/RV-1	2
NASA-Lewis Research Center 21000 Brookpark Road Spacecraft Technology Division Cleveland, Ohio 44135	
Attention: C. C. Conger, MS 54-1	1
D. A. Petrash, MS 54-1	1
W. J. Masica, MS 54-3	50
J. A. Salzman, MS 54-3	2
I. I. Sonkin, MS 500-110	1
N. T. Musial, MS 501-3	1
Library, MS 60-3	2
Report Control Office, MS 5-5	1
NASA Scientific and Technical Information Facility Box 5700 Bethesda, Maryland 20014 Attention: NASA Representative	6
Southwest Research Institute 8500 Culebra Road San Antonio, Texas 78206	
Attn: Dr. H. Norman Abramson	1
Dr. Daniel D. Kana	1
Dr. Wen-Hwa Chu	1
4043 Cody Road Sherman Oaks, California 91403 Attn: Dr. Marvin Adelberg	1
TRW Space Technology Laboratory One Space Park Redondo Beach, California 90277	
Attn: Dr. Pravin Bhuta	1
Dr. R. E. Hutton	1

Address	Number of Copies
NASA-John F. Kennedy Space Center Kennedy Space Center, Florida 32899	
Attn: Mr. J. P. Claybourne/MC	1
Mr. W. H. Boggs/MC	1
Office National D'Etudes Et De Recherches Aerospatiales 29, Avenue de la Division LeClerc 92 Chatillon France	
Par Michel Delattre	1
Par Jean Maulard	1
Bell Aerosystems Buffalo, New York 14240	
Attn: Minas Ensanian	1
University of California Los Angeles, California 90024	
Attn: Dr. K. E. Forster	1
Advanced Technology Laboratories General Electric Company Schenectady, New York 12308	
Attn: Mr. R. F. Gaertner	1
Massachusetts Institute of Technology Cambridge, Massachusetts 02138	
Attn: Dr. Peter Griffith	1
Space and Information Systems Division North American Aviation, Inc. 12214 Lakewood Blvd. Downey, California 90241	
Attn: Dr. Francis C. Hung	1
Mr. Donald J. Simkin	1
Dr. Ta Li GB 33	1
Midwest Research Institute 425 Volker Boulevard Kansas City, Missouri 64110	
Attn: Dr. Sheldon Levy	1

Address	Number of Copies
University of Kentucky Lexington, Kentucky 40506 c/o College of Engineering Attn: Dr. John H. Lienhard	1
University of Michigan Ann Arbor, Michigan 48107 Attn: Dr. H. Merte, Jr. Dr. John A. Clark	1 1
Astronautic/Propulsion Martin Denver Division Denver, Colorado 80201 Attn: Howard L. Paynter MS 1662	1
Marshall Space Flight Center Huntsville, Alabama 35812 Attn: A. L. Worland Frank Swalley H. Trucks/R-P&VE-PTP L. J. Hastings	1 1 1 1
Manned Spacecraft Center 2101 Webster-Seabrook Road Houston, Texas 77058 Attn: Jerry C. Smithson	1
Mechanical Engineering Department Tufts University Medford, Massachusetts 02155 Attn: Dr. Lloyd Trefethen	1
Department of Mechanical Engineering New York University New York, New York 10453 Attn: Dr. Novak Zuber	1

Address	Number of Copies
McDonnell-Douglas Corporation 3000 Ocean Park Blvd. Santa Monica, California 90406	
Attn: R. A. Madsen	1
J. B. Blackmon	1
Battelle Memorial Institute 505 King Avenue Columbus, Ohio 43201	
Attn: Mr. Clarkson L. Coffin	1
Mr. Alan U. Hare	1